FINAL REPORT

PROJECT NO. A-635

HEAT TRANSFER TO A GAS CONTAINING A CLOUD OF PARTICLES

EDWARD Y.H. KENG AND CLYDE ORR, JR.

Research Grant NGR-11-002-003

Covering the Period
1 June 1962 through 31 May 1968
Printed January 1969

Prepared for
National Aeronautics and Space Administration
Washington, D. C.

Engineering Experiment Station
GEORGIA INSTITUTE OF TECHNOLOGY
Atlanta, Georgia

GEORGIA INSTITUTE OF TECHNOLOGY
Engineering Experiment Station
Atlanta, Georgia

FINAL REPORT

HEAT TRANSFER TO A GAS CONTAINING A CLOUD OF PARTICLES

By

Edward Y.H. Keng
and
Clyde Orr, Jr.

Covering the Period
1 June 1962 through 31 May 1968

Printed January 1969

Research Grant NGR-11-002-003

Prepared for
NATIONAL AERONAUTICS AND SPACE ADMINISTRATION
WASHINGTON, D. C. 20005

TABLE OF CONTENTS

This report contains 134 pages.

LIST OF FIGURES

I. SUMMARY

The objective of this research was to provide fundamental information on radiant heat transfer to particle clouds. The analysis performed was intended to be useful in the evaluation of various nuclear rocket engine designs and in industrial high temperature applications. The information gained should also contribute to basic knowledge in the field of heat transfer and particle technology.

This investigation has involved a wide variety of problems, including particle cloud generation, optical properties of particle clouds, and particle gasification in addition to radiant heat transfer to particle clouds. Four types of particle cloud generators were designed and tested. Their merits and shortcomings are discussed. Extinction coefficients and the transmissivity of particle clouds were measured. Discussions are included on the dependence of the wavelength of the radiation and the concentration of the particle cloud. Experimental measurements of particle gasification were not obtained due to the lack of a sufficiently intense radiant source.

Rates of radiant heat transfer to clouds composed of well-dispersed non-luminous, solid particles of known concentrations were measured. In agreement with theoretical predictions, clouds of the smaller particles absorbed more radiant energy than those having the same mass concentration of larger particles. The absorption coefficient was found to be directly related to the cross-sectional area of the particles per unit volume of cloud. Equations are given describing the rate of radiant heat transfer to particle clouds in terms of the mean beam length, particle concentration, density, and size. Reflective particles were also investigated; the

results here were in accord with theoretical approximations. View factors have been evaluated for a number of conditions when a cylindrical wall is the emitter. Both black and non-black walls were studied. Equations have also been derived to calculate view factors among zones of any size. Discussions are also included relative to non-isothermal and variable absorption coefficient systems.

A cylindrical tungsten furnace was built and the rate of radiant heat transfer to clouds was measured. The data of carbon black clouds were in good agreement with theoretical values calculated from view factors. The data of alumina particle clouds were lower than carbon black due to low emissivity. Tungsten particles were found to deposit on the heating element after each test with a tungsten cloud. This phenomenon was not noticed when carbon black and alumina clouds were used.

II. INTRODUCTION

The principles describing the transfer of heat by radiation were formulated in the latter part of the previous century, and their application to practical problems has been the subject of many investigations since that time. The majority of these, however, have related to furnace technology because here sufficiently high temperatures were first attained for thermal radiation processes to have commercial significance and to merit the scrutiny of engineers. The problems were primarily associated with the transfer of radiation between solid surfaces or between solid surfaces and absorbing gases such as carbon dioxide and water vapor. These analyses are of limited applicability to this investigation because of the numerous empirical assumptions about combustion rates, furnace shapes, fuel characteristics, stoichiometric relationships, etc., that were required.

Radiation heat transfer is currently undergoing a renewal of interest, the advent of plasma generators, re-entry missiles, and novel concepts in nuclear technology having focused attention on these new radiation problems. Solutions are now needed to basic as well as practical problems where temperatures are much above those in conventional equipment and where radiation is the dominant mode of heat transfer.

Detailed information on the absorption of radiation by particle clouds has applications in other areas as well. X-ray and nuclear radiations, for instance, are known to produce chemical reactions in dispersed systems; just how is of much interest currently to the process industries, for example. Particles can be subjected to thermal energy in plasma generating devices to produce spherical particles, crystal transformations, and size

reductions. For protection in a time of national emergency, particle clouds might be produced to absorb radiation, both nuclear and thermal, that could otherwise prove lethal.

Radiant heat transfer is the most important mechanism of transfer at the temperatures involved in gaseous, nuclear, rocket concepts. It is dependent on the opacity characteristics of the propellant gas which may be hydrogen containing small, absorbing particles. Hydrogen gas is practically transparent below $5000^{\circ}K$[1,2] even under high pressures, thus the radiant heat transfer in this region would depend mainly on the particles.

Carbon was initially considered to be the most suitable seeding material. It has good absorptivity, high boiling point, and low density. Also it is available in large quantities having very small particle sizes. Recently, however, irregularities have been observed in the absorption of carbon particles in hydrogen gas during flash experiments.[3] These may arise as a result of a chemical reaction at the surface of the particles at high temperature. More information is needed to determine if carbon particles and hydrogen gas are indeed a suitable combination for gas-core, nuclear reactors. In the meantime, the use of several other materials, such as tungsten, rhenium, and tantalum, has been suggested. These materials are reported[4,5] to exhibit no significant difference in opacity at a wavelength of 0.579 micron, and all of them have a high boiling point. Also they do not react with hydrogen gas at high temperatures. However, the theoretical maximum extinction parameter for carbon at a wavelength of 0.4 micron is approximately three times that of tungsten per unit mass of powder.

Theoretical studies of radiant heat transfer to absorbing gases and particle clouds have been performed by many investigators.[6,7,8,9] In general, the emitting surface and the absorbing gas have been treated mathematically as if divided into zones. For cylindrical systems, the enclosed gas was divided into right cylinders and coaxial cylindrical rings by Erkku.[7] The wall and gas were divided into zones of length equal to the diameter and called unit zones by Hoffman and Gauvin.[8] Many approaches have been used since then to attack the radiant heat transfer problems for various systems.[10,11,12,13,14]

In this study, a new approach was used. The solutions were first obtained by integration for a conduit of various length and the curves of various absorption strength were constructed. Then simple mathematical maneuvers were suggested to attack difficult problems. The applications were thus widened. Properties of emitting surfaces and suspended particles were also discussed. Solutions have been obtained for cylindrical systems; however, the methods suggested are good for all conduits provided the cross-sectional areas are uniform.

III. GENERATION OF PARTICLE CLOUDS

Many types of particle cloud generators have been employed in studies of particle cloud properties, each type being good only for limited conditions. Some types produce uniform clouds but are poor in the degree of dispersion they produce. Some types work well only when particles are relatively large. Therefore, choosing a suitable generator is one of the prime factors in the success of any particle cloud study. Four types of generators have been used in this investigation for various purposes; they are described separately in the following sections. The effect of pressure on the initial dispersion is also discussed.

A. Retaining partition type

The distinctive components of this type of generator are a retaining partition within a rotating powder container.[15] The unit is shown in detail in Figure 1. As shown in section A-A, powder is retained behind a partition in a slowly rotating container. A thin layer of powder is thus produced along the bottom of the container. This layer is carried by the revolving container under nozzle pickups where the powder is entrained in air passing upward. Particle deagglomeration results from the shear forces generated by the flow through small passages.

Numerous exploratory experiments were required in order to achieve a suitable deagglomerating nozzle to handle a comparatively large flow rate and still produce a uniformly dispersed cloud with steady flow characteristics. Originally, a venturi reducing the channel diameter to about 0.03 inch was employed at the point where the powder-air mixture issued from

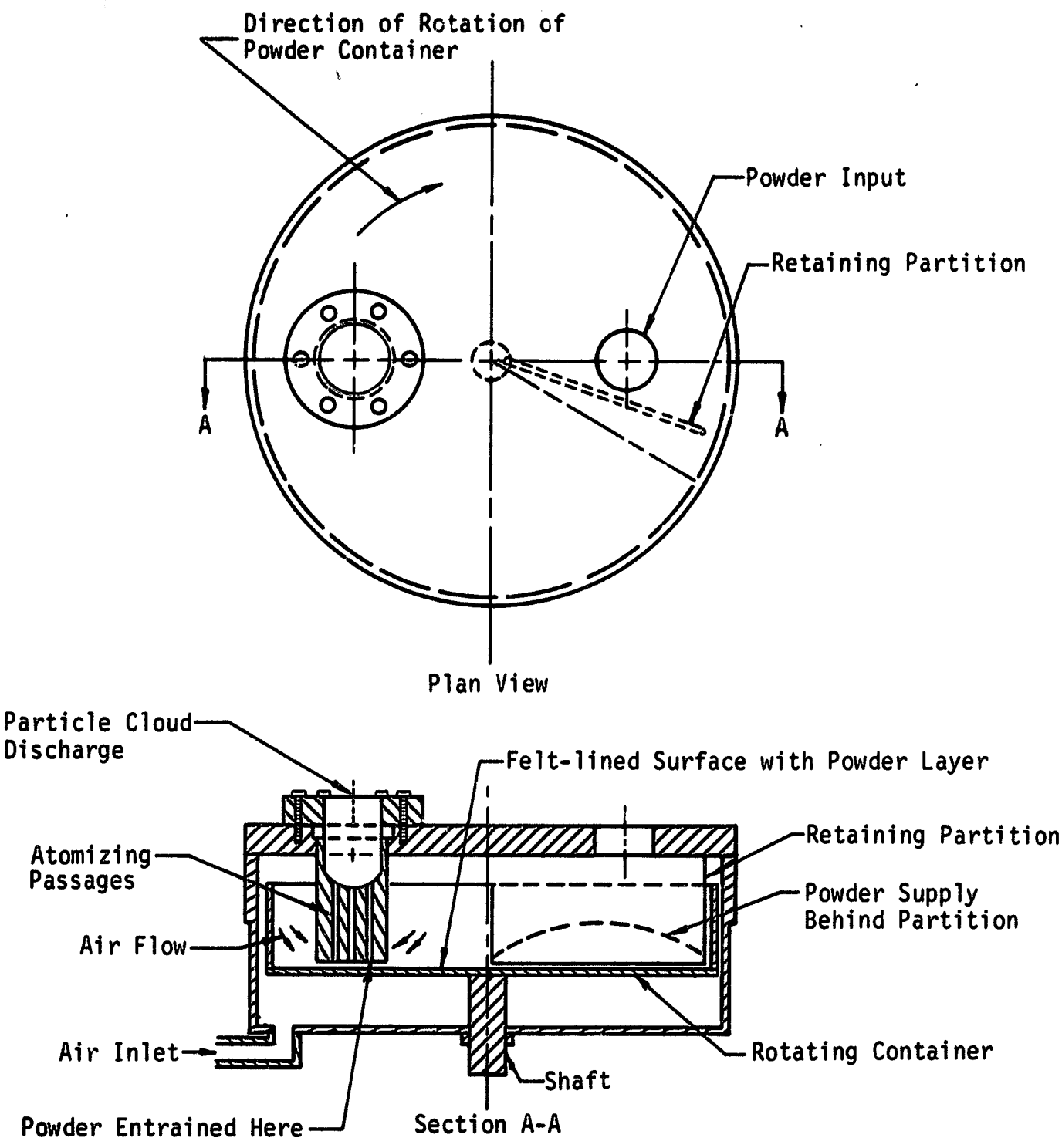

Figure 1. Retaining Partition Type of Particle Cloud Generator.

the generator assembly. At that time the powder was made airborne by entrainment with air passing through a perforated plate that covered the inlet to the aerosol conduit. In practically every instance, heavy agglomerates would form a fluidized bed in the pipe leading to the venturi. The venturi was then placed inside the aerosol generator to avoid the fluidizing effects, but now the powder entrainment was unsteady. The most satisfactory arrangement employed multiple, small-diameter passages inside the generator which served both as pickup tubes and as deagglomeration nozzles.

The final unit was found to be very good for large flow rate operations. Particle clouds generated by this unit are fairly uniform provided a smooth layer of powder is produced by the retaining partition. Dispersion is generally quite good for particles with mean diameters down to 5 microns but is only fair for particles smaller than that. Adding particles continuously to the powder container assured long-time operation without shutdown. The unit could, it is thought, be modified for high pressure conditions to improve the dispersion efficiency.

B. Vibration type

The principle of a vibrating cloud generator involves transporting particles from a powder container to a gas-solid mixing chamber by means of vibration and then expanding this mixture through a dispersion nozzle. The feed rate of the powder is controlled by the intensity of the vibration and the size and number of openings between the powder container and the mixing chamber. The gas flow rate is controlled by the differential pressure

and the size of the dispersion nozzle. Thus the concentration and quantity of the particle cloud can be controlled.

The arrangement of the vibration type cloud generator is shown in Figure 2 and the detailed design in Figure 3. As may be seen from the figures, a powder supply, contained within a high pressure cylindrical enclosure, rests on an orifice plate having six small, sharp-edged orifices. The powder is caused to feed through small openings into a mixing chamber by the vibratory action of a vibrator (Model F-010, Syntron Company, Homer City, Pennsylvania) on which the generator is mounted. Carrier gas, in this case high pressure nitrogen, swirls through the mixing chamber and entrains the particle clusters. From there the newly formed suspension flows through a short, small tube and emerges from one of the sharp-edged orifices. The rapid expansion and associated high shearing action effectively transforms the agglomerated suspension into a good dispersion of particles.

Tests have also been made by using a 3-inch long and 1/16-inch I.D. tube as the dispersion nozzle. Powder was first found to accumulate at the entrance end of the nozzle where it either plugged the flow or produced intermittent surges. This behavior was eliminated by smoothing all edges in the system against which powders might accumulate and always being sure that carrier gas was flowing through the system before turning on the vibrator.

This type of generator is easy to construct and to operate when particle diameters are above 5 microns. High pressure can be used to achieve excellent dispersion. However, problems develop when very fine particles are used. Such powders may plug the holes in the orifice plate

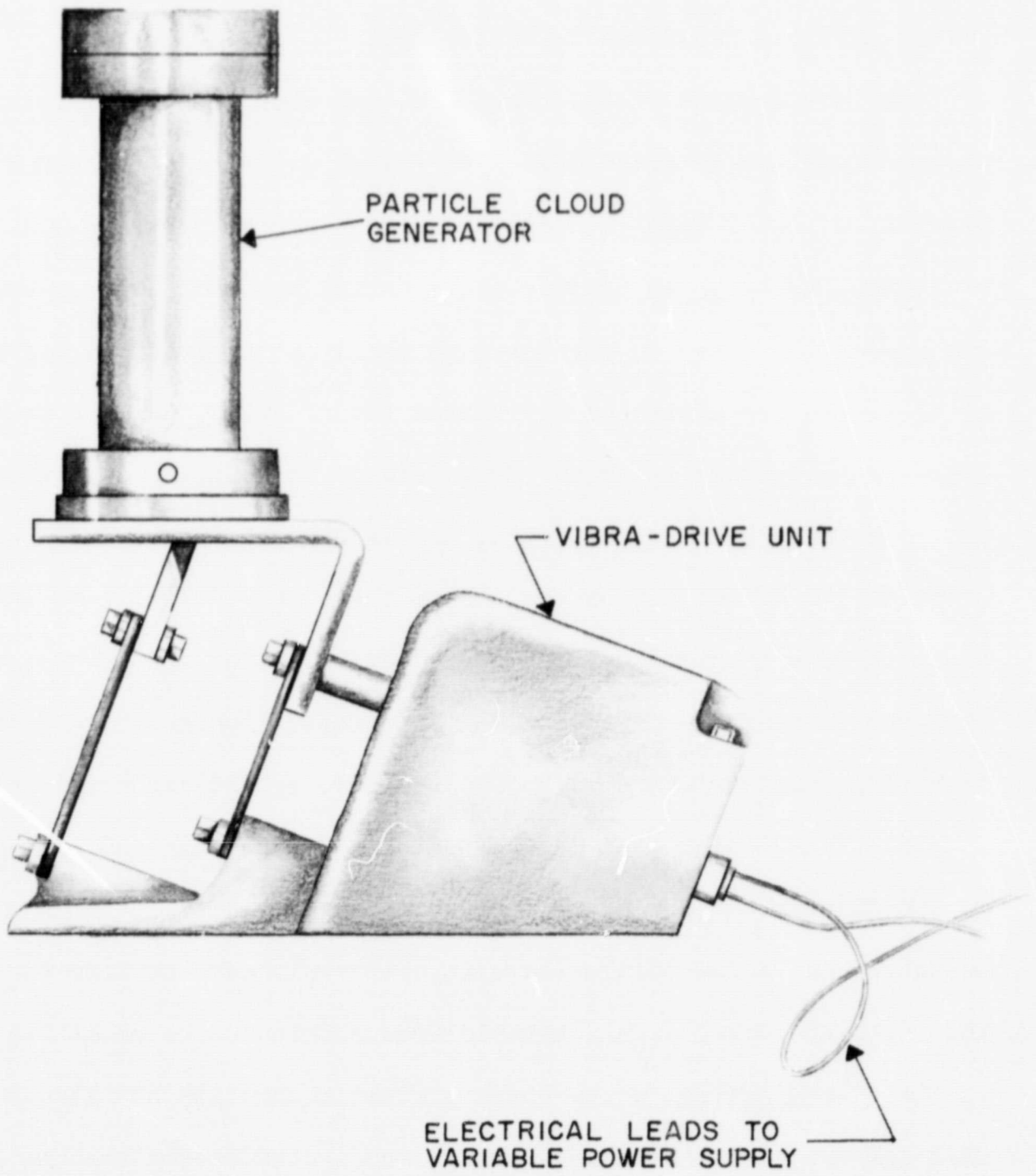

Figure 2. Syntron Vibra-Drive Unit and Particle Cloud Generator Assembly.

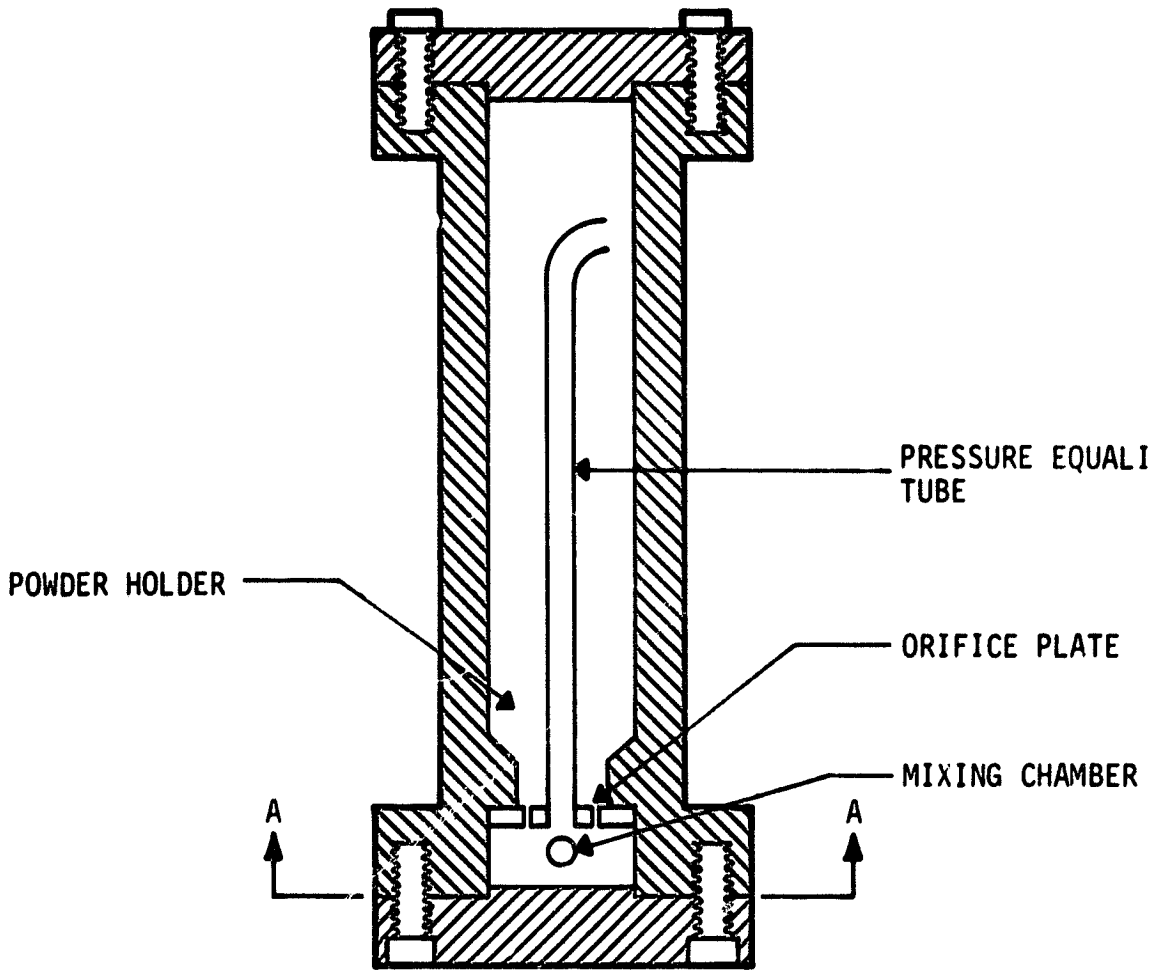

LONGITUDINAL SECTION OF POWDER FEEDER

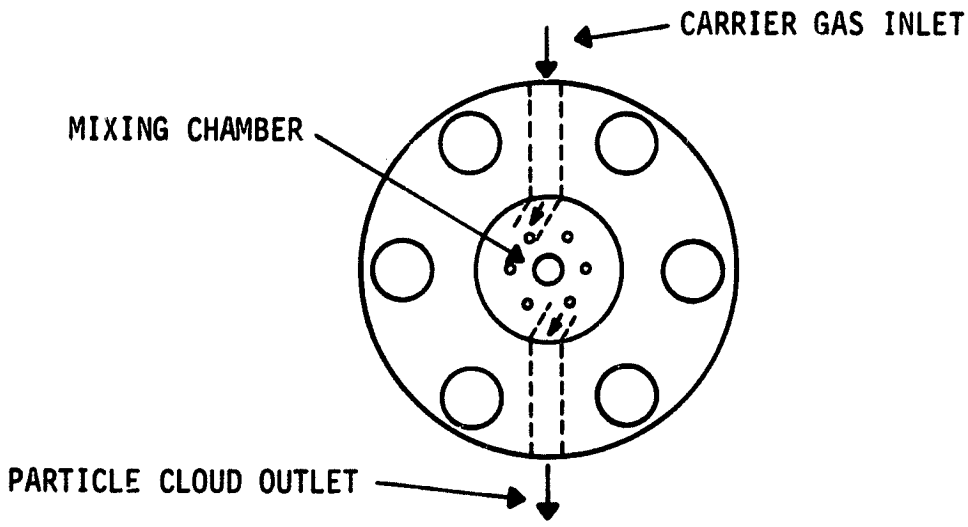

SECTION A-A

Figure 3. Vibrating Type Particle Cloud Generator.

when the holes are small. Big holes allow too much powder to fall into the mixing chamber which plugs the dispersion nozzle. Experiences gained through experiments show that a right combination of all factors is very important. These factors include particle properties, number of holes leading into the mixing chamber, shape of the mixing chamber, carrier gas pressure, and type and size of the dispersion nozzle. This type of generator can be made to operate under very high pressures to achieve good dispersion. No internal moving parts are involved in this design.

A modified model was made for the production of clouds from very fine powders. A fluidized bed was employed in this design. A schematic diagram is given in Figure 4. Ceramic or steel balls were employed to distribute the carrier gas evenly as well as to prevent powder caking at the bottom or on the chamber wall. The balls move vigorously inside the chamber when the flow rate is high. The major problem here is that very fine powders do not feed into the fluidizing chamber evenly. This difficulty was overcome by installing a large valve and tube between the two chambers and adjusting both the valve opening and the intensity of the vibration simultaneously. One end of the dispersing nozzle was extended inside the fluidizing chamber to avoid accumulation of particles at the inlet opening. The number, material, and size of the balls in the fluidizing chamber is dictated by the particle characteristics and the gas flow rate. The balls can be illiminated when the particles neither agglomerate nor adhere to the wall.

C. Aspirator type

A particle cloud generator built on the principle of an aspirator is shown schematically in Figure 5. A venturi is located on top of the

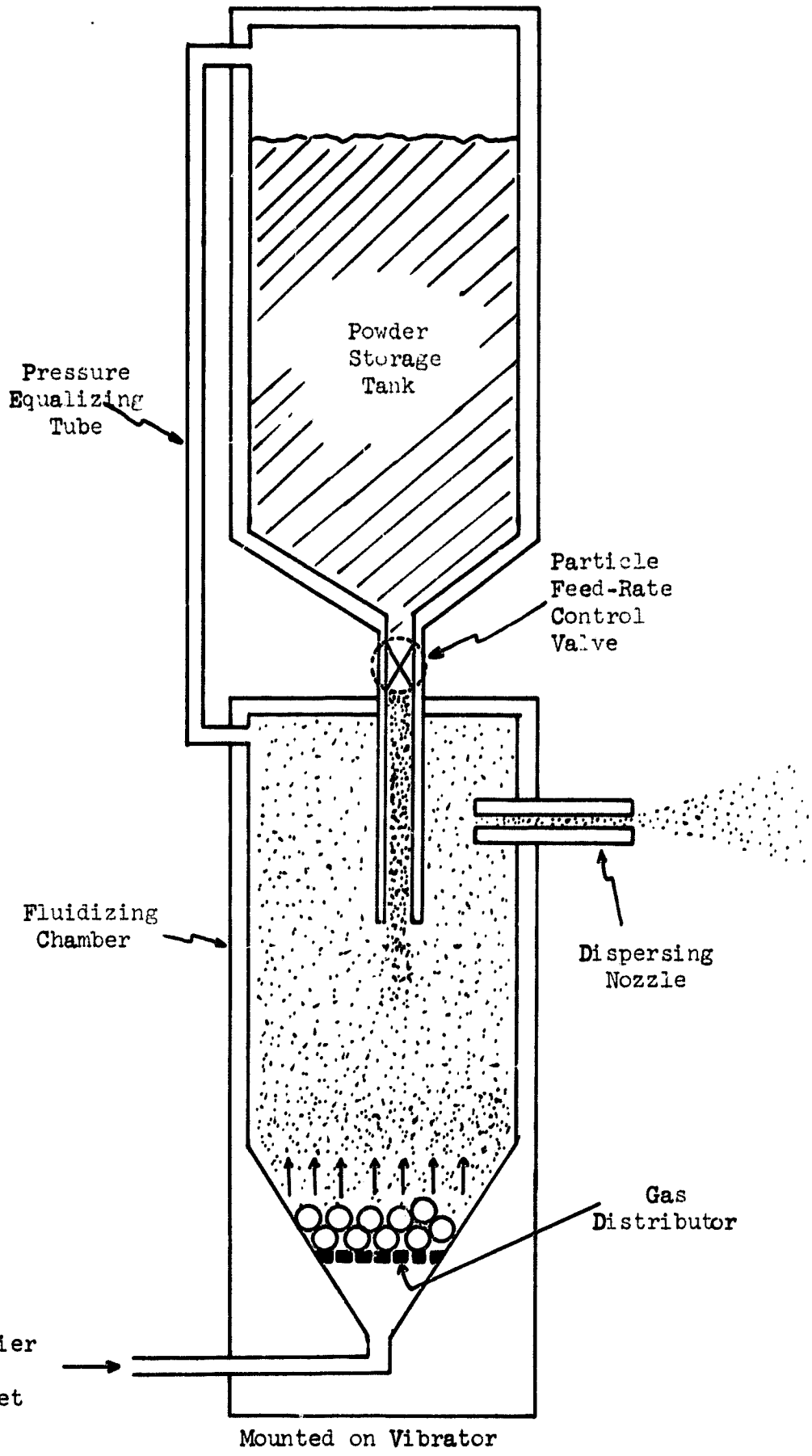

Figure 4. Particle Cloud Generators of Vibration and Fluidization Type.

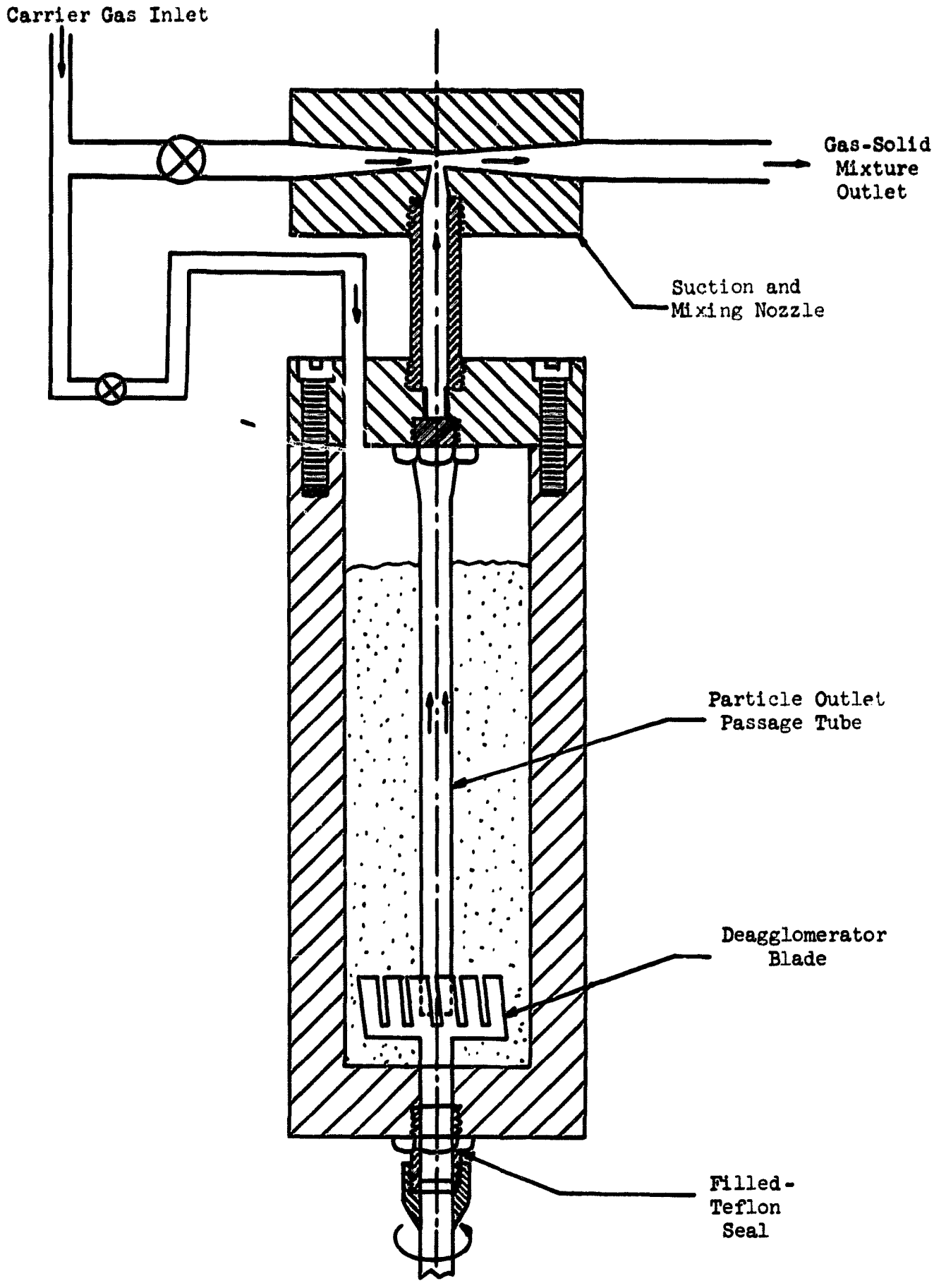

Figure 5. Particle Cloud Generator of Aspirator Type.

generator. The chamber pressure is regulated by connecting it to the carrier gas inlet through a valve. The increase in kinetic energy in the venturi is accomplished by a corresponding decrease in static pressure. Thus the dense gas-particle mixture in the chamber is sucked into the venturi. Particles are deagglomerated by the shear forces created in the venturi and are thus dispersed into a particle cloud. A deagglomerator blade is located at the bottom of the chamber near the inlet of the particle outlet tube as shown in the figure. The deagglomerator blade keeps the powder loose and uniform for easy pick-up through the tube. The shaft of this blade is sealed against pressure loss by filled teflon rings.

The concentration of the particle cloud is controlled by the valves on the inlet lines to the venturi and to the chamber. A higher gas velocity in the venturi creates greater suction and shear force. A higher flow rate to the chamber expells more particles from the chamber and produces higher particle concentration in the resulting cloud. With a proper sized venturi, well-dispersed, particle clouds of the desired concentration and at the desired rate can be produced by adjusting the valves. An additional dispersion nozzle can be employed to improve particle deagglomeration if needed. A powder must be dry before use to prevent caking and the creation of gas "bubbles" inside the powder. The motor driving the deagglomerator blade should always be turned on first, then the valve letting carrier gas through the venturi should be opened. After this, the valve on the line connected directly to the chamber is adjusted until the desired cloud concentration is obtained. This generator can also be modified for long time operation by adding a storage tank and feeding particles into the generator chamber continuously at the same rate as the particle output.

D. Stirrer type

It is sometimes difficult to transport carbon black particles, for example, from one tank to another at a small but constant rate, especially when the system is operated under high pressure conditions. When long-time operation is the problem, a large capacity generator is desirable. A relatively large generator was built having heavy walls for high-pressure operation. This unit could produce a uniform cloud for a much longer time than either of those described in Sections B and C and it could be operated at a much higher pressure than the one described in Section A giving also better dispersion.

The design of this generator is shown in Figure 6. Powder is "mobilized" by a mechanical stirrer. The size, shape, and location of the blades depend on the powder property and the rotating speed. Two thin scraper bars were installed between the top and bottom blades to scrape deposited particles from the wall. Three valves were employed; they are designated valves Nos. 1, 2, and 3 on the figure and the following discussion. Valve No. 1 allowed gas to bypass the particle chamber in order to control the dilution ratio of the cloud and also to produce shear force for the deagglomeration of the particles. Valve No. 2 let carrier gas into the chamber to pick up gas-suspended particles. Valve No. 3 permitted some of the gas to flow through the powder mass in the lower portion of the chamber and to push out a denser cloud than was possible with valve No. 2 alone. All three valve settings could be changed independently or simultaneously. If valve No. 3 was to be used during the operation, it should be opened before valves Nos. 1 and 2 to avoid particles being pushed into the tube where they might cause plugging. Placing valve No. 3 near the chamber also minimizes this problem.

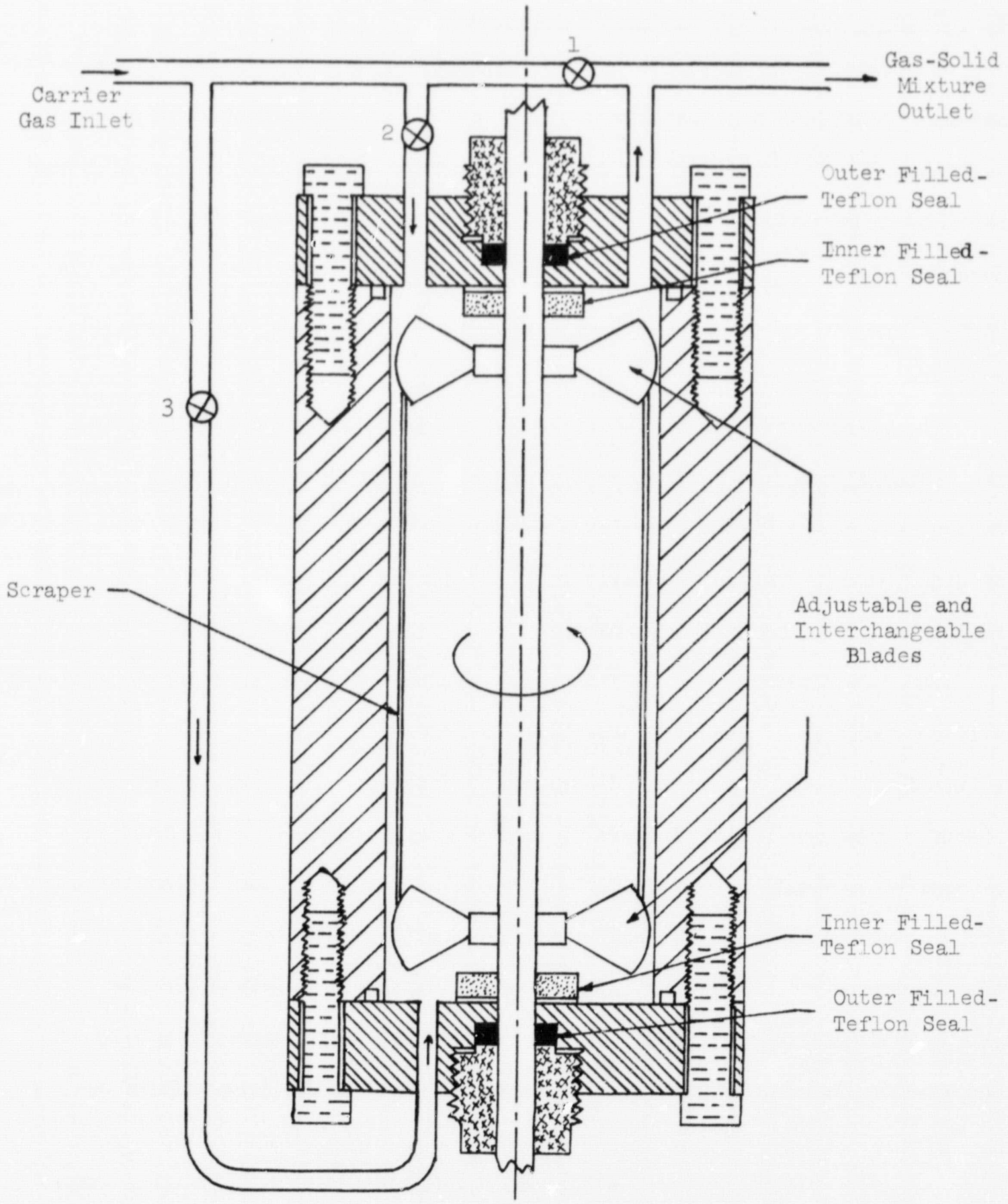

Figure 6. Particle Cloud Generator of Stirrer Type.

E. Effect of pressure on the initial dispersion

Cohesion among particles is the inevitable result of van der Waals forces and the cohesiveness of water and other vapors that may be adsorbed on the particles.[16,17,18,19,20,21] These forces must be overcome if a powder mass is to be dispersed. Application of shear is the usual means and it is developed by passing the gas-solid mixture through a dispersion nozzle. As shown above the nozzle is often nothing more than a round tube or an orifice.

The shear forces acting on particle agglomerates are proportional to the dispersion pressure if other factors such as the particle mass, nozzle design, etc., are fixed. Some investigators have reported[21] that the degree of dispersion increased regularly with increasing pressures. This was investigated in the following manner.

The test system shown in Figure 7 consisted of a pressure tank containing a fixed quantity of gas at a prescribed pressure, a solenoid valve for initiating flow of gas to the dispersing device, and the dispersing device itself. This particular dispersing device was a stainless steel holding chamber of a simple U-bend geometry with an exit tube of small diameter as the dispersing nozzle. The powder was dispersed into a large chamber and the transmittance of the particle cloud was measured. Linde-A alumina (Linde Division, Carbide and Carbon Chemical Corp.) was employed giving the results shown in Figure 8. The dispersion parameter η is defined by

$$\eta = - \frac{\rho}{C_{mo} L} \ln \left(\frac{I_L}{I_o} \right) \qquad (1)$$

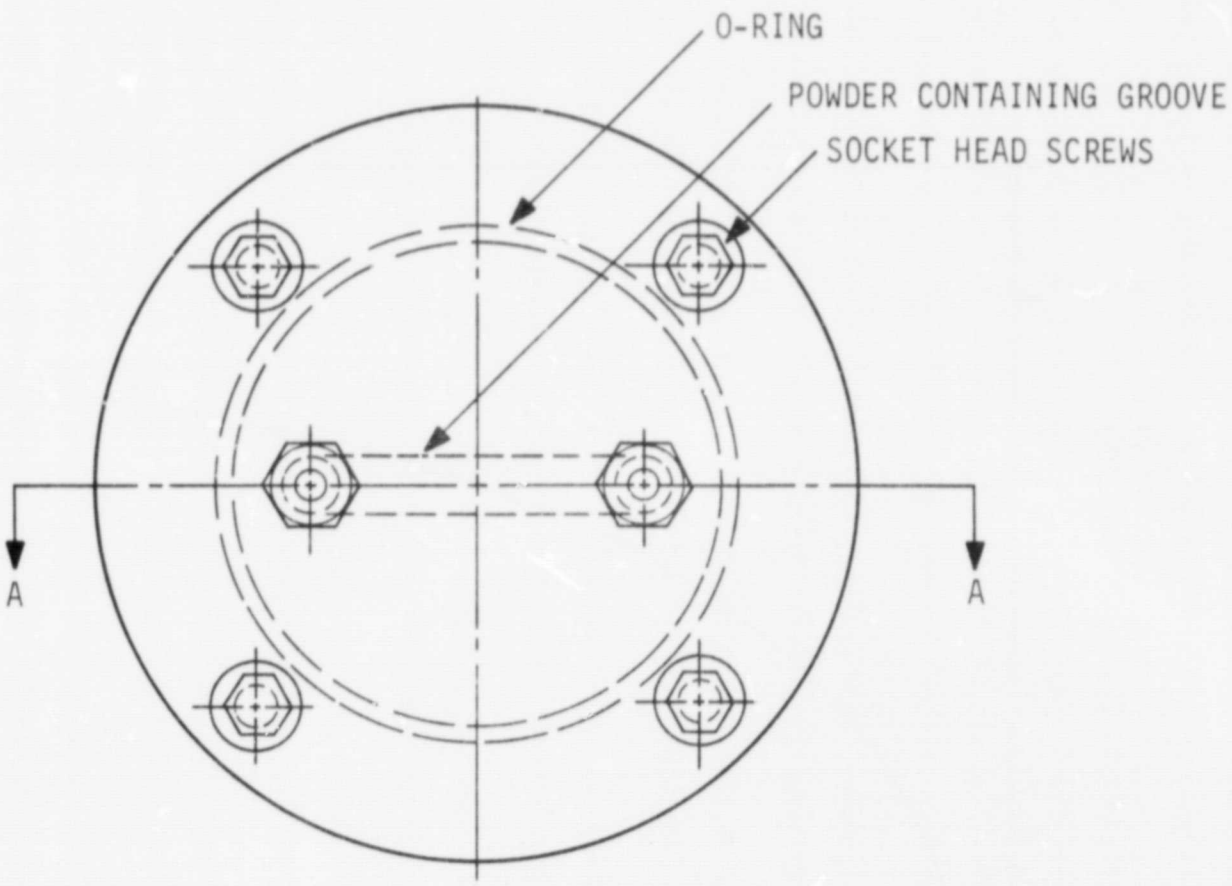

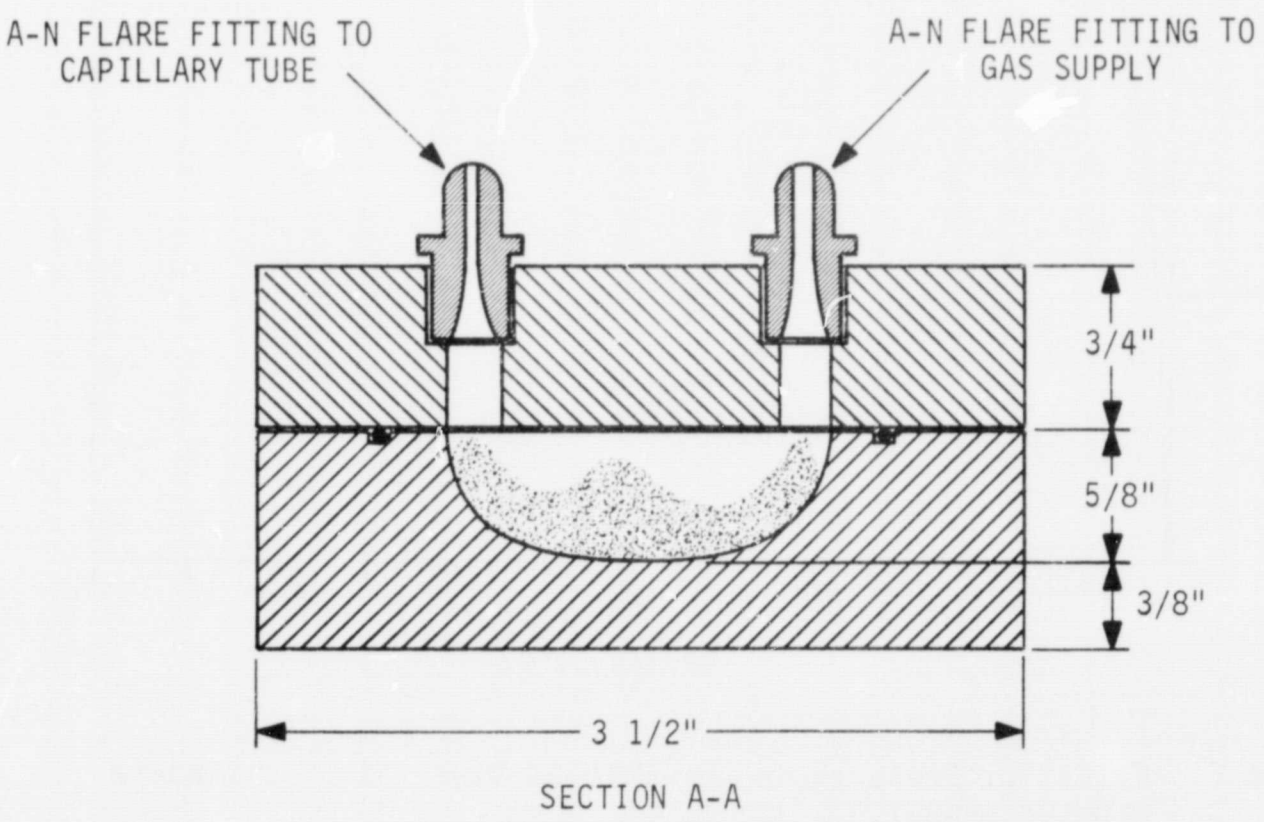

Figure 7. Powder Dispersing Device with U-Bend Geometry.

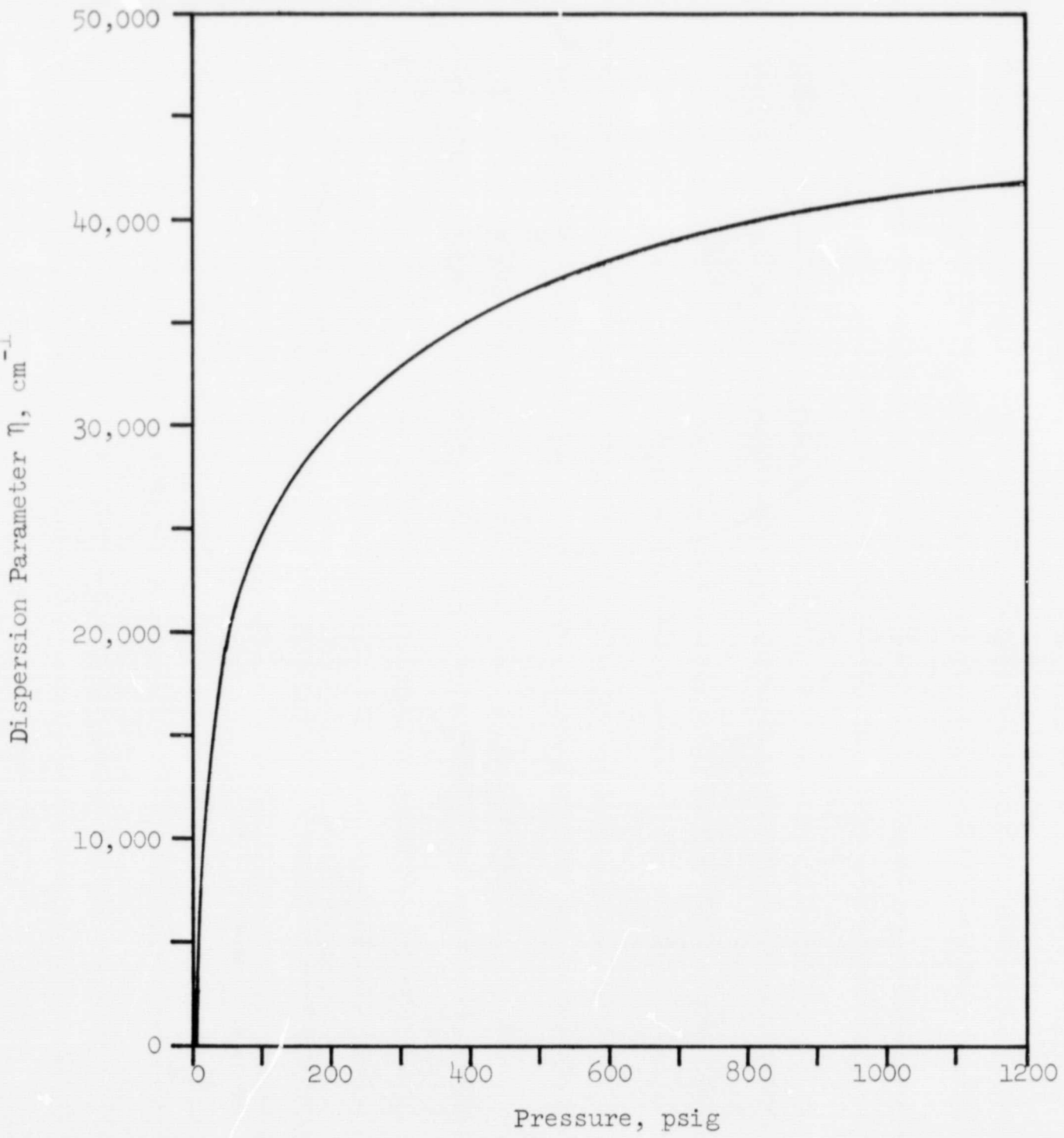

Figure 8. Effect of Pressure on the Initial Dispersion of Linde-A Alumina Powder.

where ρ is the particle density, C_{mo} the initial particle mass concentration, L the beam length, and I_L/I_o the transmittance.

The dispersion parameter is a direct measure of the degree of dispersion of a particle cloud.[22] The results show that the degree of dispersion is affected very strongly by the dispersing pressure. A coating of antistatic agent on the walls of the exit tube of the dispersing device generally decreased the amount of charge developed on dispersion. Consequently, the degree of dispersion was improved. Quantitative measurements are still needed of the influence of antistatic agents on dispersion. Both the effectiveness of agents on initial dispersion and on stability after dispersion are important. It has also been reported[21] that dispersing through an arc discharge improves powder dispersibility as well as cloud stability. The presence of a more nearly unipolar charge distribution appears to account for this effect. Exposure to ionizing radiation has been found to result in no noticeable increase in the initial degree of dispersion but measurably to increase cloud stability.

IV. OPTICAL PROPERTIES OF PARTICLE CLOUDS

A. Extinction coefficients of particle clouds

Radiation passing through a particle cloud has its intensity reduced. The reduction on passage through a differential path length dx may be expressed as

$$dI = -k\, I\, dx \tag{2}$$

where k is the extinction coefficient and I the intensity of the radiant beam. If k is constant in the direction of radiation, Equation 2 gives

$$I_\ell = I_0\, e^{-k\ell} \tag{3}$$

where I_0 and I_ℓ are the initial and final intensities before and after passing through the cloud for a distance of ℓ.

This relationship was known as the Bouguer-Lambert Law for monochromatic radiation. For a radiant beam of multiple wavelengths, the relationship may be expressed by

$$I_\ell = \int_0^\infty I_{\lambda 0}\, e^{-k_\lambda \ell}\, d\lambda \tag{4}$$

where $I_{\lambda 0}$ and k_λ are the initial intensity of the radiant beam and the extinction coefficient at wavelength λ, respectively. If k_λ is independent of wavelength, which is nearly the case for particle clouds in many applications,[24] Equation 4 becomes

$$I_\ell = e^{-k\ell} \int_0^\infty I_{\lambda 0}\, d\lambda = I_0\, e^{-k\ell} \tag{5}$$

which is the same as Equation 3. The extinction coefficient k may be considered as just a proportionality constant in Equation 2 for a certain radiant energy beam which may or may not be monochromatic. Rearranging Equation 5 gives

$$k = -\frac{1}{\ell} \ln \frac{I_\ell}{I_0} \tag{6}$$

where I_ℓ/I_0 is the transmissivity of transmittance of the particle cloud with a thickness ℓ.

The extinction of electromagnetic radiation by small particles in gases is of primary interest in the process of radiant heat transfer to particle clouds. Extinction is generally considered to include absorption and scattering both by particles and the gas if the latter is not transparent. A portion of the radiant energy is removed by the particle cloud and converted into heat; it is called absorption. The combination of reflection, refraction, and diffraction is called scattering. Sometimes the diffracted light deviates only slightly from the original path[25] and a portion of it still may be received by the light-measuring device unless the device is placed at a great distance.[26] If the radii of the particles are larger than the wavelength of the radiation,[27] the diffracted radiation can be treated as transmitted radiation in radiant heat transfer problems. Caution must be exercised, however, if the extinction measurement is used for size distribution measurement.

Since a large portion of the scattered radiation travels in the forward direction and part of it can reach the light-measuring device, the radiation

received and detected by the device includes not only the directly transmitted radiation but also part of the forward scattered radiation. Since, in this study, radiant heat transfer is of the major interest, all the radiation passing through the particle cloud is considered as transmitted radiation. The portion lost during the process is considered to be extincted; it includes the portion absorbed by the cloud and the portion scattered by the cloud and not detected by the light-measuring device.

Figure 9 is a diagramatic representation showing the experimental arrangement and the dimensions of the test apparatus. Smoothed data for I_ℓ/I_0 were used in Equation 6 to calculate the extinction coefficient. Carbon black particle clouds apparently extincted more radiation than Linde-B clouds of the same volume concentration. Particles of both materials were examined with the electron microscope. Both materials were still agglomerated to some degree even though various methods of dispersion were tried. Sizes of single particles were estimated from examinations of the better dispersions. Carbon black particles were judged to be more or less monosized and to have a mean diameter about 0.03 micron. Linde-B particles had a wide size distribution with most of them being below 0.1 micron in diameter but a few big particles were noticed in the samples examined. The reflectivity of alumina is higher than that of carbon black. Particle size and reflectivity may explain why carbon black clouds have higher extinction coefficients than Linde-B clouds of the same volume concentration. Figure 10 presents measured results; from it the concentration of particles needed to achieve a desired extinction value may be estimated. It is important to note that the dispersion efficiency of the cloud generating system, the time between

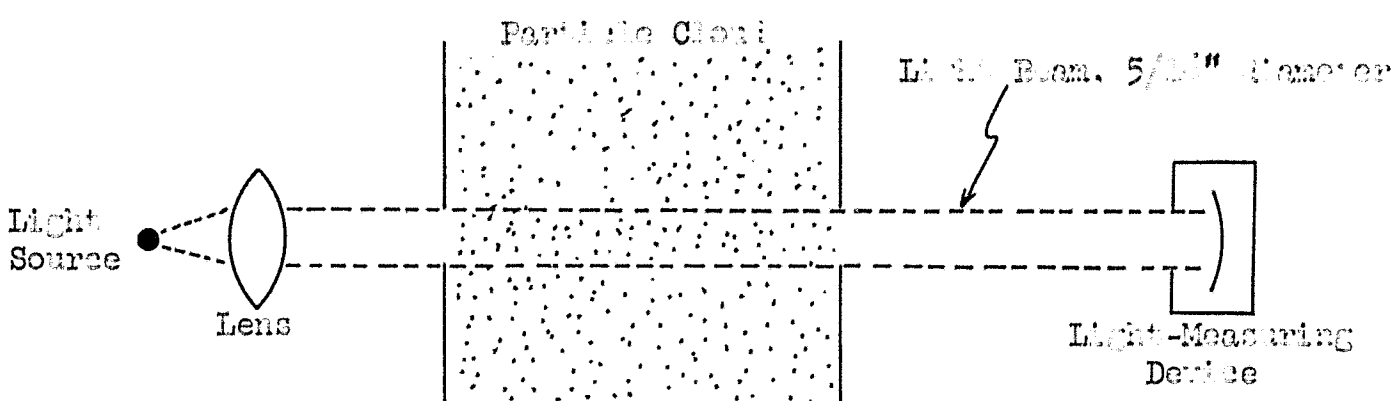

Figure 9. Schematic Diagram of the Arrangement for Extinction Coefficient Measurement.

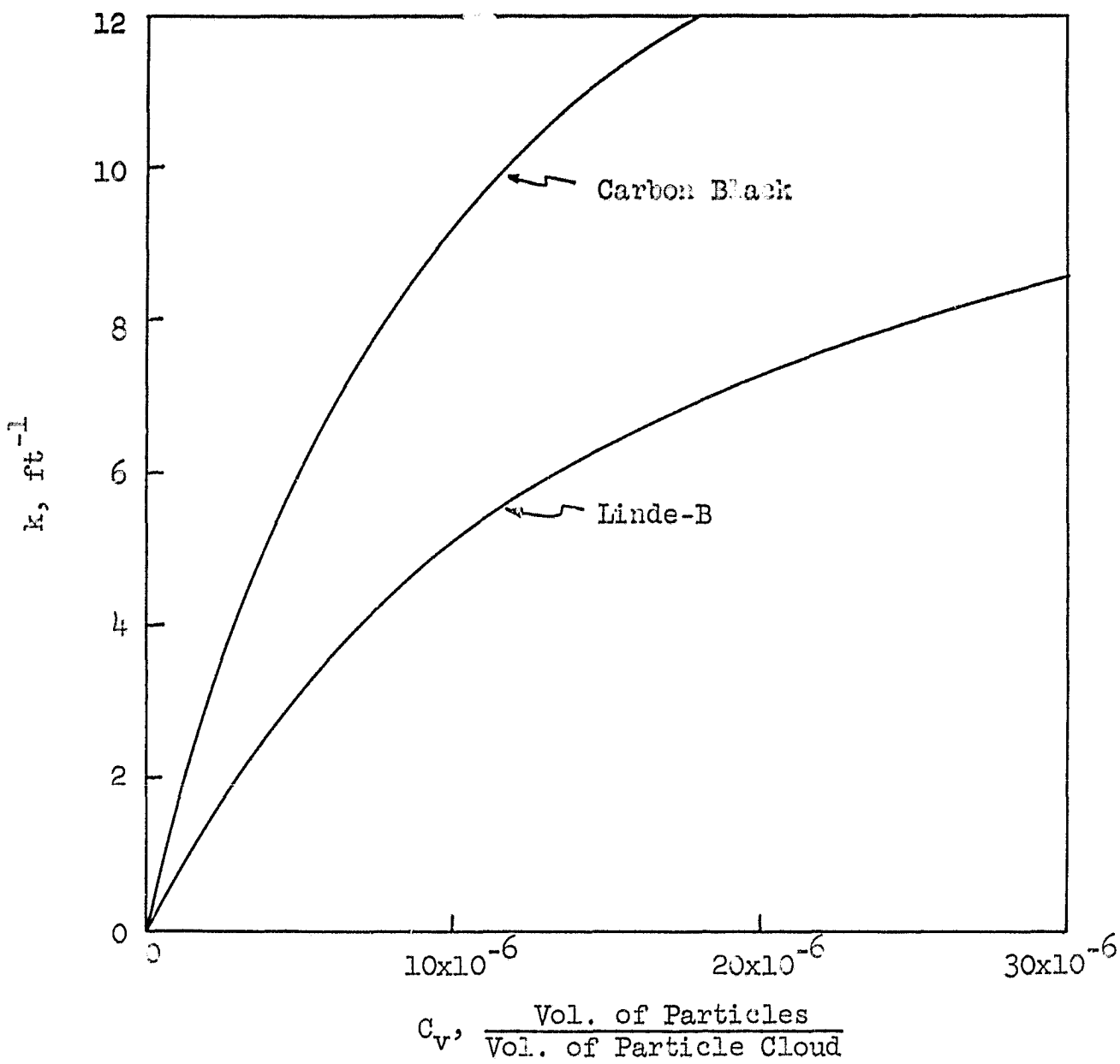

Figure 10. Extinction Coefficient of Carbon Black and Linde-B Particle Clouds Calculated from Measured Transmission Data.

generation of the clouds and the extinction measurement, and the turbulence condition are all important factors to the extinction property. The initial conditions and the coagulation rate must be considered when the required quantity of powder is to be calculated for many applications. A comparison can be made among various clouds only when all the conditions are identical.

B. Transmissivities of particle clouds

Effective dispersion of particles in a gaseous media is a problem of fundamental importance to the measurement of particle cloud transmissivity. It is meaningless to report transmissivities for any kind of powder unless the degree of dispersion is described. A well-dispersed particle cloud has a much lower transmissivity than one having extensive agglomerates. The purpose of the measurements given in this section is to furnish information for estimating the amount of carbon black needed to constitute a particle cloud having a desired transmissivity and also to check the dependence upon the wavelength of the radiation.

Agglomerates in particle clouds arise from the incomplete separation of powders initially into discrete particles and from particle coagulation after dispersion. The degree of dispersion depends on the nature of the powdered material and the effectiveness of the particle-cloud generating mechanism. Particles have mutual attraction mainly because of van der Waals and electrostatic forces; interfacial adhesion is also caused by surface film and adsorbed components. Obvious means for improving dispersion are to treat powdered materials so as to remove surface contaminants and to include additives for minimizing electrostatic effects. Another, of course,

is to devise methods that produce a severe shearing action across small agglomerates, thus effecting better separation of them.

While there are many different types of particle cloud generators, some of which are described previously, much improvement in the resulting suspensions is still desirable, particularly for submicron particles. In this study it was essential that agglomeration be reduced to a minimum and that particle clouds be of invariant concentration. The experimental device utilized was of the vibration type in which a gas-particle mixture is caused to expand suddenly through a small, sharp-edged orifice.[28] Rapid gas expansion at the orifice creates intense shear across agglomerates, breaking them apart. Details of this device have been described in Section III.

Clouds of carbon particles (Spheron 6, Cabot Corporation, Boston, Massachusetts) were produced and their degree of dispersion was deduced from micrographs. The particles were collected with a Goetz, model E, spectrometer (Zimney Corporation, Monrovia, California) and a Numinco, model MIC-501, thermal precipitator (Numinco, Monroeville, Pennsylvania). While these sampling instruments appeared to be adequate for the present studies, it is to be noted that the indicated degree of dispersion is highly dependent on the collection procedure, the location of sampling equipment, and the method of examination. Caution must be exercised in deducing particle and agglomerate sizes from such suspension deposits. For this electron micrographs are required.

The Goetz aerosol spectrometer is a device that affords essentially quantitative collection and size classification of air-borne particles. Its principle of operation is based on the application of intensive centrifugal

forces to a continuous, laminar-flowing stream of the cloud or aerosol. The device is constructed with two identical helical channels on a conical rotor such that, when the rotor is turning at a high rate of speed, particles passing through the channels are deposited according to size along the outer surface of the helical channels. The covering surface is formed by paper, plastic, or a thin metal sheet wrapped around the rotor which may be removed for examination of the collected particles. While the instrument is capable of fractionating small particles, the submicron carbon particles employed here were not separated according to size. At a rotor speeed of 12,000 rpm, however, a suitably dilute deposit for microscopic study was obtained. The collection efficiency was not high as determined by passing the exhaust gas through a millipore filter (Type GS, Millipore Filter Corporation, Bedford, Massachusetts). The low collection efficiency was a further indication that the dispersion was very good. Many particles, including agglomerates, were less than 0.2 micron in diameter. A micrograph of the particles collected by the spectrometer is given in Figure 11; the larger agglomerates are well represented.

Particles not collected by the Goetz aerosol spectrometer were collected by thermal precipitation and the deposits were photographed. Figure 12 is one of the micrographs of such a deposit. As shown, the agglomerates still consist of quite a few particles but the total size of the agglomerates is quite small.

The concentration of the cloud produced was fairly constant after adjustment of the hole sizes in the orifice plate and the size of the dispersion nozzle. It remained difficult to maintain a desired concentration

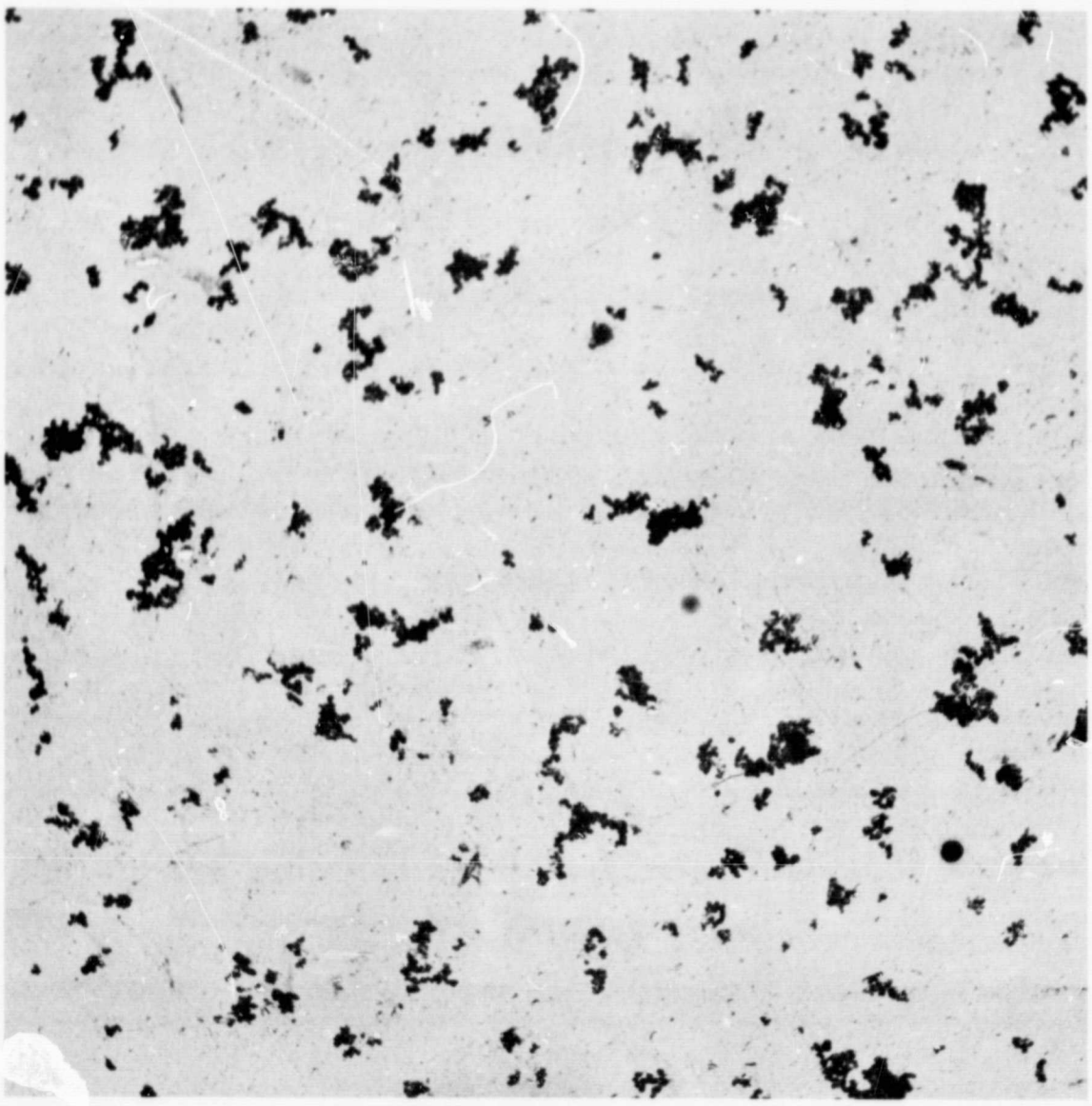

Figure 11. Carbon Black Particles Collected by Goetz Aerosol Spectrometer

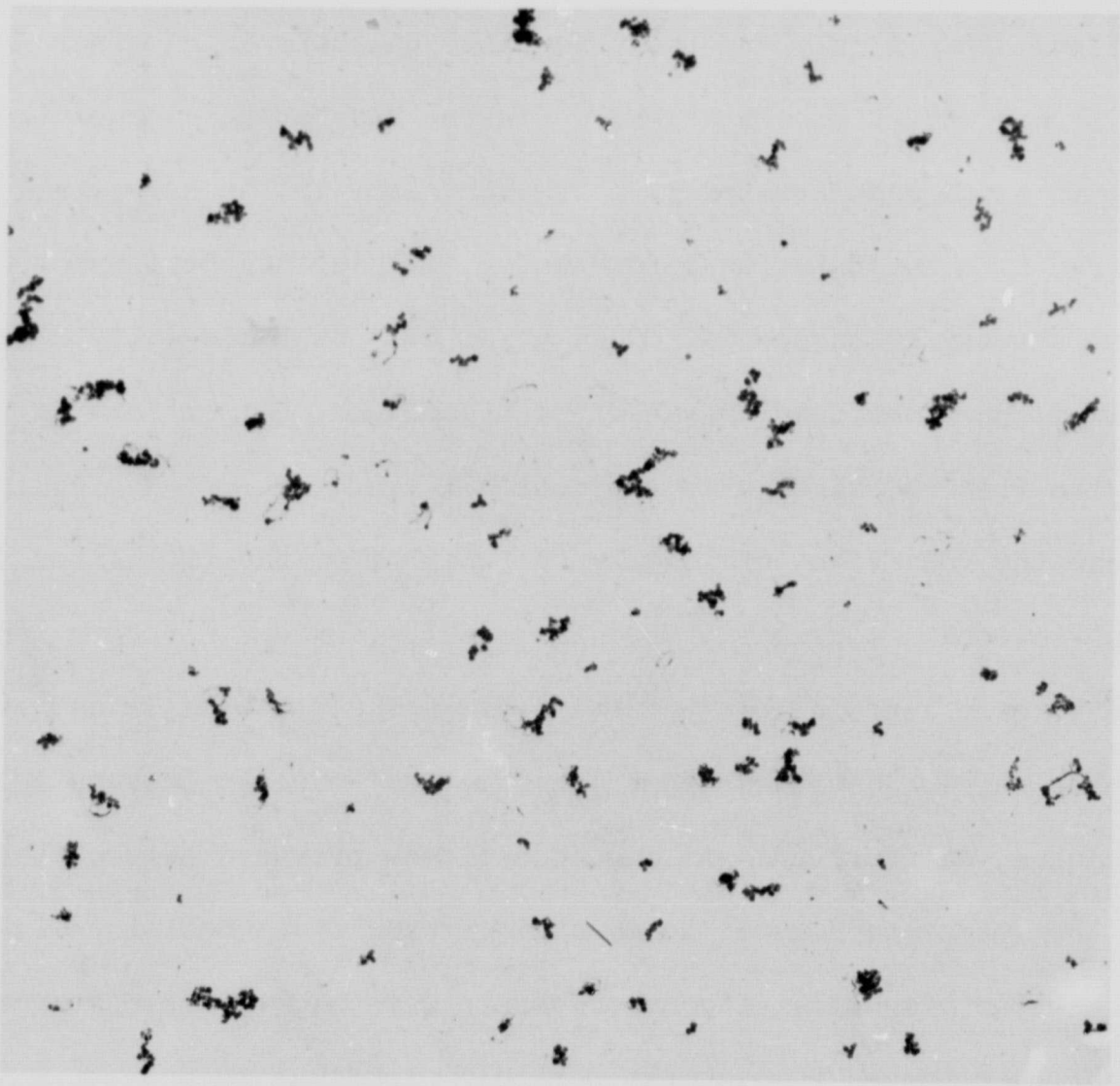

Figure 12. Carbon Black Particles Leaving the Goetz Aerosol Spectrometer and Collected by Thermal Precipitator.

for an extended period to allow a large sample to be collected. Usually, sampling several hundred liters of cloud was required to give about one gram of carbon black deposit. A large surge tank was constructed to solve this problem. It not only smoothed the small pulsations in powder discharge from the feeder but it also aided in measuring the particle concentration. The particle cloud was directed from the generator to the surge tank and was then stirred by a built-in fan before being sent to the spectrophotometer for transmissivity measurements. Once a reliable transmissivity measurement was obtained, particle feeding was discontinued and the contents of the chamber were filtered through an extraction filter. The powder collected was weighed and the result was divided by the chamber volume (246 liters) to give the weight-to-volume concentration. The results, except for very dense concentrations, were reproducible to within ±10 per cent. The transmissivity measurements were made with a spectrophotometer (Model B, Beckman Instruments, South Pasadena, California). A long channel was provided between the surge tank and the spectrophotometer to maintain steady flow conditions in the region where the transmissivity measurements were made. The distance which the radiant beam passed through the particle cloud was seven centimeters. Results are given in Figure 13.

The results show that the transmissivities of carbon black particle clouds are independent of the wavelength of the radiation within the range measured. Unfortunately, the range of the spectrophotometer was quite narrow. If all the light scattering by the carbon black particles is assumed to be in the forward direction, the results in Figure 13 represent a cloud consisting of particles having a mean volume-surface diameter of 0.6

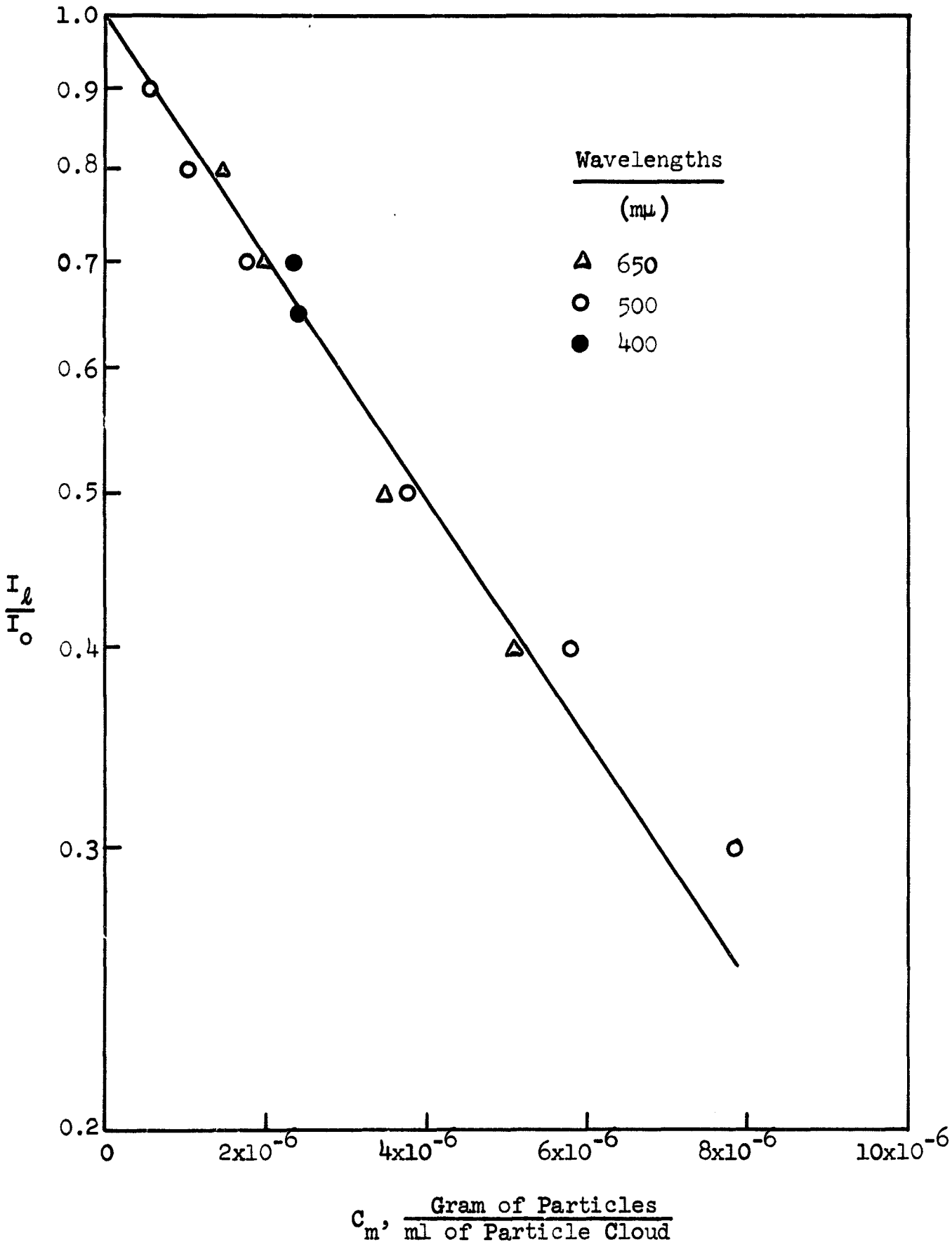

Figure 13. Transmissivity of Carbon Black Particles as a Function of Concentration for Radiation Wavelengths of 400, 500, 650 Millimicrons.

micron. This value is appreciably larger than the particle size indicated by Figures 11 and 12. This is likely due to the carbon black particles reagglomerating inside the surge tank before the transmissivity was measured. Samples coming from the exhaust duct of the spectrophotometer were examined with the electron microscope. These examinations confirmed that the apparent diameter of the particles and particle agglomerates was of the higher order of magnitude given.

At high concentration conditions the results were not as consistent due to the large number of agglomerates created in the particle cloud.

The method described was found to be sufficient to detect the dependence of particle cloud transmissivity on the wavelength of the radiation and to yield reasonably good values for the quantity of carbon black requirea to produce a given transmissivity at the existing dispersion condition.

V. PARTICLE SIZE AND THE RATE OF RADIANT HEAT TRANSFER TO PARTICLE CLOUDS

The transfer of radiant energy to systems consisting of nonluminous particl well-characterized as to particle size and concentration suspended in a gas is described here. The study required the development of an experimental furnace in which a particle cloud could be exposed to intense radiation without having conduction and convection as major heat transfer mechanisms. The furnace also had to be one in which the energy absorbed by the cloud could be determined by enthalpy balances before and after exposure.[26]

A. Apparatus and procedure

Clouds were exposed to thermal radiation while passing through a quartz tube that transmitted to its interior a sizable portion of the radiation falling on it externally. The quartz tube was protected from extraneous heat transfer effects other than radiation by enclosing it first within an evacuated space and then by an outer, annular region that was air-cooled. The surrounding, protective tubes were also quartz. The particle cloud was generated at a constant rate and pre-conditioned to a constant, known temperature. Then, after passing through the radiation, the cloud was cooled calorimetrically to determine the heat absorbed. A filter mechanism removed the suspended particles from the suspending gas--air--and returned them to the cloud generator for re-use. The system was thus designed for continuous operation. Figure 14 is a diagramatic representation of the system showing the arrangement of the principal components.

The generator produced uniform and well-dispersed particle clouds. In it a thin layer of powder was created in the bottom of a pan-like container

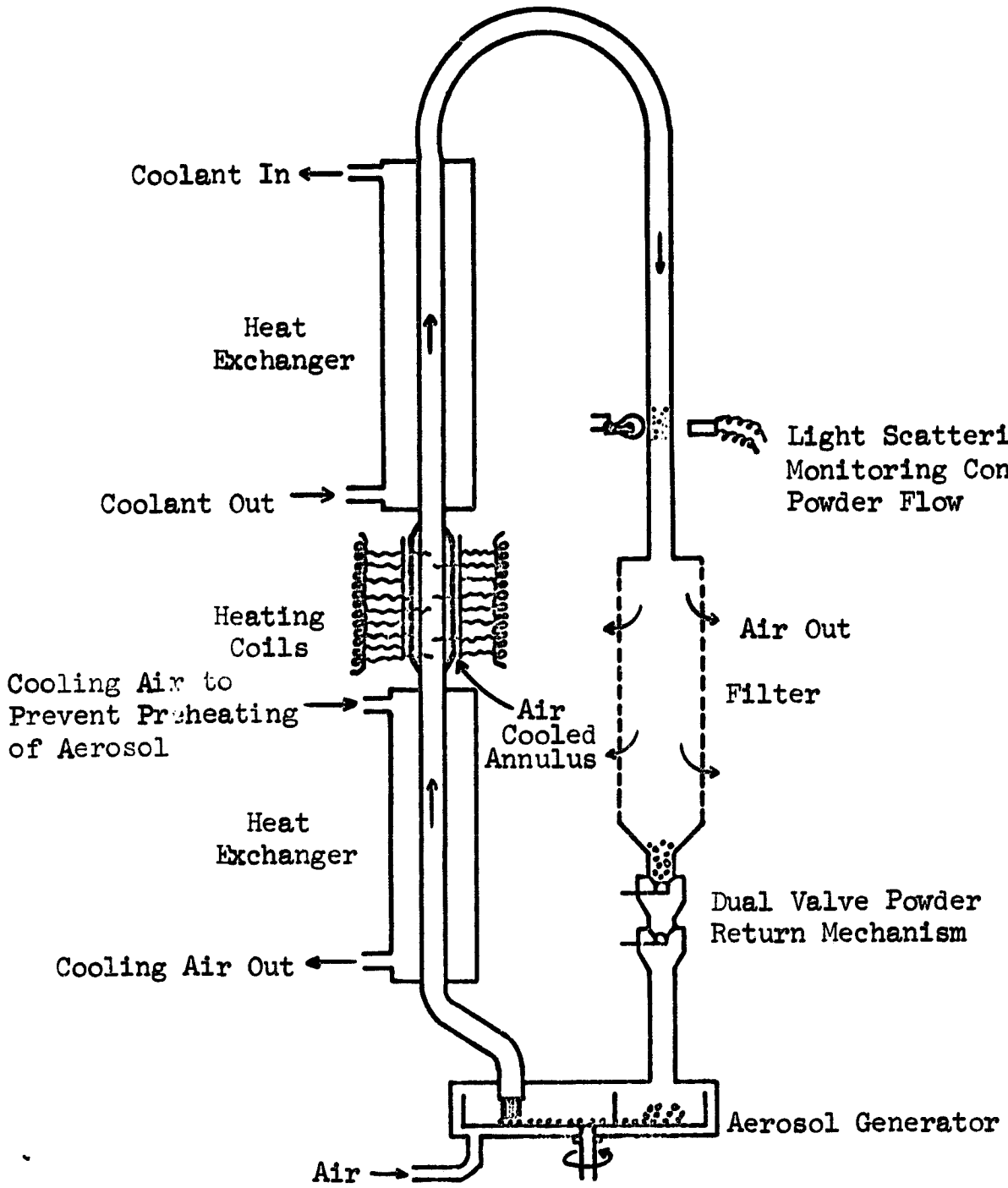

Figure 14. Diagramatic Representation of the Kanthal Wire Furnace and Components.

due to the latter's rotating continuously beneath a retaining partition. This layer was then carried under a pickup nozzle where the powder was entrained in air passing upward. Particle deagglomeration resulted from the shear force generated by the subsequent flow through small passageways. Details of this device have been described in Section III. The newly formed cloud next passed through an air-cooled, constant-temperature chamber to allow the streams from the nozzles to mix thoroughly and to bring the cloud to a known temperature.

The heating elements of the furnace were prepared from Kanthal wire, (Kanthal Company, Stanford, Connecticut) and supported to grooves spiraling inside the inner walls of a refractory brick enclosure. Two heating elements were employed, one for the upper and the other for the lower half of the furnace. Each was composed of 30 feet of 0.333-ohm per foot wire wound into a 0.375-inch diameter coil. The coil helices were spaced closer to one another at the ends of the furnace to compensate for heat losses there and to give a more nearly uniform temperature over the heated area. Further, the temperatures of the two coils were controlled independently. This arrangement reduced the temperature differences arising from convective currents within the furnace. The maximum operating temperature was 2300°F; the actual operating temperature was held constant at 2280°F.

The quartz tube through which the cloud passed had an inside diameter of 0.5 inch and a wall thickness of 0.04 inch. It was directly irradiated for a length of 12.5 inches. The two other surrounding tubes had 1.0-inch and 2.1-inch inside diameters. The middle tube was sealed to the inner conduit, and the annular enclosure thus formed was evacuated to a pressure of less

than 0.01 mm of mercury to reduce heat transfer by conduction and convection. Air was circulated in the outer annulus to protect the outer quartz tubes from the high furnace temperature. By this arrangement relatively little heat was transferred other than by radiation to the cloud. Some energy was transferred, of course, where the vacuum jacket joined the conduit, and some energy was absorbed by the quartz tube itself. The magnitude of these heat inputs was established by experiments with particle-free air.

Measurements of the inlet and exit temperature of the cooling media and the cloud exit temperature were made with copper-constantan thermocouples. These temperatures together with the mass flow rates of the streams permitted making a heat balance for each and, from these, evaluating the energy gained by the cloud while in the furnace. The inlet temperature of the cloud itself was also measured by a thermocouple installed 6.5 inches from the entrance to the heat exchange section. By assuming a linear temperature gradient for the cloud along the heat exchanger, the particle cloud temperature could be calculated just at the entrance. A supplementary heat balance on the particle cloud system exclusively was then possible. A radiation shield at the entrance to the exchanger reduced downstream radiation.

The cloud was monitored for consistency of concentration by light transmission measurements. Absolute measurement of particle concentration was made by direct sampling. The procedure was to close off the normal path around the heat transfer circuit and to open simultaneously a sample tube leading to a filter. The concentration was checked frequently and was rarely found to vary more than ±5 per cent during a test.

Finally the cloud entered the sleeve filter where the particles were

separated from the air. The filter medium was 4 inches in diameter and had 22 inches of useful length. The filter was traversed continuously outside by a ring of air jets that dislodged the filtered material and thus made possible continuous operation.

B. Particle materials

Ferrous sulfide was chosen as a first material because it was black and easy to disperse. A technical grade from the Baker Chemical Company, Phillipsburg, New Jersey, was used. Preparation consisted of first reducing it to minus 144 U.S. Standard Sieve size with a mortar and pestle. The product was then ball-milled for one-hour intervals and screened until it passed an 88-micron sieve. Thereafter, sieving was continued to yield 88 to 53, 53 to 44, and less than 44 micron diameter fractions. Sieves of the Buckbee Mears Co., St. Paul, Minn., were then employed to separate the less than 44 micron material into 44 to 30, 30 to 20, and less than 20 micron diameter fractions.

Reagent-grade cupric oxide obtained from the Baker Chemical Company was also employed. Particle size fractions were prepared by the same procedure as was the ferrous sulfide.

C. Radiant heat flux determination

The radiant energy penetrating into the quartz enclosure and available for heating the particle cloud was needed to determine the absorption efficiency of the cloud. The inner quartz conduit was coated with a highly absorbing material, lamp black mixed into a small amount of epoxy resin (Resinweld Plastic Alloy, H. B. Fullter Co., St. Paul, Minn.). Then

experiments were conducted in which water was forced upward through the conduit to remove the heat absorbed thereon. The contribution from radiation had to be separated from the total result, however, because the conduit received heat by conduction and convection as well as radiation. This was accomplished by performing additional experiments with the inner wall of the conduit being made as reflective as possible.

A gold coating baked onto the inner conduit wall was employed for this purpose. A fluid suspension of gold particles supplied by B. F. Drakenfeld and Co., Inc., Washington, Pa., was employed. Baking a deposit of this suspension to a temperature (1060°F) near the melting point of gold volatilized the suspending fluids and formed a smooth, reflective, metallic surface. The difference, then, between the results, when adjusted for the actual absorptivities of the two coatings, was the heat transferred by radiation to the particle cloud conduit.

The heat flux determinations were made with water as the coolant rather than air to permit better control of the temperature of the system. For a pair of experiments, one with each type of coating, the flow rates had to be identical since both convective and conductive heat transfer were functions of the coolant flow rate. The absorptivity of the blackened surface was taken as 0.95 and the absorptivity of the gold surface to be 0.03.

Heat fluxes were determined for a series of furnace temperatures. The results conformed very closely to the Stefan-Boltzmann law, i.e., the radiant energy was proportional to the fourth power of the absolute temperature. This was taken to indicate the general reliability of the procedure. The radiant heat flux at the operating temperature of 2280°F was 17,600 Btu/hr-ft^2.

D. Determination of heat transfer rates

A thermocouple at the upper end of the heat exchanger sensed the temperature of the cloud there, and a different thermocouple indicated the temperature rise of the cooling air as it passed through the heat exchanger. These temperatures and flow rates permit establishing an energy balance. The balance involved the sum of the heat exchanged by the air, the particles, and the heat exchanger coolant. The reference temperature was taken to be the temperature of the particle cloud at the entrance to the furnace. This temperature was quite constant; its variation was not more than a few tenths of a degree during a test.

The total enthalpy gain per unit time by air without the presence of particles may be expressed as

$$\Delta H_{ta} = \Delta H_a + \Delta H_{co} \tag{7}$$

where ΔH_{co} is the enthalpy gain per unit time by the coolant in the heat exchanger without particles in the system and ΔH_a the enthalpy not absorbed by the coolant and carried away by the air in the conduit per unit time after passing through the heat-exchange section.

The total enthalpy gain per unit time by a particle cloud can be expressed by

$$\Delta H_{tp} = \Delta H_p + \Delta H_{cp} \tag{8}$$

where ΔH_{cp} is the enthalpy gain per unit time by the coolant in the heat exchanger with particles in the system and ΔH_p the enthalpy not absorbed by

the coolant and carried away by the particle cloud in the conduit per unit time after passing through the heat exchanging section.

Air does not absorb radiation under the experimental conditions. Therefore, ΔH_{ta} can be considered to be the enthalpy gain per unit time for all cases except those in which radiation was absorbed by particles. When operating conditions were maintained the same, the enthalpy gain per unit time attributable to radiation absorbed by particles can therefore be obtained from

$$\Delta H_r = \Delta H_{tp} - \Delta H_{ta} \tag{9}$$

The temperature of air or of a particle cloud at the exit of the furnace was determined by thermocouples installed in the system. This temperature was employed to check the enthalpy gain evaluated by the method stated above and also to examine whether or not the system was operating steadily.

E. Calculation of particle cross-sectional area

The particle cross-sectional area per unit volume of cloud, A_p, can be calculated from the particle size distribution and the particle concentration. The appropriate expression is

$$A_p = \frac{3C_v}{2} \cdot \frac{\sum_i n_i \, d_i^{\,2}}{\sum_i n_i \, d_i^{\,3}} = \frac{3C_v}{2} \left(\frac{1}{d_{vs}}\right) \tag{10}$$

or

$$A_p = \frac{3C_m}{2\rho} \frac{\sum_i n_i d_i^2}{\sum_i n_i d_i^3} = \frac{3C_m}{2\rho} \left(\frac{1}{d_{vs}}\right) \qquad (11)$$

where C_v and C_m are the volume and mass concentrations, respectively; n_i the number of particles counted with a diameter of d_i; and ρ the particle density. The mean volume-surface diameter, d_{vs}, should be used when the particle cross-sectional area or the surface area of a given volume of particles is concerned.[29]

F. Theoretical predictions

Particles suspended in air reduce the intensity of a radiant beam in the direction of propagation of the beam just as do absorbing gases. The reduction along the direction of travel is expressed by Beer's law

$$I_S = I_0 e^{-kS} \qquad (12)$$

where I_S is the intensity of the radiation after a beam of intensity I_0 penetrates a distance S into the particle cloud, and k the extinction coefficient.

Equation 12 can also be expressed in terms of the true projected area of particles per unit volume of cloud, A_p, as

$$I_S = I_0 e^{-EA_pS} \qquad (13)$$

where E is the area efficiency factor for particles.

If the gaseous medium is transparent, the reduction of the intensity of a radiant beam is due wholly to absorption and scattering by the particles. Most of the scattered radiation travels in the forward direction, and all of the scattered radiation is subject to further absorption and scattering by the particles which it encounters. Therefore, when radiant heat transfer is of major consideration, the radiant energy actually removed by particles is only that absorbed by particles during the transfer process. The radiation scattered by particles may be altered from one path into others, but it does not convert into thermal energy until it is absorbed by particles. Based on probability considerations, the amount of energy absorbed from the beam by a cloud can be approximated by

$$I_a = I_o \left[1 - e^{-A_p S}\right] \tag{14}$$

Equation 14 is applicable when the particles are black or nearly black.

The conduit through which the particle clouds passed was small in comparison to the radiation enclosure. The intensity of radiation falling on the conduit was therefore essentially constant. The rate of radiant heat transfer to the particle cloud, q_a, can be written as

$$q_a = q_o \left[1 - e^{-\frac{3\bar{S}}{2}\left(\frac{C_m}{\rho d_{vs}}\right)}\right] \tag{15}$$

where $\bar{S}$ is the mean beam length. When the value of $C_m/(\rho d_{vs})$ is small, Equation 15 can be expressed as

$$q_a = \frac{3}{2} q_o \overline{S} \left(\frac{C_m}{\rho d_{vs}}\right) \qquad (16)$$

where q_o is the radiant heat flux passing through the conduit wall; it was 2400 Btu/hr in these experiments.

Methods for estimating the mean beam length for certain geometries are available in the literature.[30,31] The rate of radiant heat transfer can be readily evaluated by Equation 15 once the mean beam length is available. Unfortunately, the mean beam length for this experiment was too complex to be obtained theoretically. It was determined experimentally.

G. Discussion of results

Three or more independent tests were made for each condition and an average result was calculated. Figure 15 shows the rate of radiant heat transfer to particle clouds of constant mass concentration as a function of the mean volume-surface particle diameter. These diameters were calculated from microscopic measurements of many particles.

The smoothed experimental data are plotted as a function of $C_m/(\rho d_{vs})$ in Figure 16. When the value of $C_m/(\rho d_{vs})$ was small, the rate of transfer followed a straight line as predicted by Equation 16. The value of $\overline{S}$ as obtained from the slope of this straight line was found to be 0.053 ft. Inserting this value for $\overline{S}$ into Equation 15 then permitted the rate of radiant heat transfer to the particle cloud to be evaluated for larger values of $C_m/(\rho d_{vs})$.

The results show that Equation 15 agrees very well with the experimental data as presented in both Figures 15 and 16. Equation 16 agrees well only when the values of $C_m/(\rho d_{vs})$ are small as indicated by Figure 16.

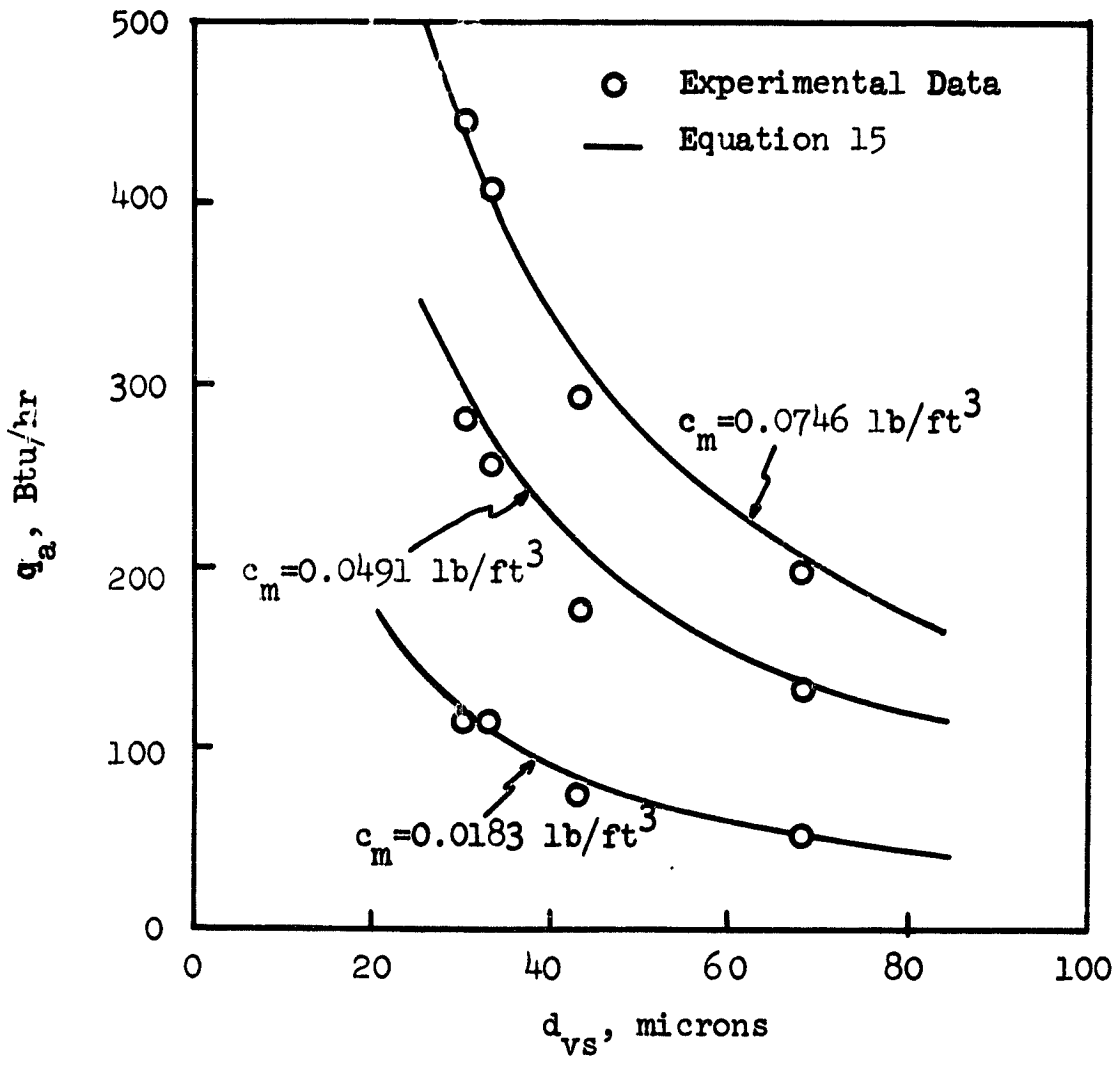

Figure 15. Rate of Radiant Heat Transfer of Ferrous Sulfide Particle Clouds as a Function of Particle Size.

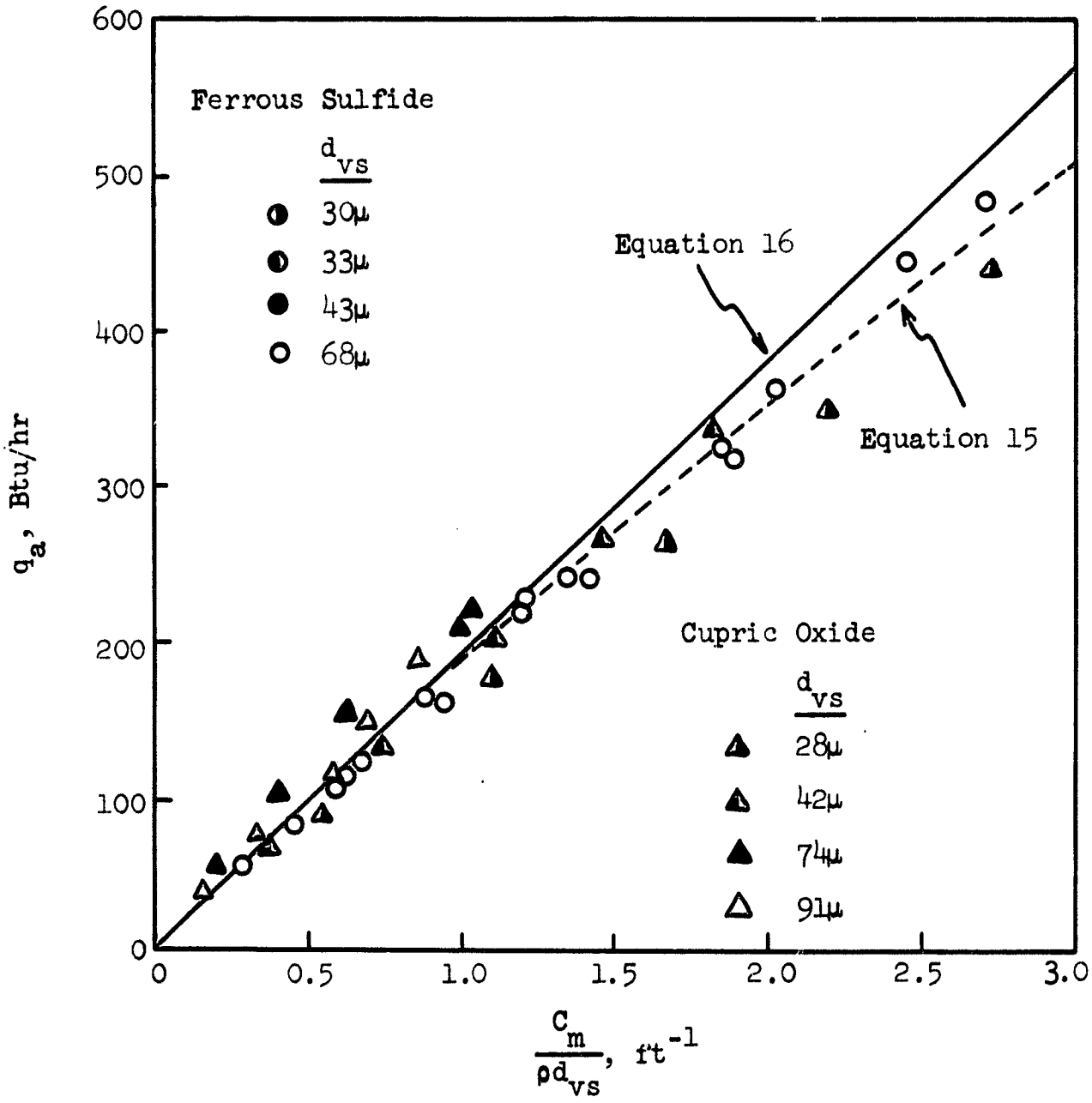

Figure 16. Rate of Radiant Heat Transfer to Ferrous Sulfide and Cupric Oxide Particle Clouds.

The results of this study show that the absorption coefficient of black or nearly black particle clouds can be calculated from particle size distribution and concentration data. The rate of radiant heat transfer to particle clouds can then be estimated theoretically when proper consideration is given to the geometry of the system.

VI. CONSIDERATION OF PARTICLE REFLECTIVITY IN RADIANT HEAT TRANSFER PROBLEMS

The rate of absorption of radiation by black particles suspended in gas is directly related to the optical density of the cloud, $k\ell$, where k is the extinction coefficient and ℓ the thickness of the cloud. The rate of absorption is linearly proportional to the values of optical density when they are small. Absorption follows the relationship $(1 - e^{-k\ell})$ as the optical density increases; it is unity when the optical density is infinity. In engineering problems, nearly black particles can be treated as black particles but the calculated rate should be multiplied by the absorption coefficient of the particle material. The absorption of the reflected radiation is small and negligible in this case. The problem becomes very complicated when materials are reflective in nature such as are some reflective metal particles and small droplets. Since analytical solutions are not available, a general discussion of absorption characteristics is given first.

A. Absorption characteristics of reflective particle clouds

Scattered radiation is not considered to be an important factor for black particle systems because there is no reflection, and the refracted and defracted radiation is usually concentrated in a small solid angle in the forward direction which means it needs not be separated from the transmitted radiation. When a radiant beam penetrates a cloud of reflective particles, however, the scattered radiation (including reflection, refraction, and defraction) plays an important roll in radiant heat transfer problems.

Assume a parallel radiant beam of uniform intensity is incident on a cloud of reflective particles as shown in Figure 17. The system under discussion here is the cylinder of length L and diameter D, which represents the path of the primary beam in the cloud. The term q_o is the radiant energy incident on one end of the cylinder and q_t the transmitted energy from the other end. The sum of the radiant energy scattered from the cylindrical wall is designated as q_s; the portion reflected back from the end as q_r; and the portion absorbed by the cloud as q_a.

The energy balance equation is expressed by

$$q_o = q_a + q_t + q_r + q_s \tag{17}$$

All the terms in Equation 17 are functions of mass concentration C_m; particle density ρ; particle size distribution or mean volume-surface diameter d_{vs}; thickness of the particle cloud L; and the particle reflectivity ρ_p, absorptivity α, and emissivity ϵ.

The rate of radiant absorption for black particles may be approximately expressed by

$$q_{ab} = q_o \left\{1 - \exp\left[- \frac{3L}{2}\left(\frac{C_m}{\rho d_{vs}}\right)\right]\right\} \tag{18}$$

as derived in Section V. For reflective particles, the radiant energy absorbed by the particle cloud q_a includes the portion absorbed from the original radiation q_{ao} and from the scattered radiation q_{as}, the result being expressed by

$$q_a = q_{ao} + q_{as} \tag{19}$$

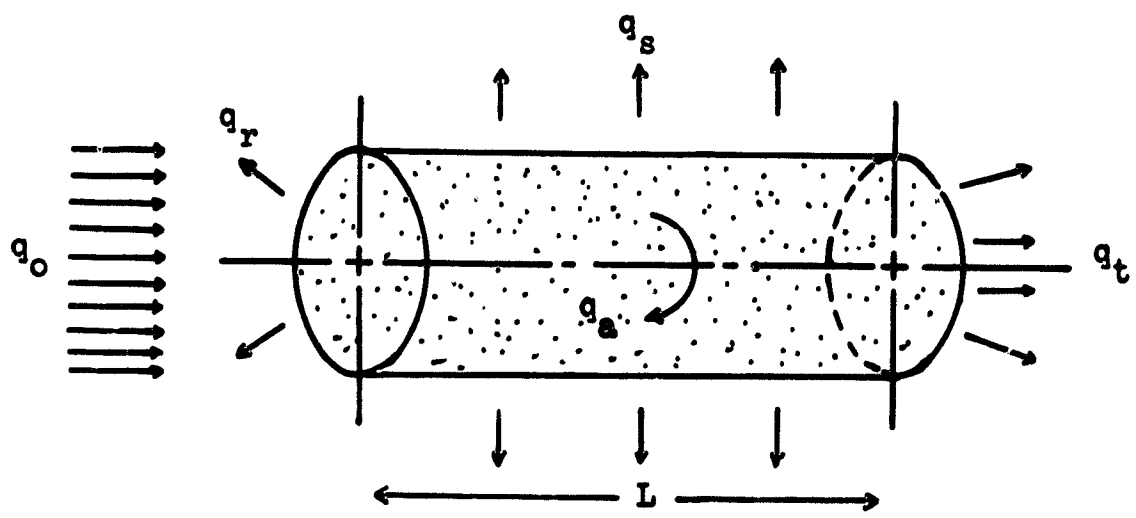

Figure 17. Diagram of a Parallel Beam Penetrating into a Cloud of Reflecting Particles.

where q_{ao} can be approximated by

$$q_{ao} = \alpha\, q_o \left\{1 - \exp\left[-\frac{3L}{2}\left(\frac{C_m}{\rho d_{vs}}\right)\right]\right\} \qquad (20)$$

The absorption rate relating to q_{as} is a strong function of the particle reflectivity ρ_ρ but it also depends on other properties of the cloud. The quantity q_{ao} is a function of $LC_m/\rho d_{vs}$ as shown in Equation 20, but q_{as} depends on L and $C_m/\rho d_{vs}$ separately instead of just the product of them. If the product of L and $C_m/\rho d_{vs}$ is kept constant, the quantity q_{as} would approach zero as L approaches zero. The value of q_{as} will gradually increase as L increases until it reaches a maximum value and then it will decrease as L further increases. This can be seen clearly if it is assumed that the particles are packed into a thin cake and stop all the radiation. The value of q_a in this case is about αq_o for fine particles, and q_{as} is nearly zero if the surface of the cake is considered to be smooth relative to the wavelength of the radiation. When the powder is dispersed in the direction of the radiant beam, particles begin to absorb additional radiation from the scattering of other particles. The concentration of particles decreases as the depth of the particle cloud increases. And last, a great portion of the scattered radiation is lost to the side and the portion which is absorbed by widely separated particles becomes less and less as L is further increased.

The cross-sectional area A of the parallel radiant beam does not affect the absorption efficiency γ which is the ratio of q_a/q_o for black particles. However, γ is affected by A for reflective particles. The quantities of q_{as} and q_s are functions of A. The quantity q_{as} increases and q_s decreases as A

increases. These phenomena arise because the mean beam length for the scattered radiation is greater for a beam with a greater cross-sectional area than for one with a smaller area.

B. Estimation of the rate of radiant heat transfer

The general characteristics of a cloud of reflective particles were discussed in the preceding section. That information may be employed in estimating radiant heat transfer rates in practical engineering problems. The following is an example of such a problem.

First, it is assumed that a solution for a cloud of black particles is already available. If the mean beam length is known, the rate of absorption for black particles is expressed by

$$q_{ab} = q_o \left(1 - e^{-\bar{S}_o A_p}\right) \tag{21}$$

where q_o is the total radiation input rate, $\bar{S}_o$ the mean beam length of the original radiation (no reflection and refraction in this case), and A_p the total projected area of particles per unit volume of cloud.

A proposed equation for reflective particles is

$$q_{ar} = q_{ao} + q_{a1} + q_{a2} + q_{a3} + \ldots \tag{22}$$

where q_{ao}, q_{a1}, q_{a2}, q_{a3}, . . . are the rates of absorption from the original radiation, for first, second, third, . . ., etc., scattering, respectively. Let $\bar{S}_1$, $\bar{S}_2$, $\bar{S}_3$, . . ., be the mean beam paths of the scattered radiation of the respective scattering steps. Then the rates of absorption can be written

$$q_{ao} = \alpha q_o \left(1-e^{-\bar{S}_o A_p}\right) \tag{23}$$

$$q_{a1} = \alpha \rho_p q_o \left(1-e^{-\bar{S}_o A_p}\right)\left(1-e^{-\bar{S}_1 A_p}\right) \tag{24}$$

$$q_{a2} = \alpha \rho_p^{\,2} q_o \left(1-e^{-\bar{S}_o A_p}\right)\left(1-e^{-\bar{S}_1 A_p}\right)\left(1-e^{-\bar{S}_2 A_p}\right) \tag{25}$$

$$q_{a3} = \alpha \rho_p^{\,3} q_o \left(1-e^{-\bar{S}_o A_p}\right)\left(1-e^{-\bar{S}_1 A_p}\right)\left(1-e^{-\bar{S}_2 A_p}\right)\left(1-e^{-\bar{S}_3 A_p}\right) \tag{26}$$

.

.

.

where α is the absorptivity and ρ_p the reflectivity of the particle materials. Substituting Equations 23, 24, 25, and 26 into 22 gives

$$q_{ar} = \alpha \left[1 + \rho_p\left(1-e^{-\bar{S}_1 A_p}\right) + \rho_p^{\,2}\left(1-e^{-\bar{S}_1 A_p}\right)\left(1-e^{-\bar{S}_2 A_p}\right) + \rho_p^{\,3}\left(1-e^{-\bar{S}_1 A_p}\right)\left(1-e^{-\bar{S}_2 A_p}\right)\left(1-e^{-\bar{S}_3 A_p}\right) + \ldots\right] q_{ab}$$

$$= \alpha_r \, q_{ab} \tag{27}$$

where the coefficient α_r is expressed as

$$\alpha_r = \alpha \left[1 + \rho_p \left(1-e^{-\bar{S}_1 A_p}\right) + \rho_p{}^2 \left(1-e^{-\bar{S}_1 A_p}\right)\left(1-e^{-\bar{S}_2 A_p}\right) \right.$$

$$\left. + \rho_p{}^3 \left(1-e^{-\bar{S}_1 A_p}\right)\left(1-e^{-\bar{S}_2 A_p}\right)\left(1-e^{-\bar{S}_3 A_p}\right) + \ldots \right] \qquad (28)$$

From the nature of the coefficient α_r, it is appropriate to call it the absorptivity of the suspended particles. The absorptivity of the suspended particles is a function of the absorptivity and reflectivity of the particle material, the mean beam lengths of the scattered radiation, and the particle projected area per unit volume. All but the mean beam length of the scattered radiation have been previously discussed.

Mean beam lengths mainly depend on the particle projected area per unit volume and the system geometry. In general, the mean beam length is directly proportional to the size of the system and inversely proportional to the particle projected area per unit volume. When the system is large and the particle concentration is high, the mean beam length depends solely on particle concentration. The mean beam length of the original radiation $\bar{S}_o$ can be estimated from information available in the literature.[30,31] The evaluation of the mean beam lengths of the scattered radiation is very much involved. Their values may be assumed to be one half of $\bar{S}_o$ if $\bar{S}_o A_p$ is small.

Caution must be exercised in evaluating the rate of radiant heat transfer to reflective particle clouds from the equations derived in this section. The analysis given here is more or less phenomenological rather than quantitative. Difficulty is to be expected in evaluating mean beam lengths. The mean beam length defined by Equation 21 may have a different

value from that calculated by integration procedures when the radiant source cannot be represented by a single value q_o. The value of the mean beam length may be assumed to be constant when the particle concentration does not vary greatly.

C. Experimental investigation on reflective particle clouds

Reflective particles usually are metal particles and liquid droplets. Zinc particles were chosen here because of their high reflectivity and the fact that they could be made to have a spherical shape. The cross-sectional area can be accurately calculated from size distribution data. The surface was smoothed and polished by extended circulation about a system. The particles should have the absorptivity and reflectivity for the pure material, mean values for commercial zinc 99.1% pure with polished surfaces being 0.05 and 0.95, respectively. Experimental apparatus and operation procedures are the same as described in Section V.

Gas-suspended small particles of high thermal conductivity flowing through a hot conduit increase the convective heat transfer above that for the gas alone. This correction was neglected in the analysis of Section V because the particles used there were relatively large and had low thermal conductivity. The actual convective heat transfer rate to a cloud of zinc particles must include the additional quantity caused by the presence of particles to the rate for gas alone.

Results relating the Nusselt number to particle loading (the ratio of the mass flow rate of particles to the mass flow rate of gas) as derived from Tien[32] and Farber and Morley[33] are given in Figure 18. Data were available down to a Reynolds number of 13,500, but the aerosol systems in this investigation had a Reynolds number of 10,000. From generalized curves,

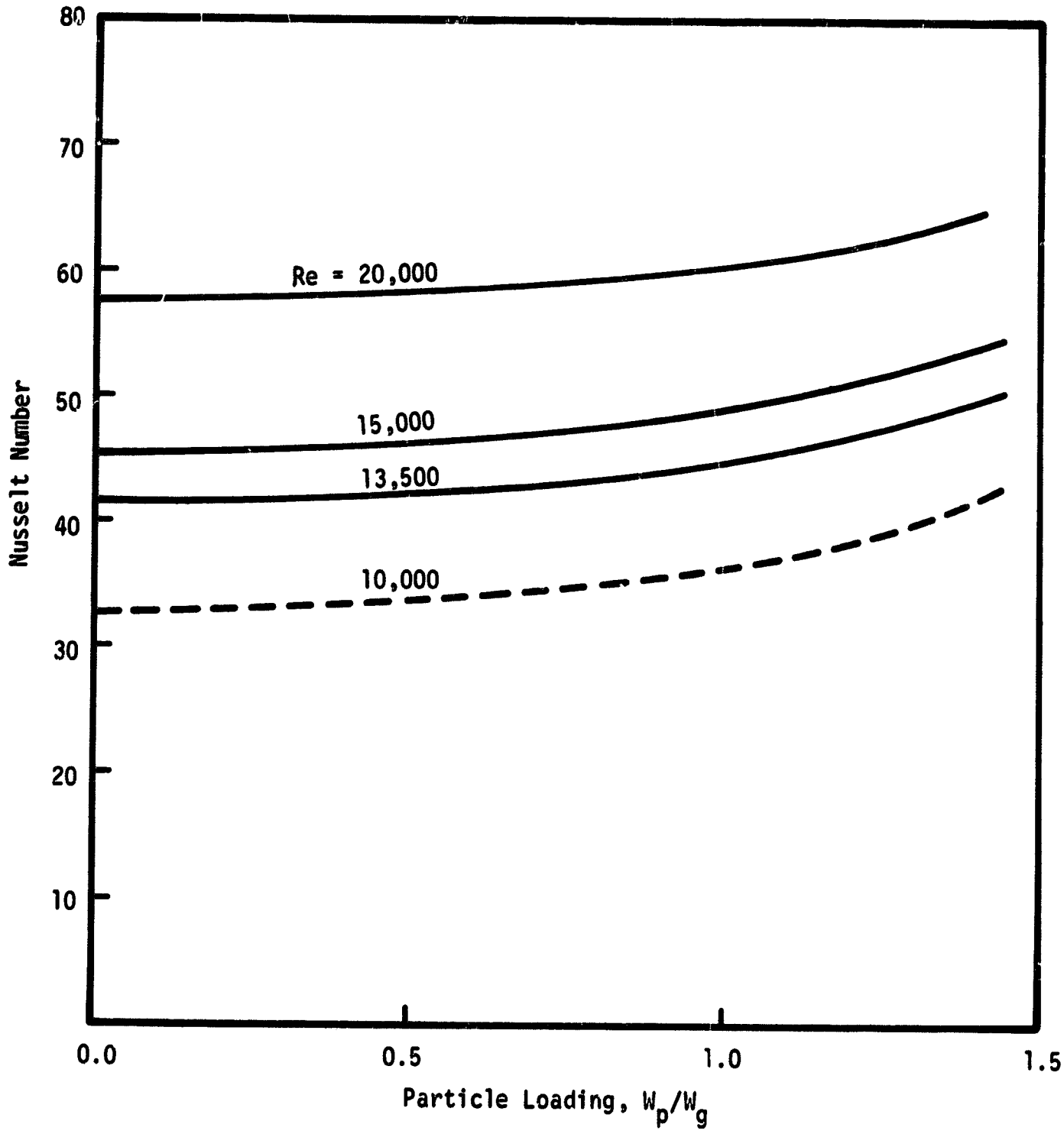

Figure 18. Nusselt Number for Particle-Gas Suspensions for Experimental System.

however, the data could be extrapolated with acceptable accuracy to the required Reynolds number for aerosols with solids-to-gas weight ratios less than 1.5.

The rate of convective heat transfer to particle-free air and to a particle cloud may be described, respectively, by

$$(q_c)_a = h_a A_w (t_w - t_a)_{mean} \tag{29}$$

and

$$(q_c)_p = h_p A_w (t_w - t_p)_{mean} \tag{30}$$

where h is the heat transfer coefficient, t the temperature, and A_w the inside surface area of the conduit. The subscripts a, p, and w indicate a property of air, particle cloud, and wall, respectively. The ratio of these two equations is

$$\frac{(q_c)_p}{(q_c)_a} = \frac{h_p A_w (t_w - t_p)_{mean}}{h_a A_w (t_w - t_a)_{mean}} \tag{31}$$

During heating, t_a was never different from t_p by more than $10^{\circ}F$ and in many cases $5^{\circ}F$. The wall temperature, while not measured, was probably reduced slightly because of the increase in heat transfer. It was assumed that the mean temperatures were very nearly equal and the heat transfer with and without particles was essentially determined by

$$\frac{(q_c)_p}{(q_c)_a} = \frac{h_p}{h_a} \tag{32}$$

The ratio of heat transfer coefficients was numerically equal to the ratio of Nusselt numbers given in Figure 18. Since $(q_c)_a$ was found by experiment to be 7.8 Btu/min, $(q_c)_p$ could be estimated.

The rate of radiant heat transfer to a particle cloud thus can be evaluated by

$$q_{ar} = q_T - (q_c)_a - [(q_c)_p - (q_c)_a] \tag{33}$$

where q_T is the total heat transfer rate to the particle cloud, $(q_c)_a$ the convective heat transfer rate to particle-free air, and $[(q_c)_p - (q_c)_a]$ the additional convective heat transfer due to the presence of particles.

D. Discussion of results

The experimental results for zinc particle clouds were evaluated using Equation 33; they are presented in Figure 19. The absorptivity of the suspended particles was calculated by

$$\alpha_r = \frac{q_{ar}}{q_{ab}} \tag{34}$$

where q_{ab} may be calculated by Equations 11 and 15 in Section V. At least three independent tests were made for each condition; mean values are presented in Figure 20. The dotted line shown in the figure was calculated by Equation 28 by assuming all the mean beam lengths of the reflective radiation equal to 0.006 ft which is about the length of cloud ($A_p = 59$ ft^{-1}) when half of the radiation was absorbed. The small discrepancy between the calculated experimental values and the theoretically predicted values is

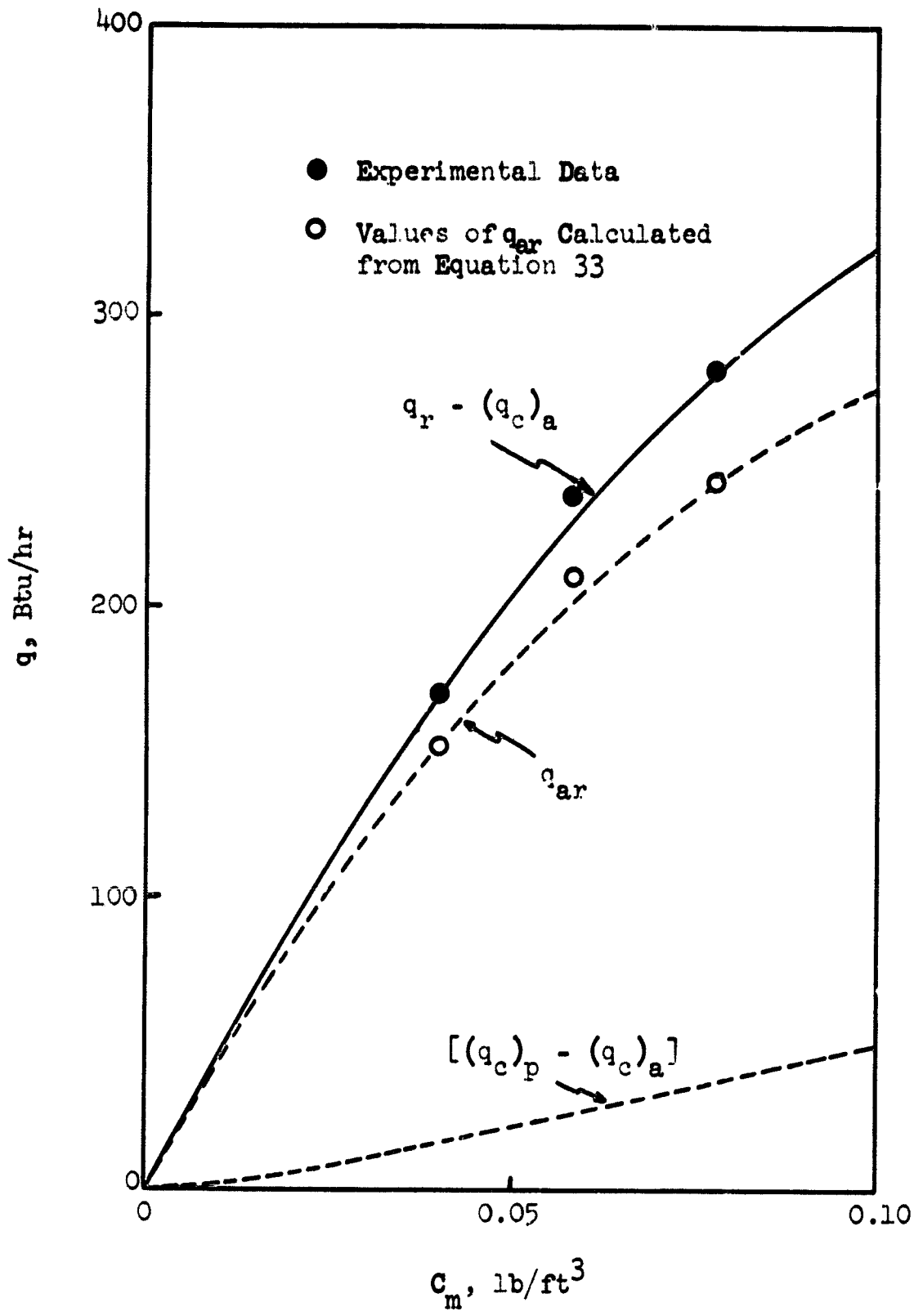

Figure 19. Experimental Data and Quantities Correlated by Equation 33 for Zinc Particle Clouds.

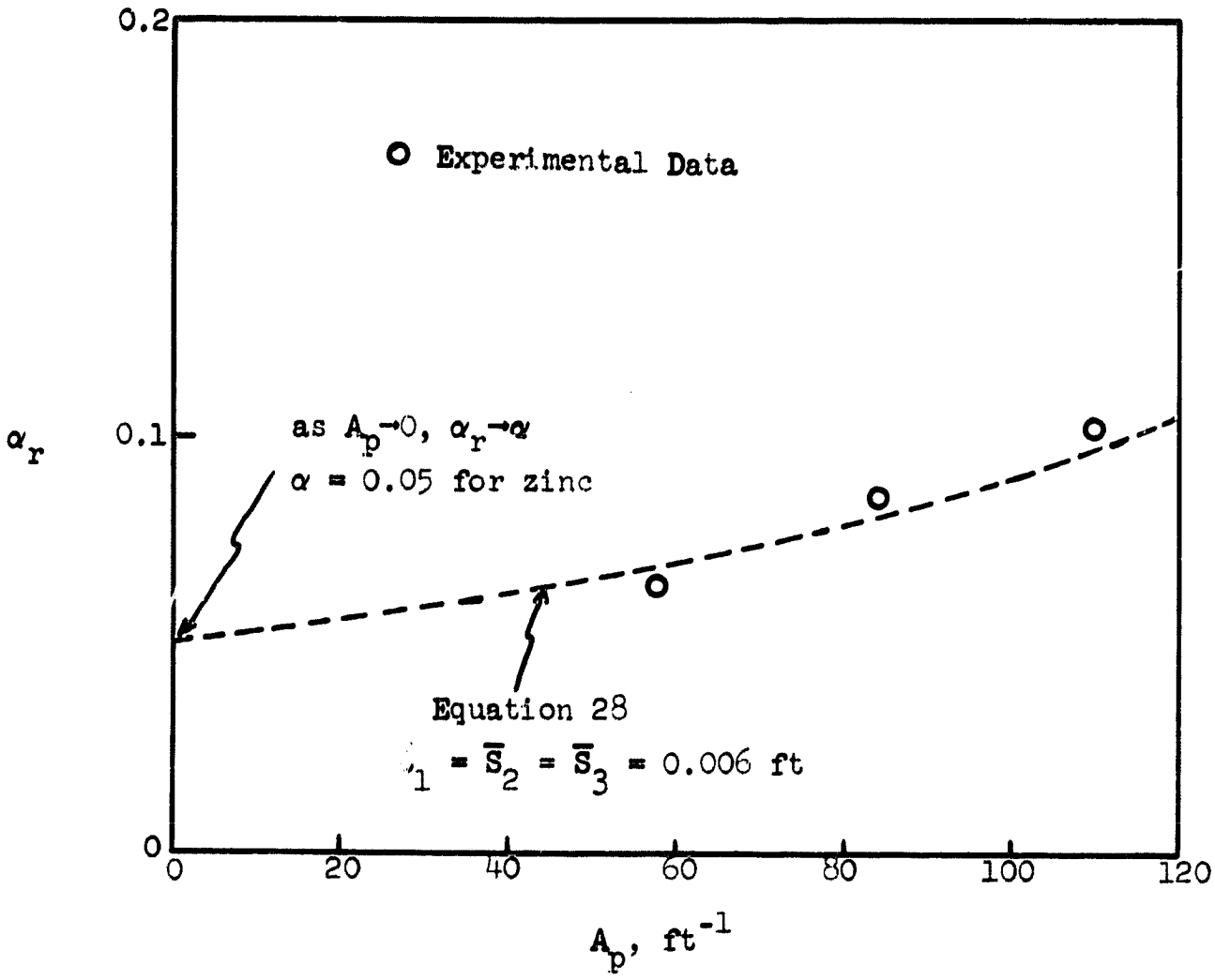

Figure 20. Absorptivity of Suspended Zinc Particles as a Function of the Total Projected Area of Particles Per Unit Volume of Cloud.

probably attributed to the approximation of mean beam lengths and experimental errors. Results are in good agreement generally.

VII. THEORETICAL ANALYSIS OF RADIANT HEAT TRANSFER IN HIGH TEMPERATURE CONDUITS

The rate of heat transfer to a particle cloud in a radiant field of known flux has been discussed in previous sections. The dependence of the rate of radiant heat transfer on particle properties has been the major concern.[34] In this section, both the characteristics of the emitting wall and the absorbing medium are considered. Sometimes the term "aerosol" is used in place of particle cloud to indicate that the gaseous medium may also be absorbing. A cylindrical geometry is chosen in the analysis primarily because of its simplicity as well as being generally applicable to high-temperature technology. Most equations with the exception of the integral ones can be easily adapted or directly applied to systems other than cylindrical ones provided their cross-sectional areas are uniform. The term "gray body" is used to refer to surfaces that emit and reflect diffusely.

A. Statement of the problem

The general treatment of radiant heat transfer from an emitting wall to a gas containing particles involves, separately, the energies absorbed by the carrier gas and by the suspended particles. The combination of these two factors is termed here the radiant heat transfer to the aerosol. Therefore, the absorption coefficient k represents the total absorption coefficient of the aerosol. In the case of an absorbing gas free of particles, k is the absorption coefficient of the absorbing gas alone. In the case of a non-absorbing gas containing absorbing particles, k is the absorption coefficient of the particles. The view factor F is defined as the fraction of energy

emitted from a black surface and received by the aerosol. For gray surfaces, f is employed as the view factor. Due to the fact that infinite reflections occur in a gray-surface system, f is always larger than F for systems of the same geometry. It is to be noted that the view factors represent only the fraction of the emitted energy incident on a surface or absorbed by the aerosol. They are dimensionless and do not show by any means the magnitude of the actual heat transfer.

B. View factors for black body systems

In general, the radiant transfer of heat from an isothermal black surface of area A_w to an aerosol nearby or flowing over the surface can be expressed as

$$q_{w \to a} = A_w F_{wa} \sigma T_w^4 \tag{35}$$

where the subscript w denotes the wall surface and a the aerosol.

If the absorption coefficient of the aerosol, k, is assumed constant, the view factor from wall to the aerosol F_{wa} can be written for a cylindrical system as

$$F_{wa} = \frac{1}{\pi A_w} \int_{A_a} \int_{A_w} \frac{e^{-kS} \cos \beta_w \cos \beta_a}{S^2} dA_w \, dA_a \tag{36}$$

where S is the distance between an emitting surface element and a receiving differential volume of aerosol. The angles between the direction of the radiation and the normal direction to the surfaces of the wall and the aerosol are, respectively, β_w and β_a. The quantities of Equation 36 can be expressed by the coordinates shown in Figure 21 as:

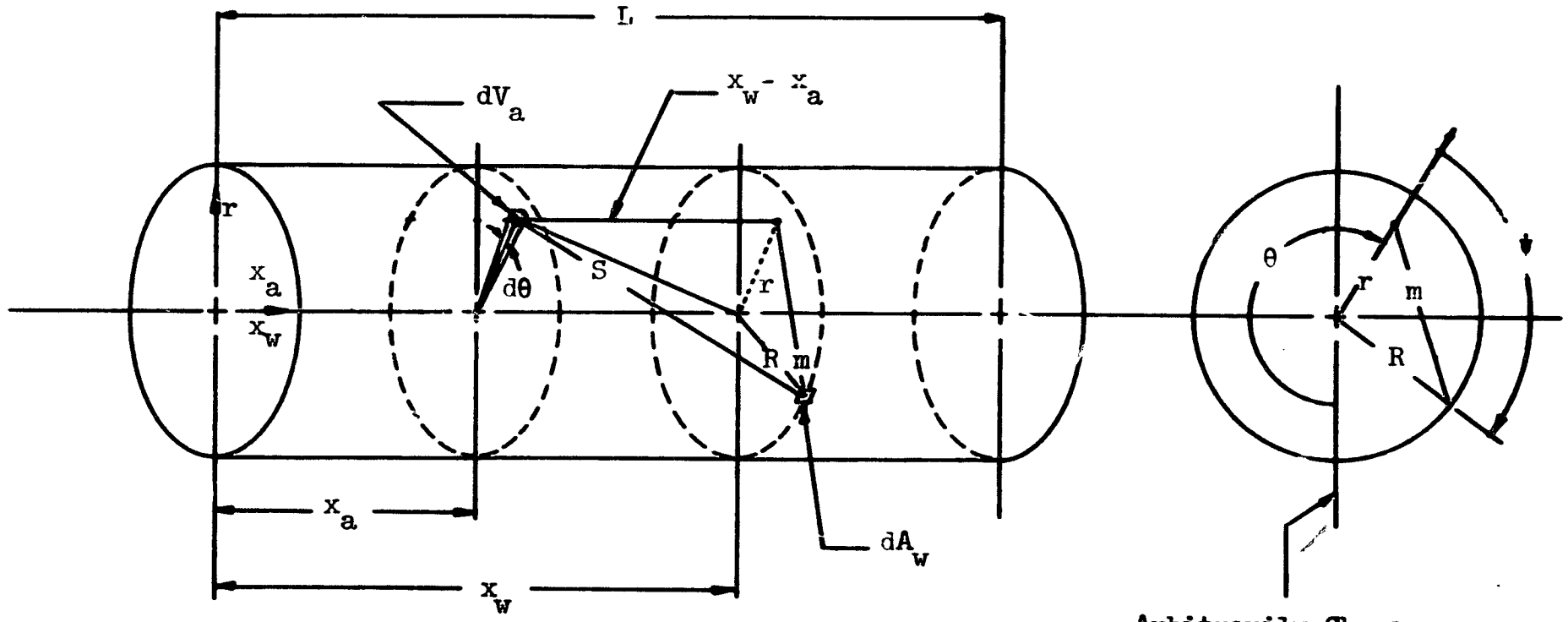

Figure 21. Definitions of Geometric Variables for the Wall-to-Aerosol View Factor Formulations.

$$\cos \beta_a \, dA_a = k \, dV_a = kr \, dr \, dx_a \, d\theta \tag{37}$$

$$dA_w = R \, d\Psi \, dx_w \tag{38}$$

$$\cos \theta_w = \frac{R - r \cos \Psi}{[(x_w - x_a)^2 + R^2 + r^2 - 2Rr \cos \Psi]^{1/2}} \tag{39}$$

and

$$S = [(x_w - x_a)^2 + R^2 + r^2 - 2Rr \cos \Psi]^{1/2} \tag{40}$$

Thus Equation 36 becomes

$$F_{wa} = \frac{k}{\pi L^2} \int_0^R \int_0^{2\pi} \int_0^{L_a} \int_0^{L_w} \frac{r(R - r \cos \Psi)}{[(x_w - x_a)^2 + R^2 + r^2 - 2Rr \cos \Psi]^{3/2}}$$

$$\cdot \exp\left\{-k[(x_w - x_a)^2 + R^2 + r^2 - 2Rr \cos \Psi]^{1/2}\right\} dx_w \, dx_a \, d\Psi \, dr \, d\theta \tag{41}$$

If the absorbing aerosol is completely within the cylinder, then $L_a = L_w = L$. Thus Equation 41 becomes

$$F_{wa} = \frac{k}{\pi L^2} \int_0^R \int_0^{2\pi} \int_0^L \int_0^L \frac{r(R - r \cos \Psi)}{[(x_w - x_a)^2 + R^2 + r^2 - 2Rr \cos \Psi]^{3/2}}$$

$$\cdot \exp\left\{-k[(x_w - x_a)^2 + R^2 + r^2 - 2Rr \cos \Psi]^{1/2}\right\} dx_w \, dx_a \, d\Psi \, dr \tag{42}$$

where L and R are the length and radius of the cylindrical system, respectively.

The integrations against x_w and x_a were performed analytically by means of a series expansion of the exponential term. The subsequent integrations for Ψ and r were performed numerically by use of closed-form, Newton-Cotes, quadrature formulae.[15] The results for aerosols of various absorption parameters, kR, are presented in Figure 22 as a function of the length-to-radius ratio, L/R. The radiant heat transfer rate can be easily evaluated by inserting the value read from the figure into Equation 35.

C. View factors for gray body systems

Classical radiant heat transfer problems assume black-body behavior. In general, systems existing in practice are very seldom black. Analysis of a non-black-body system is complex, but an approximate result can be obtained relatively easily provided assumptions are made. If a system can be assumed to have surfaces that are perfectly diffuse emitters and reflectors, the analysis can be much simplified. A surface usually can be assumed to be diffuse if it is relatively rough compared to the wavelength of the incident radiation. This means that all surfaces will behave more diffusely when the incident radiation comes from a higher temperature source with the same emitting property.

In a black-surface, cylindrical system, that portion of the radiation passing through the aerosol and reaching the wall of the cylinder is absorbed completely by the wall. But in a gray-wall system, the portion reaching the wall is partially absorbed and partially reflected. The reflected energy is available for further absorption by the aerosol. This infinitely continuing process adds to the absorption as more reflection occurs. If f_{wa} is assumed to be the view factor for the gray-surface system which includes the initial

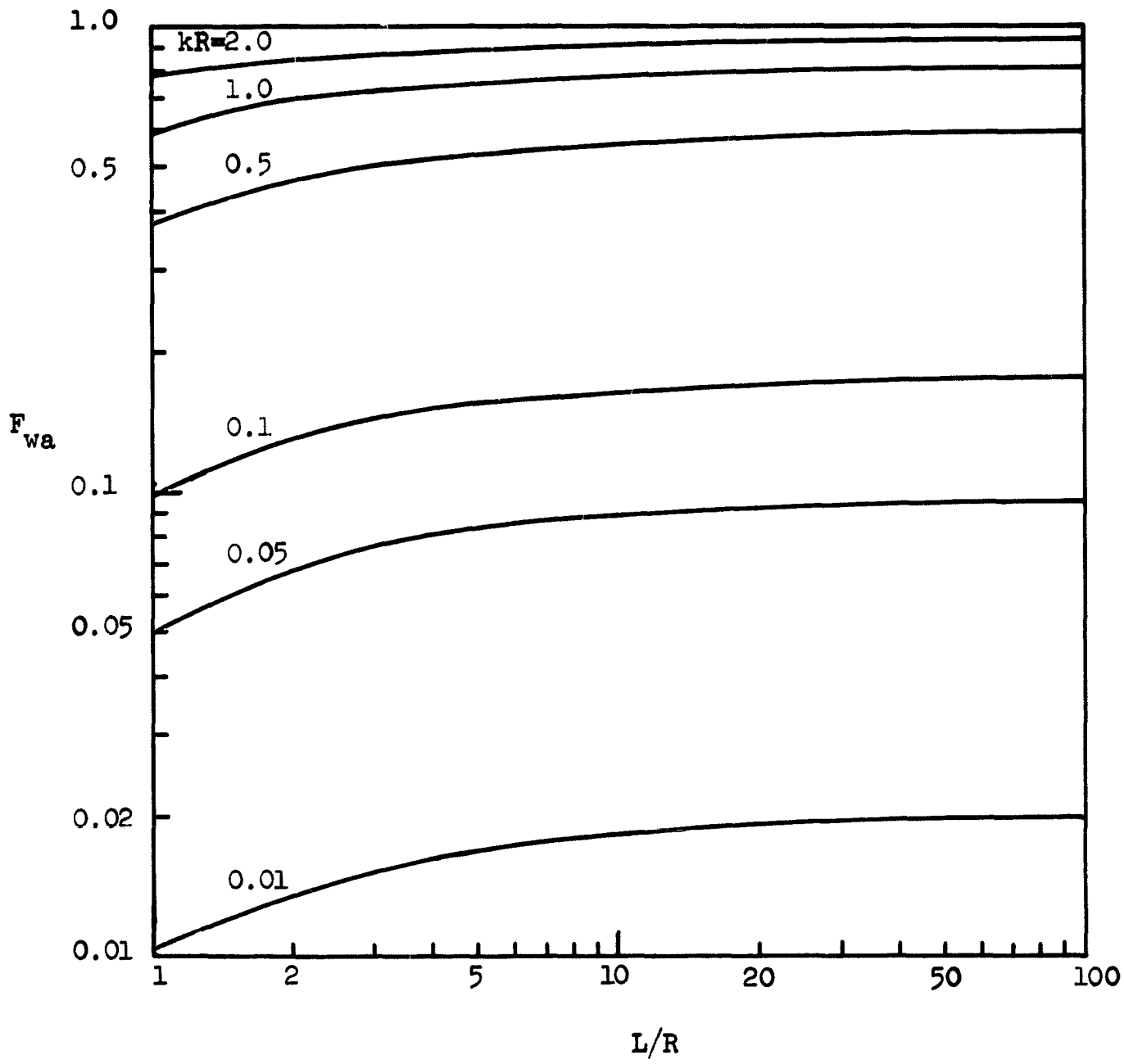

Figure 22. Wall-to-Aerosol View Factors for Black-Wall Cylinders Containing Aerosols Having Various Absorption Coefficients.

view factor and the view factors of the continuing process of reflection, then the radiant heat transfer from the wall to the aerosol can be expressed as

$$q_{w \to a} = A_w \, f_{wa} \, \epsilon \, \sigma \, T_w^4 \tag{43}$$

where ϵ is the total emissivity of the wall surface. The view factor f_{wa} can be expressed by an infinite series as

$$f_{wa} = F_{1a} + \rho_w \, F_{1w} \, F_{2a} + \rho_w^2 \, F_{1w} \, F_{2w} \, F_{3a}$$

$$+ \rho_w^3 \, F_{1w} \, F_{2w} \, F_{3w} \, F_{4a} + \ldots\ldots \tag{44}$$

where ρ_w is the reflectivity of the wall surface. The view factors, F_{1a}, F_{2a}, F_{3a}, . . ., represent, respectively, the fractions of the radiant energy leaving the wall that are intercepted by the aerosol in the first pass, second pass, third pass, etc. The view factors F_{1w}, F_{2w}, F_{3w}, . . ., represent the fraction of radiant energy leaving the wall that pass through the aerosol and are incident again on the wall during the first pass, second pass, third pass, etc.

A gray surface is assumed to be a perfectly diffuse emitter and reflector. Thus it may be assumed that

$$F_{1a} = F_{2a} = F_{3a} = \ldots = F_{wa} \tag{45}$$

and

$$F_{1w} = F_{2w} = F_{3w} = \ldots = F_{ww} \tag{46}$$

Equation 44 now can be reduced to

$$f_{wa} = F_{wa}[1 + \rho_w F_{ww} + \rho_w^2 F_{w,}^2 + \ldots] \tag{47}$$

The value of $\rho_w F_{ww}$ is always less than unity. Thus the expression for f_{wa} can be further simplified to

$$f_{wa} = \frac{F_{wa}}{1 - \rho_w F_{ww}} \tag{48}$$

Substituting f_{wa} into Equation 43 gives

$$q_{w \to a} = A_w \left(\frac{\epsilon F_{wa}}{1 - \rho_w F_{ww}}\right) \sigma T_w^4 \tag{49}$$

The values of F_{wa} are shown in Figure 22 for various systems. To evaluate F_{ww}, the following expression

$$F_{w1w2} = \frac{1}{\pi A_w} \int_{A_{w2}} \int_{A_{w1}} \left(e^{-kS}\right)\left(\frac{\cos \beta_{w1} \cos \beta_{w2}}{S^2}\right) dA_{w1}\, dA_{w2} \tag{50}$$

may be employed, where the quantities in terms of the coordinates are:

$$dA_{w1} = R\, d\theta\, dx_{w1} \tag{51}$$

$$dA_{w2} = R\, d\Psi\, dx_{w2} \tag{52}$$

$$S = [(x_{w1} - x_{w2})^2 + 2R^2 - 2R^2 \cos \Psi]^{1/2} \tag{53}$$

and

$$\cos \beta_{w1} = \cos \beta_{w2} = \frac{R(1 - \cos \Psi)}{[(x_{w1} - x_{w2})^2 + 2R^2 - 2R^2 \cos \Psi]^{1/2}} \qquad (54)$$

Since the emitter and the receiver are the same cylinder, $L_{w1} = L_{w2} = L$. Equation 50 thus becomes

$$F_{ww} = \frac{R^3}{2\pi^2 L} \int_0^{2\pi} \int_0^{2\pi} \int_0^{L} \int_0^{L} \frac{(1 - \cos \Psi)^2}{[(x_{w1} - x_{w2})^2 + 2R^2 - 2R^2 \cos \Psi]^2}$$

$$\cdot \exp\left\{-k[(x_{w1} - x_{w2})^2 + 2R^2 - 2R^2 \cos \Psi]^{1/2}\right\} dx_{w1}\, dx_{w2}\, d\Psi\, d\theta \qquad (55)$$

or

$$F_{ww} = \frac{R^3}{\pi L} \int_0^{2\pi} \int_0^{L} \int_0^{L} \frac{(1 - \cos \Psi)^2}{[(x_{w1} - x_{w2})^2 + 2R^2 - 2R^2 \cos \Psi]^2}$$

$$\cdot \exp\left\{-k[(x_{w1} - x_{w2})^2 + 2R^2 - 2R^2 \cos \Psi]^{1/2}\right\} dx_{w1}\, dx_{w2}\, d\Psi \qquad (56)$$

The value of F_{ww} can be obtained similarly as stated for F_{wa} except one less integral term is involved than for F_{wa} because of the constant radius R. Hoffman and Gauvin[8] obtained solutions for cylinders of length equal to one, two, and three times that of the diameter. Their results are modified and are presented in Figure 23 with interpolation and extrapolation added.

The view factors calculated by Equation 48 are nearly exact for relatively dense aerosols. For systems of dilute aerosols, very small errors

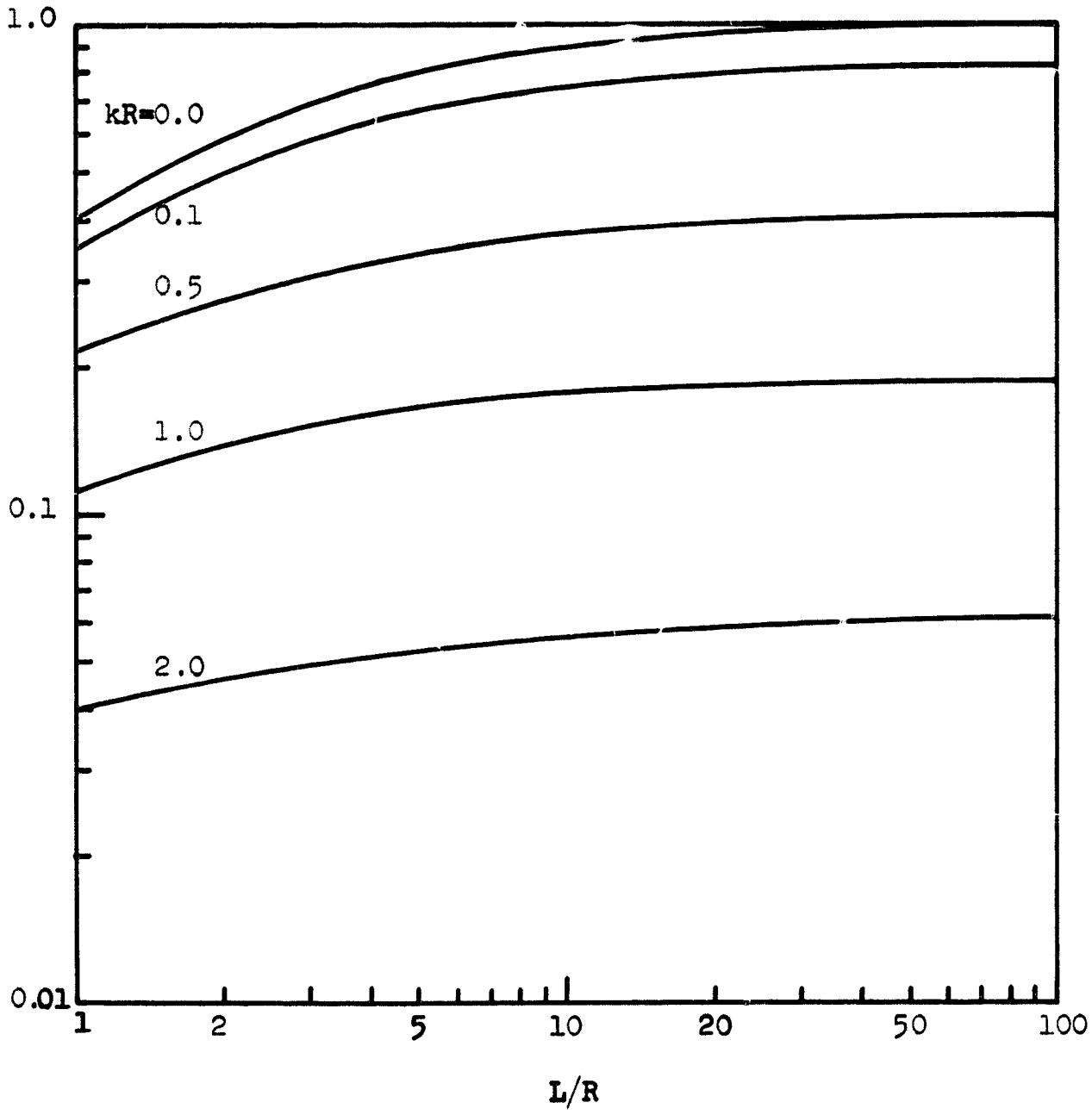

Figure 23. Wall-to-Wall View Factors for Black-Wall Cylinders Containing Aerosols Having Various Absorption Coefficients.

are to be expected for short (length less than radius) or long (length greater than five times radius) cylinders. This results from the nearly uniform irradiation within short cylinders and the negligible end effects for long cylinders. For intermediate cylinders, the center portion receives more radiant energy per unit area than each of the end portions. For example, the center portion of a cylinder having a length equal to three times the radius receives about three per cent more of the emitted radiant energy than each of the end portions receives if the absorption parameter, kR, is assumed to be 0.1. An error analysis with consideration of this uneven irradiation for a surface of reflectivity of 0.5 was performed, and the final result showed no significant difference from that obtained by Equation 48 in which the assumption of uniform irradiation was made. Apparently, the increase in absorption due to uneven irradiation is very small.

If the temperature and size of a conduit is fixed, the rate of related radiant heat transfer to the same absorbing medium within it is proportional to the emissivity of the conduit wall. To show this relation, it may be written that

$$q_\epsilon = \delta\, q_b \tag{57}$$

where q_ϵ is the rate of radiant heat transfer of a gray wall conduit having emissivity ϵ and q_b of a black wall conduit. The coefficient δ can be expressed by

$$\delta = \frac{\epsilon}{1 - \rho_w F_{ww}} \tag{58}$$

The values of F_{ww} for cylinders can be obtained from Figure 23.

The coefficient δ may be called the apparent emissivity of the wall because it is the ratio of the total radiant energy leaving the gray conduit wall per unit time (including emitted and reflected radiation) to that if the wall is black. The values of δ for a cylindrical conduit (L/R = 1) are shown in Figure 24 with the wall emissivity as parameter. The rate of radiant heat transfer from the cylindrical conduit to the absorbing medium within it can be evaluated by

$$q_e = 2\pi RL\ \delta\ F_{wa}\ \sigma\ T_w^4 \qquad (59)$$

where δ is the value obtained from Figure 24 by the correspondent emissivity curve.

The absorption efficiency γ, which is defined as the portion of the emitted radiation absorbed by the aerosol, of a cylindrical conduit (L/R = 1) is shown in Figure 25 with reflectivity ρ_w as parameter. The rate of radiant heat transfer in this case (non-black conduit) is calculated by

$$q_\rho = \gamma\ q_e \qquad (60)$$

where q_e is the radiant energy emitted from the conduit wall per unit time and is $2\pi RL\epsilon\sigma T_w^4$. For black conduit, $\gamma = F_{wa}$. The values of γ for reflective surfaces approach it for black surfaces when the value of kR is large because the radiation is absorbed by the aerosol and the amount that reaches the wall is very small.

Even though the absorption efficiency of a reflective conduit is higher than a black or less reflective one, the rate of radiant heat

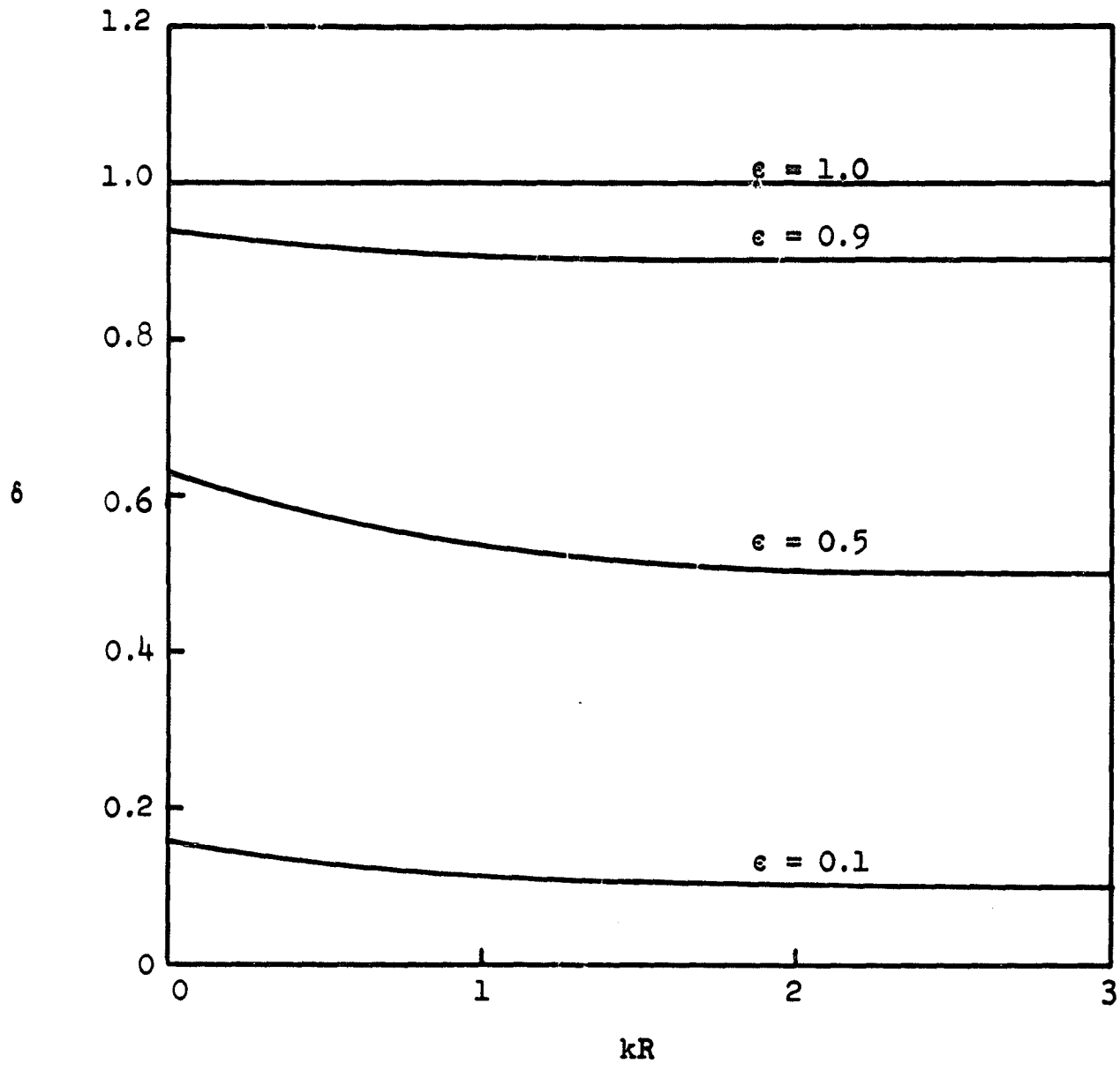

Figure 24. Ratio of the Rate of Radiant Heat Transfer of a Gray Wall and a Black Wall Cylinder (L/R = 1) to the Absorbing Medium Within When the Wall Temperature is Constant.

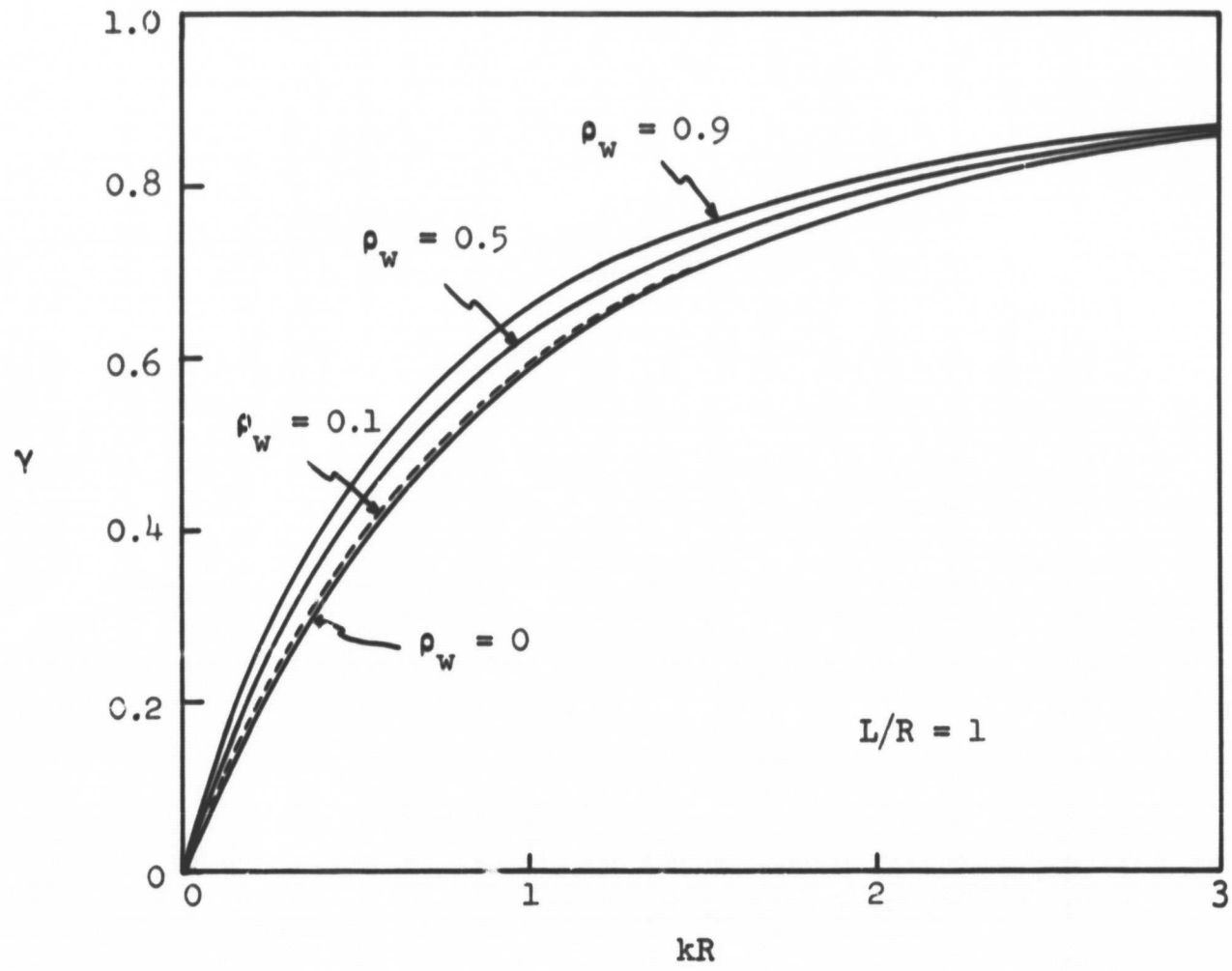

Figure 25. Absorption Efficiency of Aerosols in a Cylinder as a Function of kR Having Reflectivity of the Wall as a Parameter.

transfer is always lower if the conduit wall temperature is the same. It must be remembered that higher absorption efficiency means the higher rate of radiant heat transfer only if the radiant heat flux is constant. For example, if conduit temperature is constant and at equilibrium, i.e., $\epsilon = \alpha$ and $\epsilon = 1 - \rho_w$, a cylindrical conduit (L/R = 1) with emissivity of 0.5 will emit at a rate of 50 per cent of that of a black conduit but the rate of radiant heat transfer is 57 per cent when kR is 0.5. If the rate of the radiation emitted from the conduit is fixed at 100 Btu/min the rate of radiant heat transfer to the absorbing medium (kR = 0.5) within the conduit is about 38 Btu/min for a black conduit and 43 Btu/min for a conduit having a reflectivity of 0.5.

D. View factors for specular-reflection systems

Specular reflection refers to the process in which the angle of reflection equals the angle of incidence but with reduced intensity. Many smooth metal surfaces reflect specularly. Whether or not a surface is optically smooth depends on the wavelengths of the incident radiation. Some surfaces that appear rough to the eye may be considered smooth for long wavelength radiation. So the justification of specular reflection depends on the wavelength of the incident radiation and the relative roughness of the receiving surface. It has been stated[35,36] that a surface may be nearly a diffuse emitter even if it is a specular reflector. Here, it has been assumed that the surfaces of the cylinders are perfectly diffuse emitters and specular reflectors.

The view factors for a specular-reflection system are very difficult to evaluate analytically. The situation is unlike a diffuse-reflection

surface for which the view factors of each reflection pass can be assumed to be as given by Equations 45 and 46. For a cylinder of infinite length, however, the solution will be the same as for a diffuse-reflection surface. It can be shown by an analysis using an arbitrarily chosen beam of initial intensity i_o that the total absorption by the aerosol for this beam is expressed by

$$q_{i_o} = i_o(1 - e^{-kS}) + \rho_w\, i_o e^{-kS}(1 - e^{-kS}) + \rho_w{}^2\, i_o e^{-2kS}(1 - e^{-kS}) + \ldots$$

$$= i_o(1 - e^{-kS})(1 + \rho_w\, e^{-kS} + \rho_w{}^2\, e^{-2kS} + \ldots)$$

$$= i_o\left(\frac{1 - e^{-kS}}{1 - \rho_w\, e^{-kS}}\right) \tag{61}$$

where S is the distance that the arbitrarily chosen beam travels through the aerosol until it reaches the wall.

If a beam length, $\bar{S}$, is employed, than an overall radiant heat transfer equation may be written

$$q_{w\to a} = A_w\, \epsilon\, \sigma\, T_w{}^4 \left(\frac{1 - e^{-k\bar{S}}}{1 - \rho_w\, e^{-k\bar{S}}}\right) \tag{62}$$

where the view factor f'_{wa} for a specular-reflection system can be expressed by

$$f'_{wa} = \frac{1 - e^{-k\bar{S}}}{1 - \rho_w\, e^{-k\bar{S}}} \tag{63}$$

Actually, this expression is the same as Equation 48 because

$$F_{wa} = 1 - e^{-k\bar{S}} \tag{64}$$

and

$$F_{ww} = e^{-k\bar{S}} \tag{65}$$

so that

$$f'_{wa} = f_{wa} = \frac{F_{wa}}{1 - \rho_w F_{ww}} \tag{66}$$

Usually, cylinders with lengths greater than ten times their radius can be safely considered as infinitely long cylinders with even dilute aerosols in them. For a cylinder having a length equal to its diameter (as was the furnace used in this study) the maximum error will be about 5 per cent for the experiment with an aerosol having kR = 0.1 if the surface of the furnace is indeed a perfect specular reflector with a reflectivity of 0.5. In some practical high temperature systems, the surfaces can either be assumed to be diffuse or to behave in a manner between specular reflection and diffuse reflection. Equation 66 is believed to be a good compromise for most systems of smooth metal surfaces and fairly concentrated aerosols.

E. View factors among zones

If a cylinder with a black wall is arbitrarily divided into two zones, say A and B, the view factors for each of the zones to the aerosol in its zone can be obtained from Figure 22. The view factor from the wall of zone

A, w_A, to the aerosol in zone B, a_B, can be evaluated by the following equation:

$$F_{w_A \to a_B} = \frac{k}{\pi L_A} \int_0^R \int_0^{2\pi} \int_0^{L_A} \int_{L_A}^{(L_A+L_B)} \frac{r(R - r\cos\Psi)}{[(x_B - x_A)^2 + R^2 + r^2 - 2Rr\cos\Psi]^{3/2}}$$

$$\cdot \exp\left\{-k[(x_B - x_A)^2 + R^2 + r^2 - 2Rr\cos\Psi]^{1/2}\right\} dx_B\, dx_A\, d\Psi\, dr \quad (67)$$

where L_A and L_B are the lengths of zones A and B, respectively. Both of the coordinate variables x_A and x_B are along the axis of the cylinder as shown in Figure 21.

Similarly, the view factor from the wall of zone B, w_B, to the aerosol in zone A, a_A, can be expressed by

$$F_{w_B \to a_A} = \frac{k}{\pi L_B} \int_0^R \int_0^{2\pi} \int_{L_A}^{(L_A+L_B)} \int_0^{L_A} \frac{r(R - r\cos\Psi)}{[(x_B - x_A)^2 + R^2 + r^2 - 2Rr\cos\Psi]^{3/2}}$$

$$\cdot \exp\left\{-k[(x_B - x_A)^2 + R^2 + r^2 - 2Rr\cos\Psi]^{1/2}\right\} dx_A\, dx_B\, d\Psi\, dr \quad (68)$$

If two zones are separated by a third zone, an equation with some modification is needed. In Figure 26, for example, zones A and C are separated by zone B. The view factors from the wall of zone A to the aerosol in zone C and from the wall of zone C to the aerosol in zone A can be expressed by

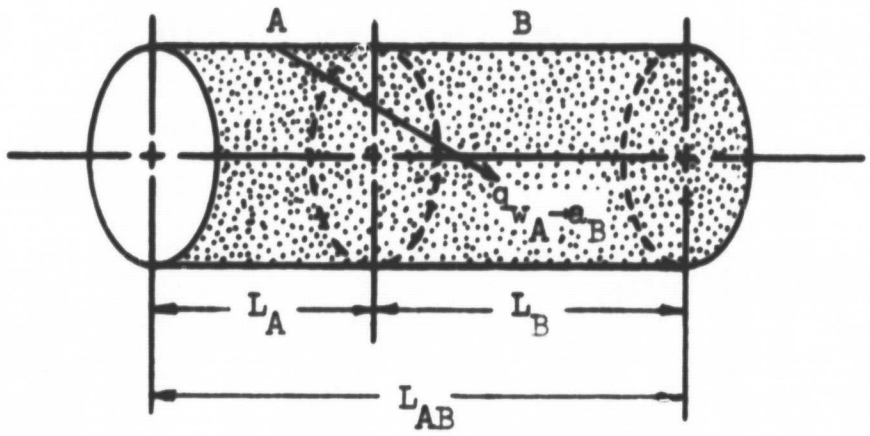

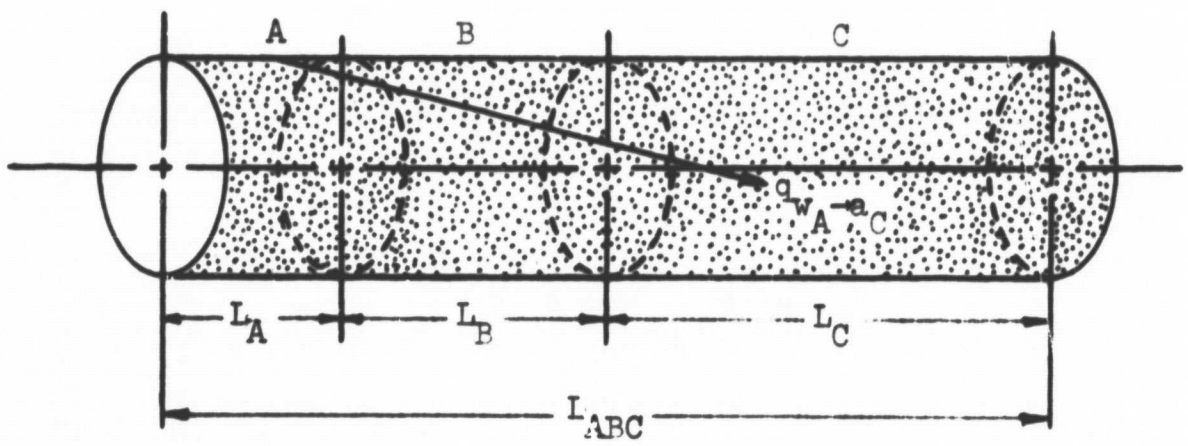

Figure 26. Radiant Heat Transfer Between Zones.

$$F_{w_A \to a_C} = \frac{k}{\pi L_A} \int_0^R \int_0^{2\pi} \int_0^{L_A} \int_{(L_A+L_B)}^{(L_A+L_B+L_C)} \frac{r(R - r\cos\Psi)}{[(x_C - x_A)^2 + R^2 + r^2 - 2Rr\cos\Psi]^{3/2}}$$

$$\cdot \exp\left\{-k[(x_C - x_A)^2 + R^2 + r^2 - 2Rr\cos\Psi]^{1/2}\right\} dx_C\, dx_A\, d\Psi\, dr \quad (69)$$

and

$$F_{w_C \to a_A} = \frac{k}{\pi L_C} \int_0^R \int_0^{2\pi} \int_{(L_A+L_B)}^{(L_A+L_B+L_C)} \int_0^{L_A} \frac{r(R - r\cos\Psi)}{[(x_C - x_A)^2 + R^2 + r^2 - 2Rr\cos\Psi]^{3/2}}$$

$$\cdot \exp\left\{-k[(x_C - x_A)^2 + R^2 + r^2 - 2Rr\cos\Psi]^{1/2}\right\} dx_A\, dx_C\, d\Psi\, dr \quad (70)$$

respectively.

By examining Equations 67 and 68, 69, and 70, the following relationships are obtained:

$$A_B F_{w_B \to a_A} = A_A F_{w_A \to a_B} \quad (71)$$

and

$$A_C F_{w_C \to a_A} = A_A F_{w_A \to a_C} \quad (72)$$

The lengths of zones A, B, and C vary with each system. If $L_B = \alpha_B L_A$ and $L_C = \alpha_C L_A$, it follows that $L_A+L_B = (1+\alpha_B)L_A$ and $L_A+L_B+L_C = (1+\alpha_B+\alpha_C)L_A$. Then the view factors can be evaluated for various values of L_A, α_B, and α_C. This procedure is complicated and also incomplete due to the limited values

of L_A selected. A method has been developed to obtain the view factors by using a simple equation.

For two adjacent cylinders, let $L_{AB} = L_A + L_B$. Then the relationship between the view factors can be expressed as

$$(AF_{wa})_{L_{AB}} = (AF_{wa})_{L_A} + (AF_{wa})_{L_B} + A_A F_{w_A \to a_B} + A_B F_{w_B \to a_A} \qquad (73)$$

From Equations 71 and 73, there is obtained

$$A_A F_{w_A \to a_B} = A_B F_{w_B \to a_A} = 1/2\left[(AF_{wa})_{L_{AB}} - (AF_{wa})_{L_A} - (AF_{wa})_{L_B}\right] \qquad (74)$$

or

$$L_A L_{w_A \to a_B} = L_B F_{w_B \to a_A} = 1/2\left[L_{AB}(F_{wa})_{L_{AB}} - L_A(F_{wa})_{L_A} - L_B(F_{wa})_{L_B}\right] \qquad (75)$$

The view factors F_{wa} for various length-to-radius ratios are available in Figure 22.

If two zones of interest, such as A and C in Figure 26, are not adjacent, the relationship between the view factors can be expressed by

$$L_A F_{w_A \to a_C} = L_A F_{w_A \to a_{BC}} - L_A F_{w_A \to a_B} \qquad (76)$$

where a_{BC} represents the aerosol in adjacent zones B and C and can be considered to be a single zone of length L_{BC}. Equation 76 may be reduced to

$$F_{w_A \to a_C} = F_{w_A \to a_{BC}} - F_{w_A \to a_B} \qquad (77)$$

The values of $F_{w_A \to a_{BC}}$ and $F_{w_A \to a_B}$ can be evaluated by Equation 74. Similarly, there is obtained

$$F_{w_C \to a_A} = F_{w_C \to a_{AB}} - F_{w_C \to a_B} \tag{78}$$

For gray-wall systems, the view factors for gray walls are used in the above equations. The values of view factors can be obtained from

$$L_A f_{w_A \to a_B} = L_B f_{w_B \to a_A} = 1/2\left[L_{AB}(f_{wa})_{L_{AB}} - L_A(f_{wa})_{L_A} - L_B(f_{wa})_{L_B}\right] \tag{79}$$

If Equation 79 is written in energy terms, it becomes

$$q_{w_A \to a_B} = 2\pi R L_A f_{w_A \to a_B} \epsilon \sigma T_w^4 \tag{80}$$

The quantity, $q_{w_A \to a_B}$, includes the radiation emitted and reflected from the wall of section A and absorbed directly by the aerosol in section B plus that portion of absorbed energy reflected by the wall of section B but originally emitted and reflected from the wall of section A. In other words, the quantity $q_{w_A \to a_B}$ represents the additional portion of absorption due to the presence of section A.

In those cases where the absorption coefficient k is not the same in zone A and zone B, say k_A and k_B, respectively, the equations discussed above cannot be applied without modification. The rate of radiant heat transfer mainly depends on two factors: the rate of radiant energy penetrating the boundary of the two zones and the absorption efficiency of the receiving zone with respect to the penetrated radiation. The former is independent

of the characteristics of the receiving zone, i.e., the rate of radiant energy penetrating the boundary will be the same regardless of whether the receiving zone has the same absorption coefficient or not. The latter factor is a function of $k\bar{S}$, where $\bar{S}$ is the mean beam length of the radiation penetrating the receiving zone.

Some view factors are defined as:

$F_{w_A \to a_B}(k_A, k_A)$ = view factor from the wall of zone A to the aerosol in zone B when both zones have absorption coefficients of k_A

$F_{w_A \to a_B}(k_A, k_B)$ = view factor from the wall of zone A to the aerosol in zone B when their absorption coefficients are k_A and k_B, respectively

$F_{wa}(k_A)_{L_A}$ = view factor from the wall of zone A to the aerosol in zone A when the absorption coefficient is k_A

$F_{wa}(k_A)_{L_B}$ = view factor from the wall of zone B to the aerosol of zone B when the absorption coefficient is k_A

$F_{wa}(k_A)_{L_{AB}}$ = view factor from the walls of zone A and zone B to the aerosol in zone A and zone B when the absorption coefficient is k_A

$F_{wa}(k_B)_{L_B}$ = view factor from the wall of zone B to the aerosol of zone B when the absorption coefficient is k_B

$F_{ww}(k_A)_{L_A}$ = view factor from the wall of zone A to the wall of zone A when the absorption coefficient is k_A.

The rate of radiant heat transfer from the wall of zone A to the aerosol of zone B, if the wall is black and the absorption coefficient is k_A in both zones, can be expressed by

$$q_{w_A \to a_B} = 2\pi R L_A \, F_{w_A \to a_B}(k_A, k_A) \, \sigma \, T_{w_A}^4 \tag{81}$$

where

$$F_{w_A \to a_B}(k_A, k_A) = \frac{1}{2L_A}\left[L_{AB}F_{wa}(k_A)_{L_{AB}} - L_A F_{wa}(k_A)_{L_A} - L_B F_{wa}(k_A)_{L_B}\right] \tag{82}$$

The rate of radiant heat transfer from the wall of zone B to the aerosol of zone A can, similarly, be expressed by

$$q_{w_B \to a_A} = 2\pi R L_B \, F_{w_B \to a_A}(k_A, k_A) \, \sigma \, T_{w_B}^4 \tag{83}$$

where

$$F_{w_B \to a_A}(k_A, k_A) = \frac{1}{2L_B}\left[L_{AB}F_{wa}(k_A)_{L_{AB}} - L_A F_{wa}(k_A)_{L_A} - L_B F_{wa}(k_A)_{L_B}\right] \tag{84}$$

The rate of radiant heat transfer from the wall of zone A to the aerosol of zone B, if the absorption coefficients are k_A and k_B, respectively, can be expressed by

$$q_{w_A \to a_B} = 2\pi R L_A \, F_{w_A \to a_B}(k_A, k_B) \, \sigma \, T_{w_A}^4 \tag{85}$$

where

$$F_{w_A \to a_B}(k_A, k_B) = \frac{1 - \exp(-k_B \bar{S}_{AB})}{1 - \exp(-k_A \bar{S}_{AB})} F_{w_A \to a_B}(k_A, k_A) \tag{86}$$

The term $\bar{S}_{AB}$ is the mean beam length of the radiation in zone B which is emitted from the wall of zone A and penetrates into zone B. Its value is assumed to be the same for k_A and k_B since they usually do not differ greatly from one another. When the values of $k_A\bar{S}_{AB}$ are small, Equation 86 can be simplified to

$$F_{w_A \to a_B}(k_A, k_B) = \frac{k_B}{k_A} F_{w_A \to a_B}(k_A, k_A) \tag{87}$$

If the system consists only of zone A and zone B, the total rate of radiant heat transfer is the sum of the rates to the aerosol in zone A and zone B. Letting T_{w_A}, k_A, and T_{w_B}, k_B be the wall temperatures and absorption coefficients of zone A and zone B, respectively, the total rate of radiant heat transfer to the aerosol in the system can be expressed by

$$q_{w \to a} = \left[q_{w_A \to a_A} + q_{w_B \to a_A}\right] + \left[q_{w_A \to a_B} + q_{w_B \to a_B}\right] \tag{88}$$

where

$$q_{w_A \to a_A} = 2\pi R L_A F_{wa}(k_A)_{L_A} \sigma T_{w_A}^4 \tag{89}$$

$$q_{w_B \to a_A} = 2\pi R L_B \left[\frac{1 - \exp(-k_A \bar{S}_{BA})}{1 - \exp(-k_B \bar{S}_{BA})}\right] F_{w_B \to a_A}(k_B, k_B) \sigma T_{w_B}^4 \tag{90}$$

$$q_{w_A \to a_B} = 2\pi R L_A \left[\frac{1 - \exp(-k_B \bar{S}_{AB})}{1 - \exp(-k_A \bar{S}_{AB})}\right] F_{w_A \to a_B}(k_A, k_A) \sigma T_{w_A}^4 \tag{91}$$

$$q_{w_B \to a_B} = 2\pi R L_B F_{wa}(k_B)_{L_B} \sigma T_{w_B}^4 \tag{92}$$

The values of the mean beam lengths, $\bar{S}_{AB}$ and $\bar{S}_{BA}$, depend on the values of k_A, k_B, L_A, L_B, and R. If the quantity of $F_{A\to AB}(k_A)$, which is the portion of radiant energy emitted from the wall of zone A and received at the boundary of zone A and zone B is known, then the value of $\bar{S}_{AB}$ can be estimated by

$$\bar{S}_{AB} = -\frac{1}{k_A} \ln\left[1 - \frac{F_{w_A \to a_B}(k_A, k_A)}{F_{A\to AB}(k_A)}\right] \tag{93}$$

Similarly,

$$\bar{S}_{BA} = -\frac{1}{k_B} \ln\left[1 - \frac{F_{w_B \to a_A}(k_B, k_B)}{F_{B\to AB}(k_B)}\right] \tag{94}$$

where $F_{B\to AB}(k_B)$ is the view factor from the wall of zone B to the boundary of zone A and zone B.

The view factors from the wall of a zone to the boundary adjacent to another zone can be evaluated by

$$F_{A\to AB}(k_A) = 1/2\left[1 - F_{wa}(k_A)L_A - F_{ww}(k_A)L_A\right] \tag{95}$$

and

$$F_{B\to AB}(k_B) = 1/2\left[1 - F_{wa}(k_B)L_B - F_{ww}(k_B)L_B\right] \tag{96}$$

The rates of radiant heat transfer between two zones of different wall temperature and absorption coefficient can be calculated by the equations given above. The information obtained will be useful in evaluating total heat transfer at a local area if the local heat transfer coefficient is known.

All the view factors $F_{wa}(k_A)_{L_A}$, $F_{wa}(k_B)_{L_B}$, and $F_{wa}(k_A)_{L_{AB}}$ can be obtained from Figure 22. For example, $F_{wa}(k_A)_{L_{AB}}$ is the value read from curve k_AR of the figure at abscissa L_{AB}/R. The view factors $F_{ww}(k_A)_{L_A}$, $F_{ww}(k_B)_{L_B}$, and $F_{ww}(k_A)_{L_{AB}}$ can be obtained from Figure 23. For example, $F_{ww}(k_A)_{L_A}$ is the value read from the figure using the curve k_AR and the abscissa L_A/R.

F. Nonisothermal emission conditions

The view factors for a black wall system and a uniform absorbing medium have been discussed in Subsection B of this section. If the wall is not isothermal, the rate of radiant heat transfer cannot be evaluated by a simple expression as given by Equation 35. The temperature term is not a constant, thus it cannot be removed from the integral function for the view factor as was done in Subsection B. The equation for a nonisothermal wall system when the absorbing medium is still assumed to be constant may be written

$$q_{w\to a} = \frac{\sigma kR}{\pi} \int_0^{2\pi}\int_0^{R}\int_0^{2\pi}\int_0^{L_a}\int_0^{L_w} \frac{\epsilon_w T_w^4 \, r\,(R - r\cos\Psi)}{[(x_w - x_a)^2 + R^2 + r^2 - 2Rr\cos\Psi]^{3/2}}$$

$$\cdot\exp\left\{-k[(x_w - x_a)^2 + R^2 + r^2 - 2Rr\cos\Psi]^{1/2}\right\} dx_w\, dx_a\, d\Psi\, dr\, d\theta \qquad (97)$$

where the wall temperature T_w is a function of x_w, Ψ, and θ, and ϵ_w is usually a function of T_w.

An analytical solution of Equation 97 has to be obtained for each individual temperature conditions. The integration procedure is very laborious even when T_w is only a simple function of x_w. Fortunately, the

solution can be approximated by the results and analysis presented in Subsections B, C, and E. The procedure of evaluating the rate of radiant heat transfer from a nonisothermal cylindrical system to an absorbing medium of constant absorption coefficient is demonstrated below. This procedure can be used for any conduit of uniform cross-sectional area provided the view factors for isothermal conditions are available.

The temperature of a high temperature conduit generally varies only longitudinally at steady state. The conduit may be so divided that each zone can be assumed isothermal. Of course, the number of zones is dependent on the temperature distribution. The length of each zone does not have to be identical. Uneven wall temperatures are generally attributed to three causes. One is that the wall is not evenly heated by the energy source. One is that the absorbing medium flows into the conduit with a greater temperature difference at the inlet than thereafter, thus the heat transfer rates by convection and conduction are different from section to section. Another possibility is that the radiant energy received by the conduit wall itself is greater at the middle than at the ends where a large part of radiation is lost. The temperature of an isothermal zone is uniform by definition but not exactly so for actual conditions. A mean temperature could be used for each zone in these cases. The mean temperature of a cylindrical zone may be evaluated by

$$T_m = \frac{\int_0^{L_z}\int_0^{2\pi} T^4 \, R \, d\theta \, dL}{\int_0^{L_z}\int_0^{2\pi} R \, d\theta \, dL} = \frac{1}{2\pi L_z}\int_0^{L_z}\int_0^{2\pi} T^4 \, d\theta \, dL \qquad (98)$$

where L_z is the length of the zone.

View factors for a black or a uniform gray body conduit have been presented in Subsections B and C. The view factors among zones discussed in Subsection E apply to the conditions here because they do not depend on the wall temperature of the receiving zones except when the optical properties vary from zone to zone. Optical properties such as emissivity and reflectivity are functions of temperature and surface conditions.

The value of emissivity of each zone is directly related to the output rate of radiant energy from that zone, so it should be used in the calculation for that zone. The reflectivity is assumed to be the same throughout the conduit so that view factors among zones for gray wall systems can be used. Errors arising from this assumption are not significant because the total contribution of the reflective energy from other zones is small compared to direct radiation. Therefore, an average value of reflectivity may be used in all the gray body view factor calculations. The emissivity of each zone is employed to calculate the energy emitted from its wall.

If a conduit is divided into n isothermal zones, the radiant energy transferred from the entire conduit wall to an arbitrarily chosen zone j can be expressed by the sum of the portion from each zone as

$$q_{w\to a_j} = q_{w_1\to a_j} + q_{w_2\to a_j} + \cdots + q_{w_j\to a_j} + \cdots + q_{w_n\to a_j} \qquad (99)$$

where $q_{w\to a_j}$ is the rate of radiant heat transfer from the conduit (which consists of all the isothermal zones) to the aerosol in zone j and $q_{w_n\to a_j}$ is the rate from the wall of zone n to the aerosol in zone j.

For black wall systems, the quantities in Equation 99 can be expressed by

$$q_{w_i \to a_j} = A_{w_i} F_{w_i \to a_j} \sigma T_{w_i}^4 \tag{100}$$

where $q_{w_i \to a_j}$ and $F_{w_i \to a_j}$ are, respectively, the rate of radiant heat transfer and view factor from the wall of zone i to the aerosol in zone j, and A_{w_i} and T_{w_i} are, respectively, the area and temperature of the wall of zone i.

For gray wall systems, it may be written that

$$q_{w_i \to a_j} = A_{w_i} f_{w_i \to a_j} \epsilon_{w_i} \sigma T_{w_i}^4 \tag{101}$$

where ϵ_{w_i} is the wall emissivity of the zone i. The view factors can be obtained from Figure 22 or Equations 75 and 77. Thus the total rate of radiant heat transfer from the wall of all zones to the aerosol of all zones is

$$q_{w \to a} = \sum_{j=1}^{n} q_{w \to a_j} = \sum_{j=1}^{n} \left(\sum_{i=1}^{n} q_{w_i \to a_j} \right) \tag{102}$$

G. Approximation for systems of variable absorption coefficient

When an absorbing medium flows through a heated conduit, its temperature rises as it moves forward. The absorption coefficient of the gaseous medium, if absorbant, will change according to the gas temperature. Particle concentration will be reduced as the carrier gas expands. In this case, an assumption of constant absorption coefficient is not applicable except when the conduit is short and a proper average value can be calculated.

Zoning techniques will be employed again. The absorbing medium is divided into several zones each of which is assumed to be uniform in wall

temperature and aerosol absorption coefficient. The radiant energy absorbed by a zone comes mainly from the wall of its own and the walls of neighboring zones. A practical example is given here in support of this contention. The length of each zone is chosen as the radius of the cylinder, and the wall is assumed to be black and isothermal. The aerosol in a zone at the center of a long conduit absorbs about one half of the total absorption of that zone from its own wall and about one sixth from each of the adjacent zones when the average value of kR is 0.01. In this case, only about one twelfth of the total absorption is from each side of this zone outside zones immediately adjacent.

Usually an absorption coefficient changes little in a short distance. Therefore, the assumption that neighboring zones have the same absorption coefficient as the one being calculated is considered acceptable. Calculations then can be performed by employing the method of the preceding section. The curve parameter kR from the corresponding value of k in Figure 22 will be used for each zone. For example, if k_j is the absorption coefficient of the medium in jth zone, then the k_jR curves will be used to evaluate all q's in Equation 99. If the absorption coefficient decreases in the direction of the flow due to thermal expansion of the carrier gas, then the actual radiant energy transferred to the jth zone from upstream zones is slightly lower than the calculated value and from downstream zones it is slightly higher. The errors, apparently both very small, are opposite and very nearly equal. The calculated results for unit zones by this approach are nearly exact for systems of constant wall-temperature. For

systems of violently changing absorption coefficient, errors, however, are incurred, but other opposing factors change also and reduce the overall error. The results are believed to be sufficiently accurate for most practical calculations.

The radiant energy transferred to the medium before it enters and after it leaves the heated-wall section can also be evaluated by Equations 80 and 81 for any extension as long as the absorption coefficient is known and the diameter of the extended sections is the same as the heated one.

A discussion is also presented in Subsection E about variable absorption coefficients. Equations have been derived for several conditions.

VIII. RADIANT HEAT TRANSFER IN A TUNGSTEN FURNACE

A. Arrangement of apparatus and general operation

The heat transfer apparatus consisted of the following basic components: a high output power supply and control, a tungsten-element furnace with a cylindrical heater, an aerosol generator, a transmissivity-measurement unit, particle-concentration sampler, thermocouples, and an optical pyrometer. A general view of the furnace showing some of its components is given in Figure 27.

To make a test, the recorder and photometer were first turned on and allowed to achieve steady-state conditions. The powder was dried in advance of a test to eliminate moisture. Next, the cooling nitrogen gas and water were turned on. The nitrogen gas was directed at the neck of the heating element where failure tended to occur otherwise. Water was used to cool the furnace jacket. A small portion of the nitrogen gas flow was employed to prevent aerosol from entering the photometer slits. The carrier gas, also nitrogen, was then set at the desired flow rate with a rotameter. After this flow rate was established, the carrier gas stream was switched so as to bypass the rotameter to avoid its plugging with aerosol during the test. The nitrogen gas was allowed to flow for a few minutes to purge oxygen from the system. The surge tank was also sealed off so that there would be little oxygen in it at the start.

The main power supply was turned on with a shorting bar placed between the two electrodes to insure against an initial voltage surge that could damage the furnace heating element. Then the shorting bar was removed. The power controller supply was then activated, and the power level was

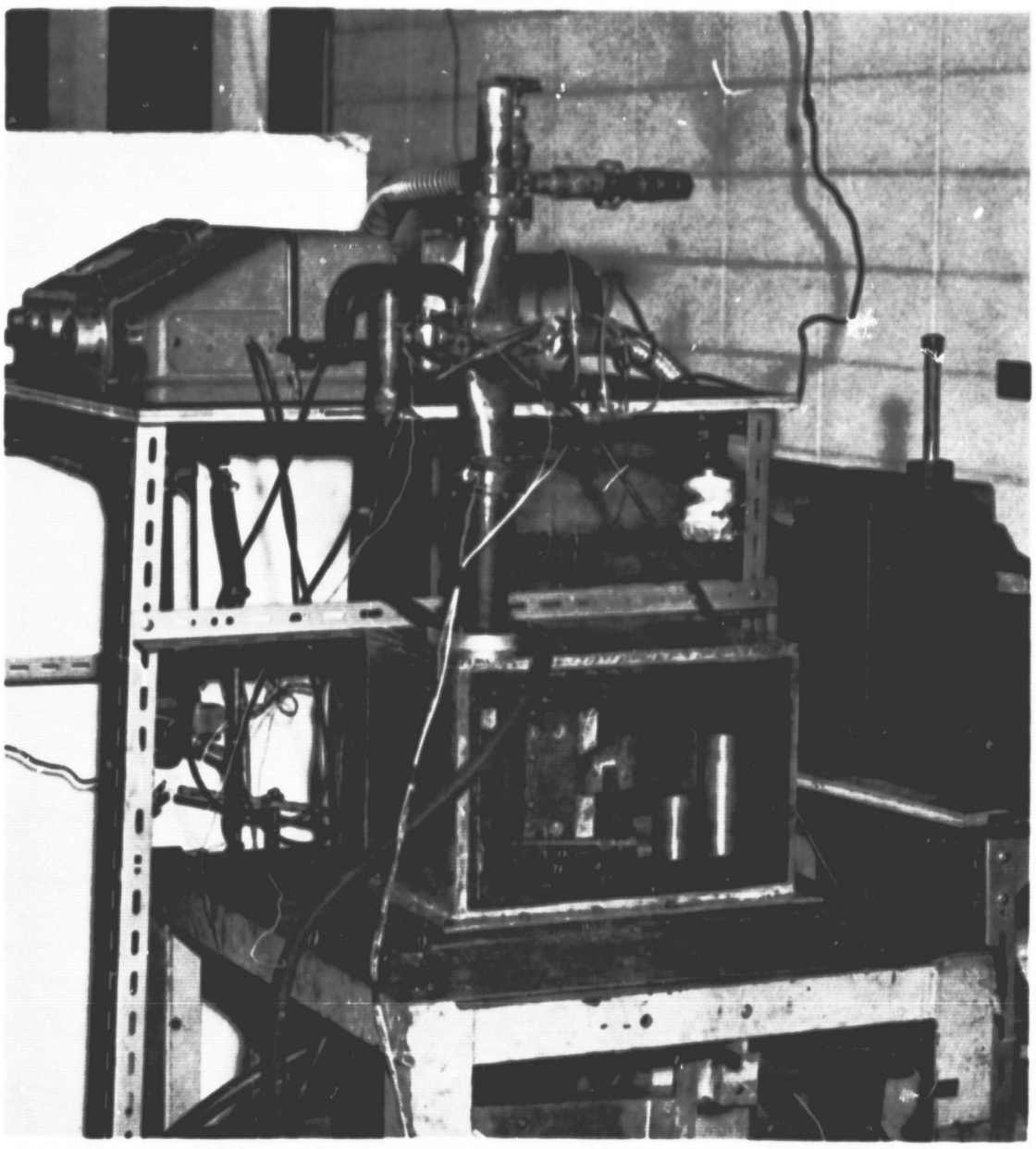

Figure 27. Tungsten Furnace and Some of its Components.

brought up slowly until the desired temperature was achieved, a recorder monitoring the temperature all the while. The temperature measurements from all thermocouples were plotted on a recorder. When they attained steady values, the particle feeder was turned on. The aerosol was introduced first into the surge tank (when the concentration of the particle cloud was not uniform) and then fed to the furnace. The desired particle concentration was detected by the photometer and adjustments were made as necessary. The temperature indications then attained another steady state, giving the data necessary for heat transfer calculations. The system was shut down following a procedure that was the reverse of that outlined except that the cooling system usually was allowed to operate longer to protect the apparatus.

The aerosol was sampled occasionally and the collection weighed to maintain a check on the feeder operation. Little or no change was ever detected unless the feeder was disturbed or a setting changed.

B. Furnace assembly and power supply

The heart of the furnace was the heating element which formed, as nearly as possible, an isothermal, cylindrical enclosure. Test gases and particle-gas mixtures were passed through it, and the gain in heat content was measured. Sheet tungsten 0.005 inch thick was selected as the heating element. A strip of this tungsten was formed into a cylinder with two parallel segments of unbent tungsten leading from one side with a 1/8-inch clearance between them. The parallel segments of the tungsten served as the power leads. Boron nitride, a very effective electrical insulator up to refractory temperatures, separated the power leads. Multiple strips of

tungsten placed in lateral contact with the power leads formed a laminated electrical conductor that reduced the electrical resistance and prevented a disproportionate dissipation of electrical energy along this portion of the circuit.

The cylindrical surface formed by the heating element was extended on both ends by similar tungsten components. These extensions were mounted on the central boron nitride insulator that spanned the total length of the furnace and served as the principal structural member for securing the inner tungsten components of the furnace. A 1/16-inch gap was provided between the heating element and the extension to confine the electrical circuit to the heating element only.

Formation of the cylindrical furnace components from flat tungsten sheet was difficult but critical since the axial alignment and the surface continuity of the heating element and its longitudinal extensions had to be preserved. To meet this requirement the properties of metal had to be considered. A sheet fastened rigidly on one side does not remain cylindrical once formed. Instead, it becomes elliptical when free of restraining forces. The desired shape was preserved, however, by stress relief while retained in the desired form by a temporary mechanical structure. In the case of tungsten, heating to 1800°F accomplished stress relief and did not embrittle the metal, the recrystallization (or embrittlement) temperature for tungsten being somewhat above 1800°F. The boron nitride insulator was cooled by removing the heat through the power leads to a water-cooled coil imbedded in the ground-potential electrode.

Both ends of the annular channel between the inner and outer tungsten

cylinders were sealed by steel caps. The gas or particle clouds could only flow through the inside of the heating element even though there was a gap between the heating element and its extensions. The heat transfer system described up to this point was surrounded by a water-cooled enclosure. The material of this case was copper, since copper has a very high thermal conductivity and provided very effective heat transmission to the cooling water. No removal of heat from the furnace would have been preferred, but the intense heat generated within the apparatus had to be confined. The addition of more adiabatic radiation shields would have been helpful but was impractical in view of the already complex assembly. A compromise was made, therefore, of one adiabatic and one isothermal radiation shield. Excessive heat loss was prevented, nevertheless, by gold plating on the outer shield to reduce radiation losses. The convection heat losses were not prohibitively high. A schematic drawing of the arrangement is shown in Figure 28.

Gas flow into and out of the furnace conduit was through connectors made of steel since temperatures in this region were relatively low. Sauereisen cement (servicable up to 3000°F) sealed the connectors to the tungsten conduit. The ends of the connectors were capped. Swagelock fittings provided for the insertion of thermocouples into the chamber. The upper conduit connector was water cooled where it passed through the protective covering of the furnace assembly. Cooling was attained by circulating water through a channel in the upper sealing ring. The removal of heat at this point was beyond the test region in the aerosol conduit; its removal prevented heat dissipation into the aluminum cover.

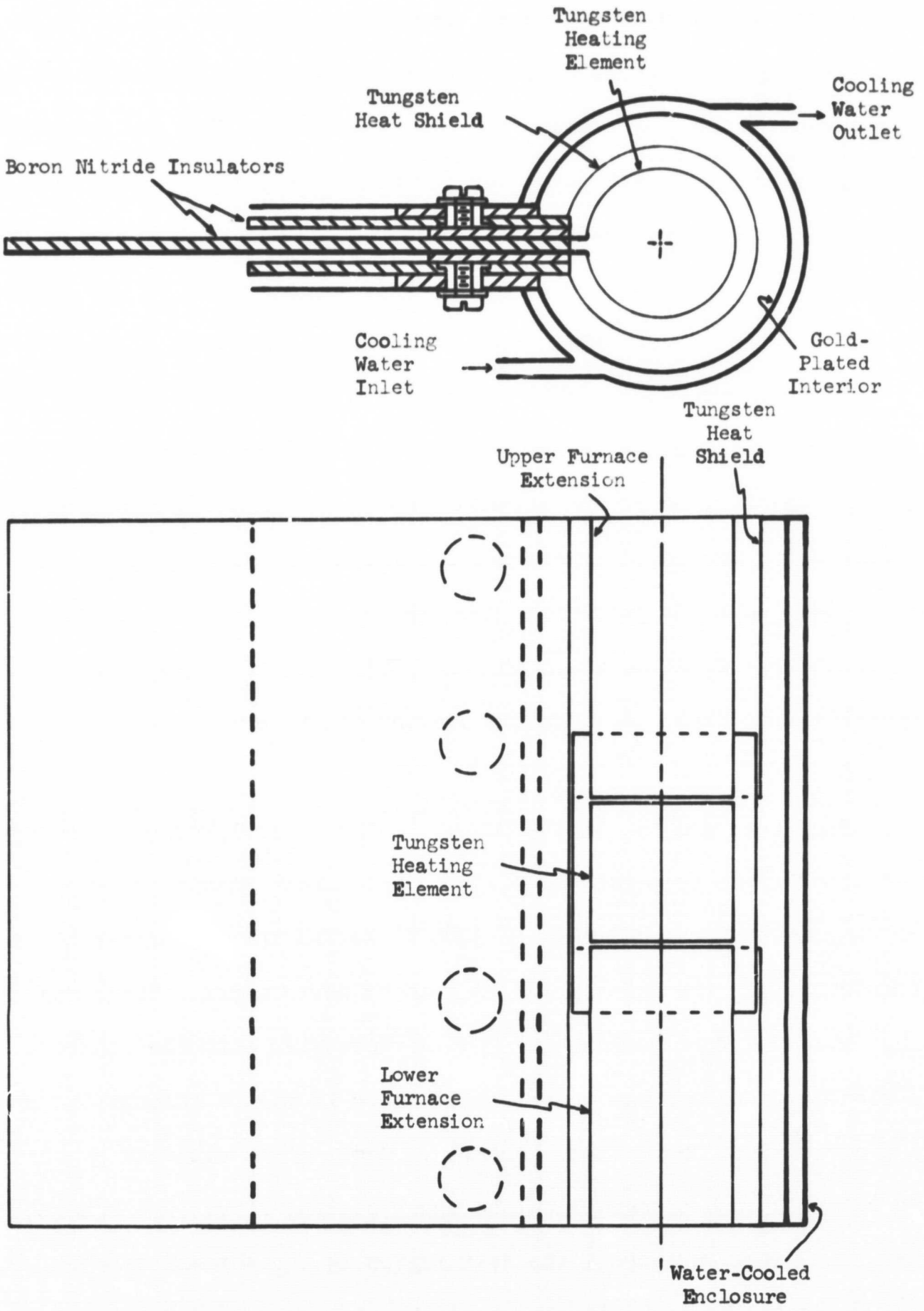

Figure 28. Diagramatic Representation of the Tungsten Furnace.

The power supply of the system could deliver a single-phase current of up to 1200 amperes at 480 volts. The input to the furnace was controlled by a saturable-core reactor, having a capacity of 125 kilowatts. Control of the reactor was achieved with a solid-state circuit that, at full power, delivered 6 amperes and 75 volts of saturating direct current. The alternating power level was monitored by a precision ac ammeter and kilowatt meter. The kilowatt meter allowed the operator to set the power input precisely at the desired level. By recording the voltage and amperage levels during a test, the resistance of the furnace under the test condition could be calculated. These values served to give a check on the furnace temperatures; an optical pyrometer was employed for this purpose. The power control panel and a temperature recorder are shown in Figure 29.

C. Particle cloud generation

A vibration-type generator was used in the early stages of the investigation. The dispersion from it was very good but the cloud was not uniform at high concentrations. An aspirator-type generator was built to solve this problem. The clouds produced from the latter unit appeared uniform to the eyes but fluctuated according to the photometer register. To overcome this the aerosols were passed through a large surge tank incorporating a fan. The aerosols emerging from this tank were quite uniform.

When a long period of operation was desired with a varying aerosol concentration but other factors held constant, a large capacity generator was needed. A stirrer-type generator was built for this purpose; it performed satisfactorily. In some instances the particle clouds produced were so uniform that the surge tank could be bypassed. This eliminated the

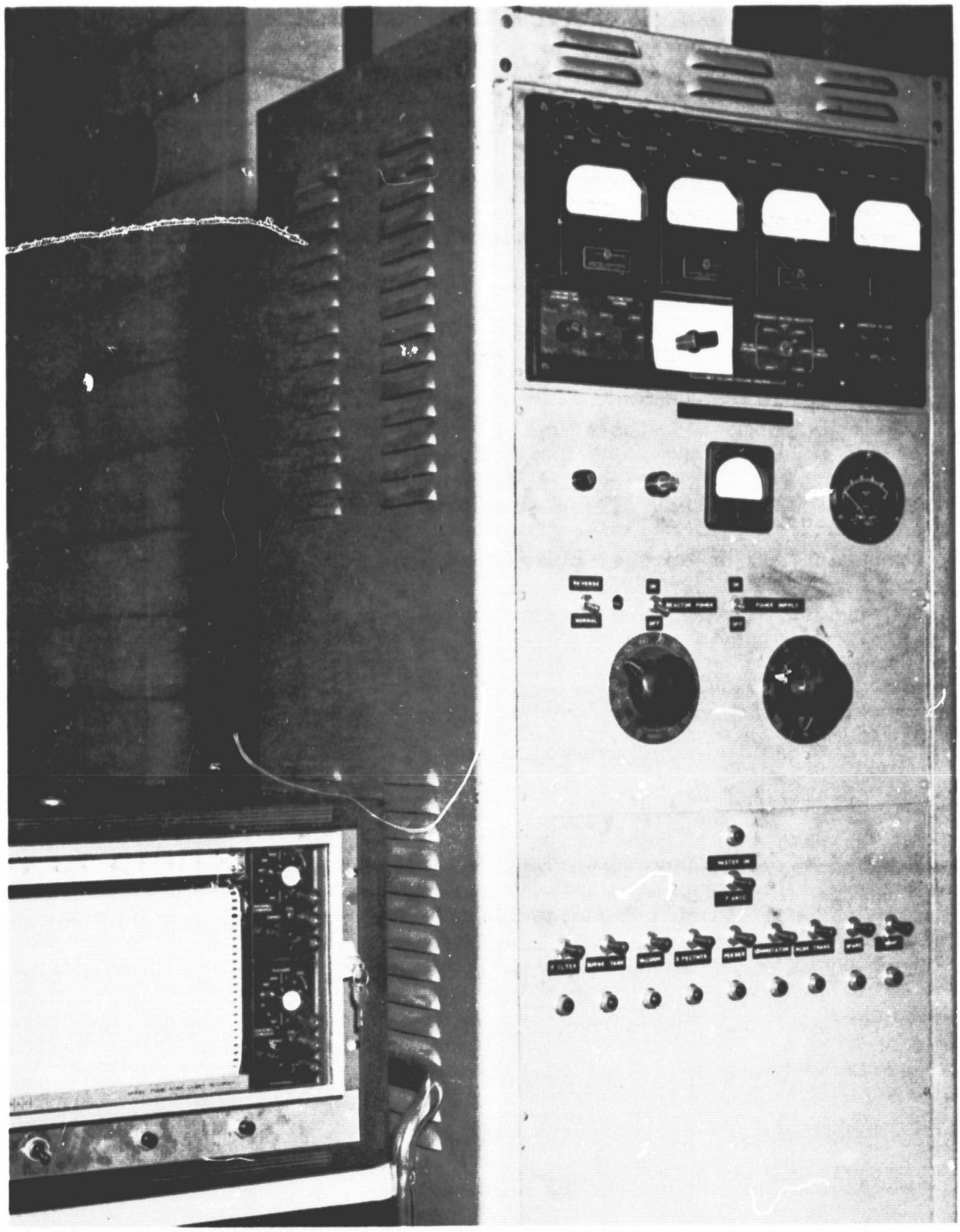

Figure 29. Power Control and Temperature Recorder.

reagglomeration of particles while in the tank and also reduced the possibility of oxygen contamination in the gas which reduced the life of the furnace.

The details of construction of each particle cloud generator are described in Chapter III. The performance of the generator depended greatly on the physical properties and pretreatment of the particles. Nevertheless, the performance of the generators was found to be different from time to time, especially when submicron particles were used, regardless of the pretreatment

D. Measurements of aerosol properties

The aerosol properties of interest were optical density, or transmissivity, and particle load. The former was employed to evaluate the absorption coefficient of the aerosol and the latter to clarify the degree of dispersion and the amount of powder required to absorb a specific quantity of radiant energy.

A Beckman, Model B, spectrophotometer was used initially to measure the transmissivities of the aerosols. It was difficult to keep the windows clean in the standard system, however. Accordingly, a fourteen-inch long by two-inch inside diameter circular section with a rectangular cross-section midway was installed on the furnace outlet. The lamp and photo cell of the spectrophotometer were then physically removed and placed in specially fabricated, air-flushed housings at the ends of the extension. A thermocouple was installed near the center of light beam passage so that the aerosol temperature could be measured as it passed through the extension. This temperature was employed to obtain the true absorption coefficient inside the furnace.

Two methods have been employed to evaluate the particle concentration of the aerosols. One utilized Greenberg-Smith impingers as collectors and a calibrated centrifugal suction pump. Another employed thimble filters instead of the impingers. Samples were taken from the gas stream only when steady-state aerosol flow has been established. With the impinger system, a small amount of detergent was added to the water to aid in the wetting and collection of the particles. The collected matter was recovered by filtering the water through a millipore filter and weighing. With the thimble filter method, the moisture content of the filter itself could have been significant in comparison to the weight of the collected particles. The filters were dried in an oven at identical temperatures before and after the sampling to avoid errors due to a weight change of the filters themselves.

E. Temperature measurements

The main sources of error in measuring the temperature of a gas by means of a thermocouple are (1) the exchange of radiation between the thermocouple and the surroundings, (2) the rate of heat flow by convection along the thermocouple from the gas, and (3) the rate of heat flow along the thermocouple leads by conduction. A protective shield on a thermocouple reduces the radiation exchange mainly to that between the shield and the thermocouple. The reduction differs with the geometry and radiation properties of the system and the shields. Fishenden and Saunders[37] and Bosanquet[38] discuss the wall effect in gas temperature measurements with a thermocouple. McAdams[30] also suggested a few methods of calculating the true gas temperature.

In this study, the measurements of aerosol temperature were made by installing three sets of two thermocouples each symmetrically about the heating element, i.e., so that both the thermocouples of each set would receive the same among the radiation from the heating element if the latter was heated uniformly. Thus it could be assumed that errors will be approximately identical for the thermocouples of a set. The thermocouples were installed at the locations within the furnace as shown in Figure 30.

Initially, the thermocouples were all of chromel-alumel and were not shielded. Soon it was found that thermocouple No. 5 always failed when the furnace temperature was raised above 3500°F. Those thermocouples near the heating element were replaced by platinum-platinum rhodium ones and shielded by rolled platinum covers. Various shapes of shields were tested; the most satisfied one was found to be cone-shaped. At the small end of the cone, a round hole of about 1/8-inch diameter was made. This hole allowed aerosol to pass the thermocouple but stopped all direct radiation from the heating element.

Most of the experimental measurements given in this report were made with thermocouples shielded so as to block more than 80 per cent of the incident radiation. The shields were made as nearly identical as they could be so that equal temperature errors could be assumed, the difference in the temperature of the aerosol entering and leaving being the major concern. As designated on Figure 30, the average value of the difference between thermocouples Nos. 1 and 4, and Nos. 2 and 5 was used as the temperature gain of the aerosol. These two values were usually very close to one another. In case thermocouple No. 5 failed or was moved to another position, the

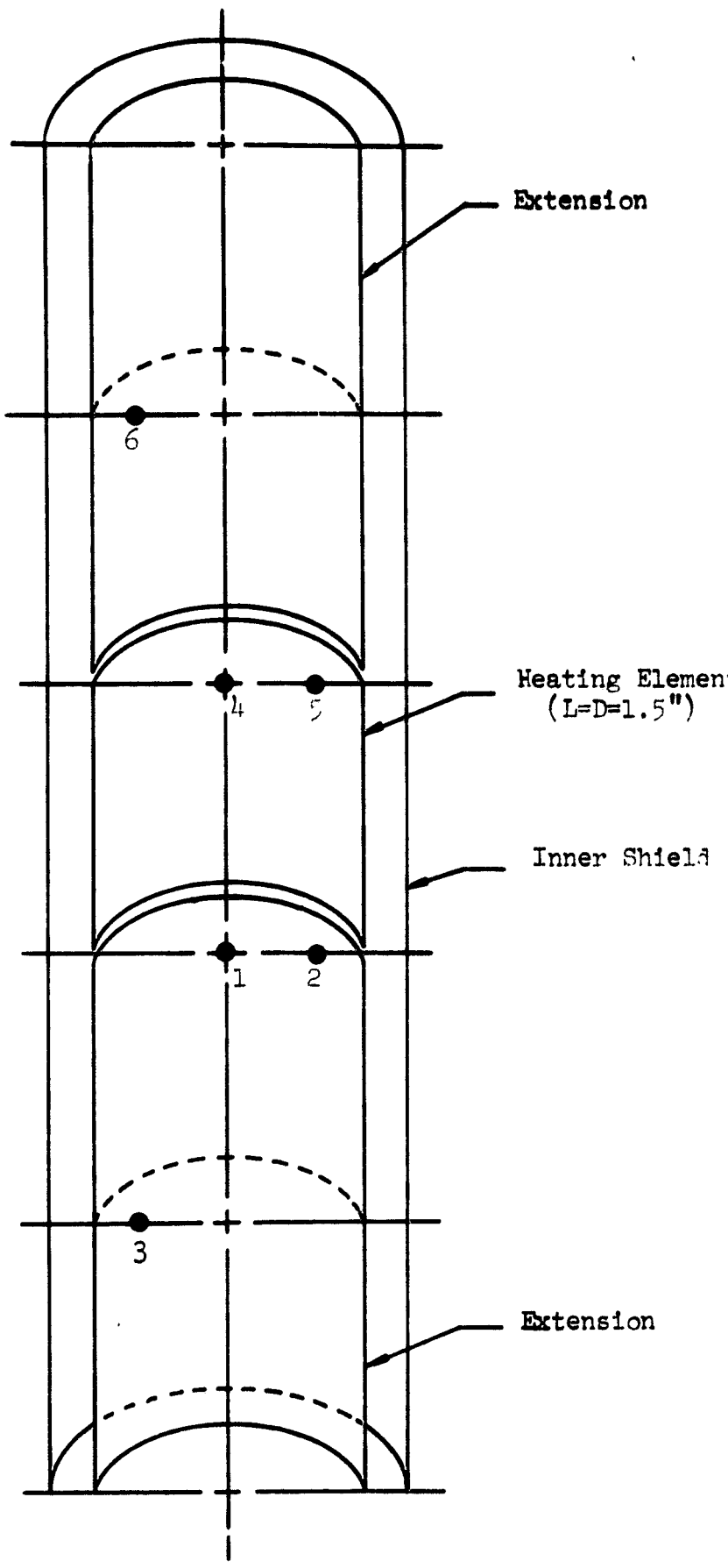

Figure 30. Positions of Thermocouples Inside the Tungsten Furnace.

temperature difference between Nos. 1 and 4 alone could be used for the calculation. Thermocouples Nos. 3 and 6 detected the least error due to radiation, so their indications were used to estimate the absolute temperature of the aerosol in the furnace.

F. Radiation properties of the heating element

An examination of the radiant properties of tungsten was made to support the assumption of angular independence of emissivity and reflectivity. Fresnel's equations are valid for a smooth and homogeneous surface. The main factors affecting radiant properties are the index of refraction n and the absorption coefficient k. The values of n and k for tungsten are 3.47 and 3.26, respectively[36,39] for incident radiation of wavelength 0.5893 micron. The angular reflectivity $\rho(\Phi)$ is one half the sum of the angular reflectivities on the plane of incidence and the plane normal to the plane of incidence with nitrogen gas, for which the index of refraction is one, being the medium.

The angular reflectivities of tungsten are calculated to be as given on Figure 31 using values reported by Holl.[39] If the general Kirchhoff-law relationship applies, the angular emissivities of tungsten can be evaluated with the results being as shown by Figure 32. The values of the monochromatic emissive power of a tungsten surface and a black surface at 4300°F are plotted for comparison in Figure 33. The assumption of diffuse emission for a tungsten surface is believed justified on the basis of Figures 31, 32, and 33. Whether or not a tungsten surface reflects diffusely depends also on the roughness of the surface and the property of the incident radiation. As discussed in Section VII, deviation from diffuse reflection has far less influence on the results than has deviation from diffuse emission.

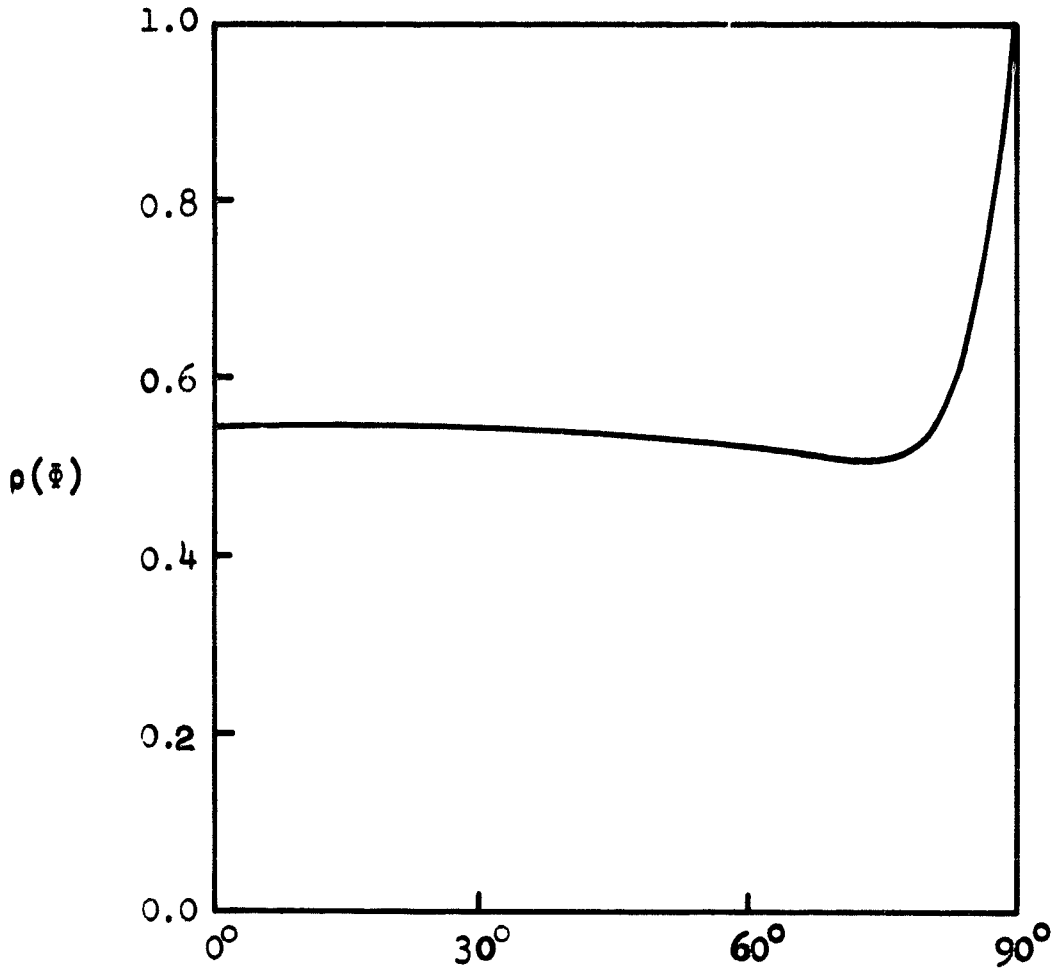

Figure 31. Angular Reflectivity of Tungsten When the Wavelength of the Incident Radiation is 0.5893 Micron.

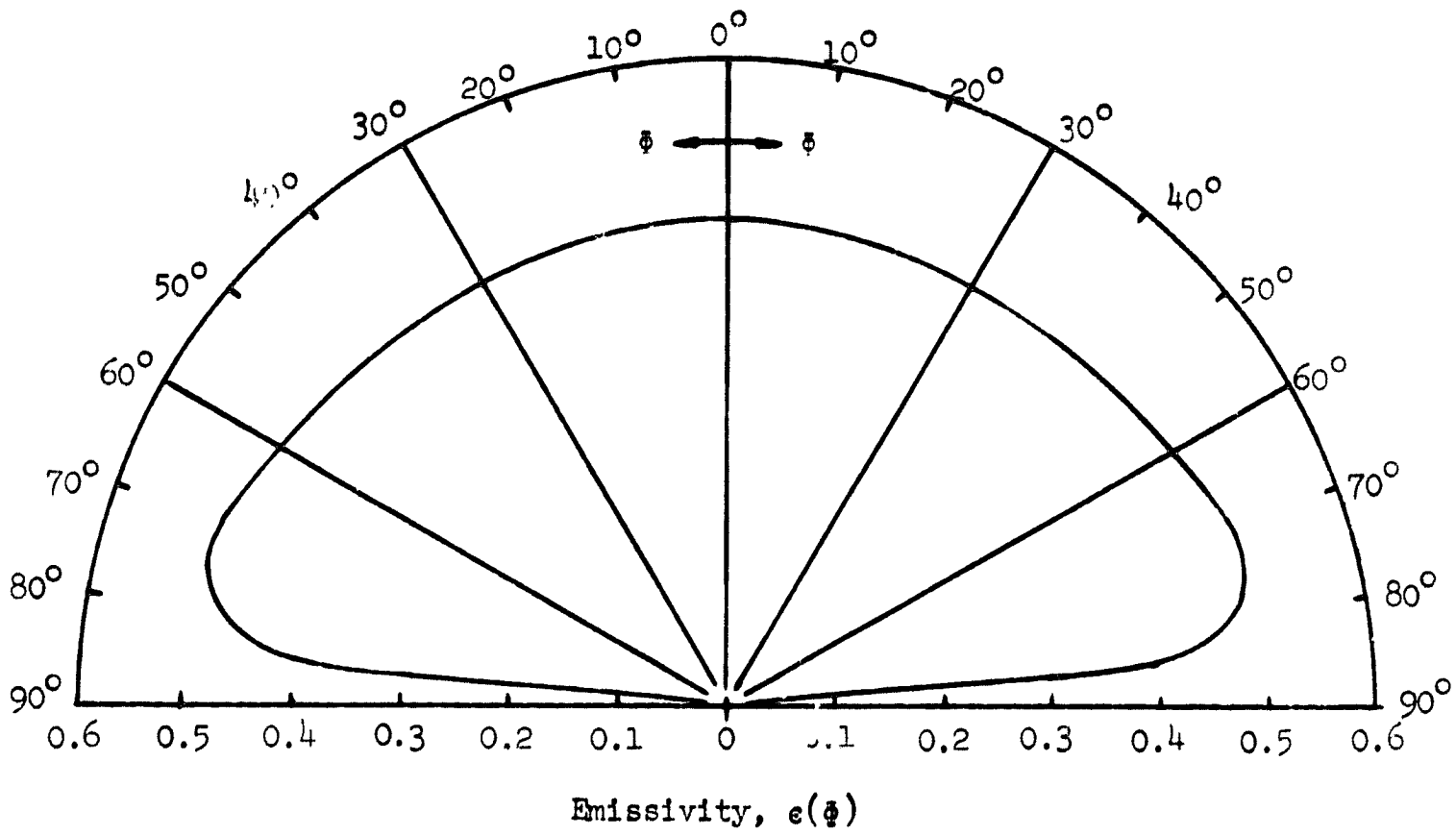

Figure 32. Angular Emissivity of Tungsten When the Wavelength of the Incident Radiation is 0.5893 Micron.

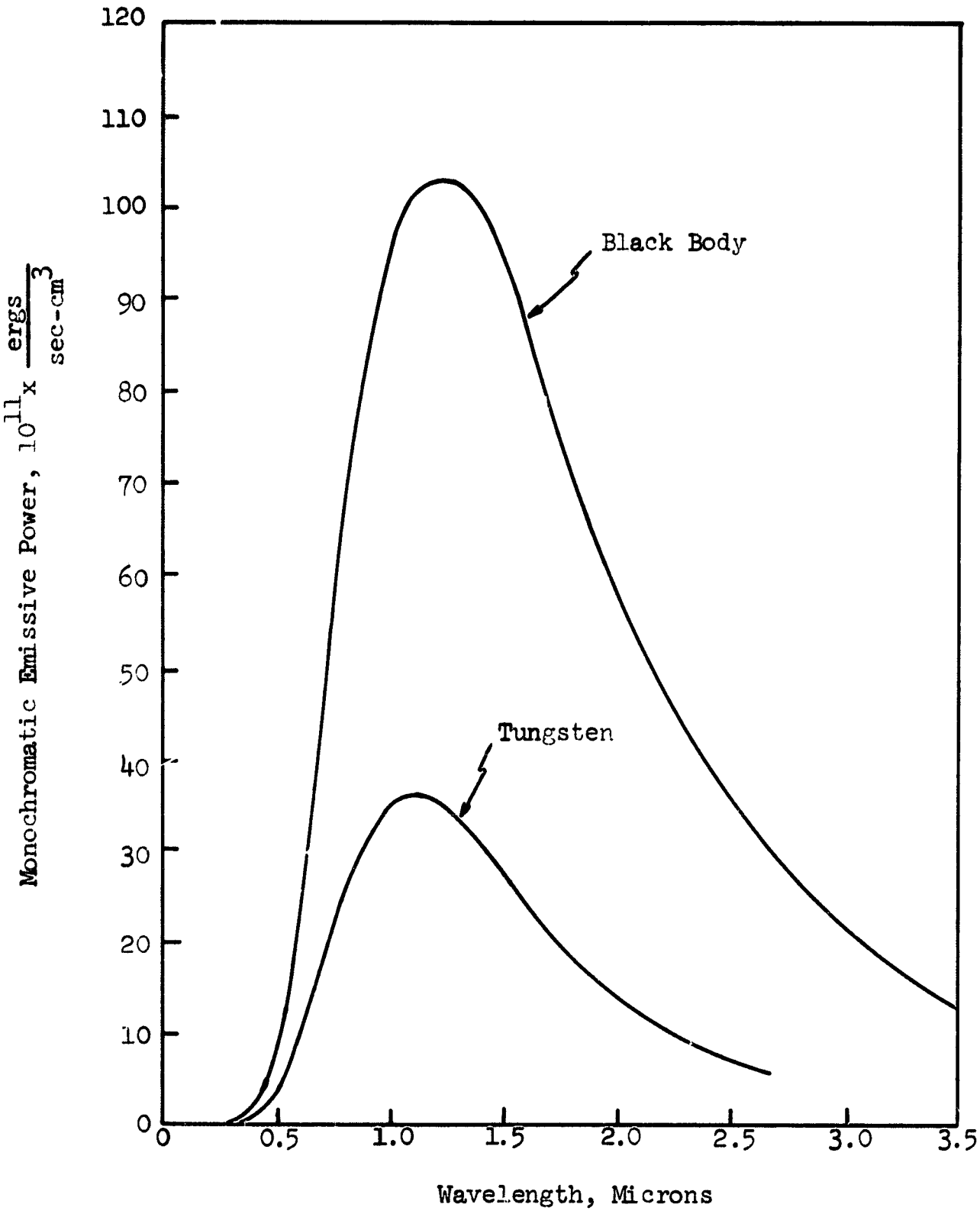

Figure 33. Monochromatic Emissive Power of a Tungsten Surface and a Black Surface at 4300°R.

The values of total emissivity of tungsten were obtained from the Handbook of Chemistry and Physics. There are very little differences between these values and those reported elsewhere.[40]

G. Results and their comparison with theoretical predictions

The total radiant energy emitted from the inside wall of the cylindrical heating element was calculated by

$$q_e = A_w \epsilon \sigma T_w^4 \qquad (103)$$

where A_w is the area of the inside surface of the cylindrical wall (= $2\pi RL$).

The value of the total energy emitted from the inside wall q_e is shown as a function of wall temperature T_w on Figure 34. The absorption efficiency of the aerosol γ is defined as the portion of emitted radiation absorbed by the aerosol. Thus the radiant heat transfer can be calculated by multiplying the emitted energy of the wall by the absorption efficiency of the aerosol.

Radiant heat-transfer rates were obtained by subtracting the heat-transfer rates by conduction and convection from the measured overall values. A blank test, or one with no particles seeded, was made prior to each test when particles were added. This approach is not quite ideal because the temperature of the gas medium is not exactly the same between unseeded and seeded gas at a given location inside the furnace. Fortunately, the temperature measurements showed that the mean temperature difference between the wall and the gas medium was nearly the same in both cases. This is to be expected because the entrance temperature of the gas was somewhat greater when unseeded than when seeded due to more radiant energy being transferred beyond the

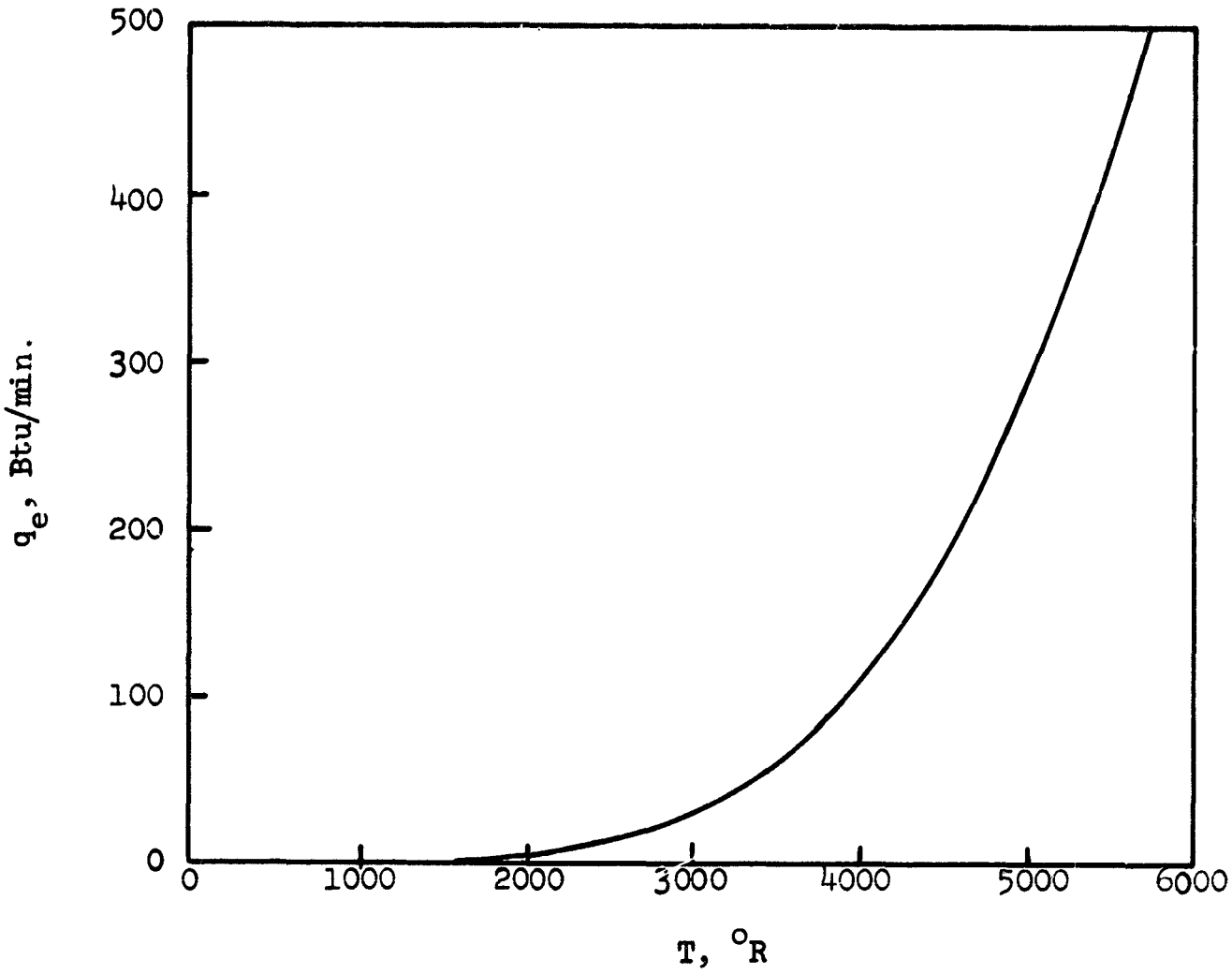

Figure 34. Total Radiant Energy Emitted from the Inside Wall of a Tungsten Cylinder with L = D = 1.5 in.

limits of the furnace. The results are presented in Figure 35. The theoretical curves are based on the assumption that a tungsten surface behaves like a gray body. The difference between the 3500°R and 4600°F curves in Figure 35 is due to the difference in emissivity and reflectivity. In general, surfaces with lesser emissivities but greater reflectivities give greater efficiencies but lesser overall radiant-heat-transfer rates. This is due to the fact that initial radiations emitted from those surfaces are less.

Total heat transfer rates at 3670°R are presented in Figure 36. The experimental data were calculated directly from the temperature measurements without corrections for convective heat transfer. The predicted curve represents the sum of the theoretically predicted radiant heat transfer rate and the experimentally measured convective heat transfer rate with particle-free nitrogen gas. Results showed that the total heat transfer rate was essentially doubled when pure nitrogen was seeded with carbon black to a volumetric concentration of only 10 ppm.

Particle clouds of Linde-B alumina (Linde Division, Carbide and Carbon Chemical Corp.) and tungsten (Fisher Scientific Company) were also tested. Linde-B alumina powder is white and the diameters of its particles are in the submicron range. Absorption efficiencies measured for Linde-B were lower than for carbon black because of its non-black surface. Particle clouds of Linde-B also contained many agglomerates. The value of the absorptivity of the material as a flat surface thus cannot be taken as the absorptivity of the surface of the particles. The absorptivity of Linde-B particles as revealed by the experimental data given in Figure 37 was about

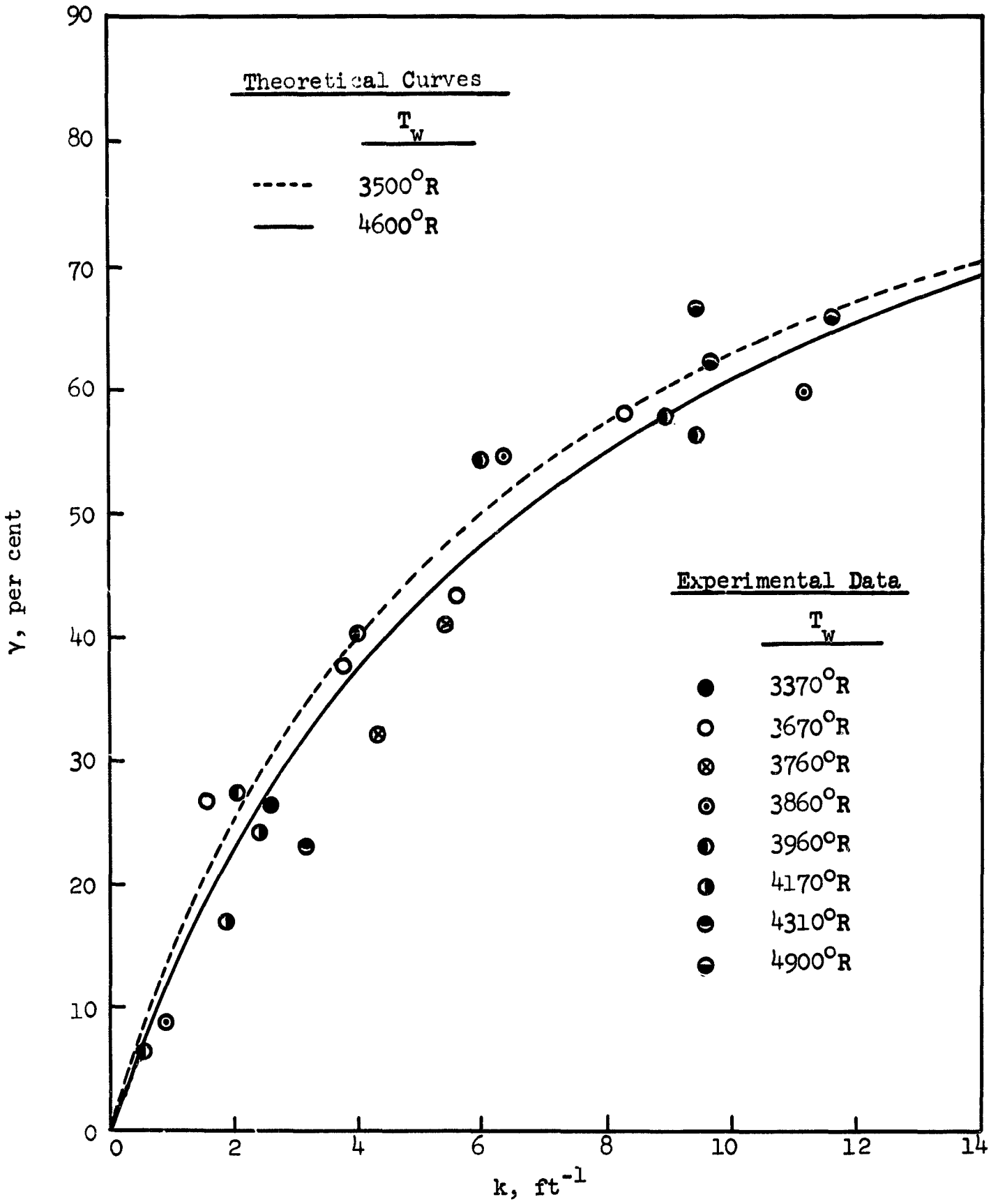

Figure 35. Absorption Efficiency of Carbon Black Aerosols in a Cylindrical Tungsten Furnace.

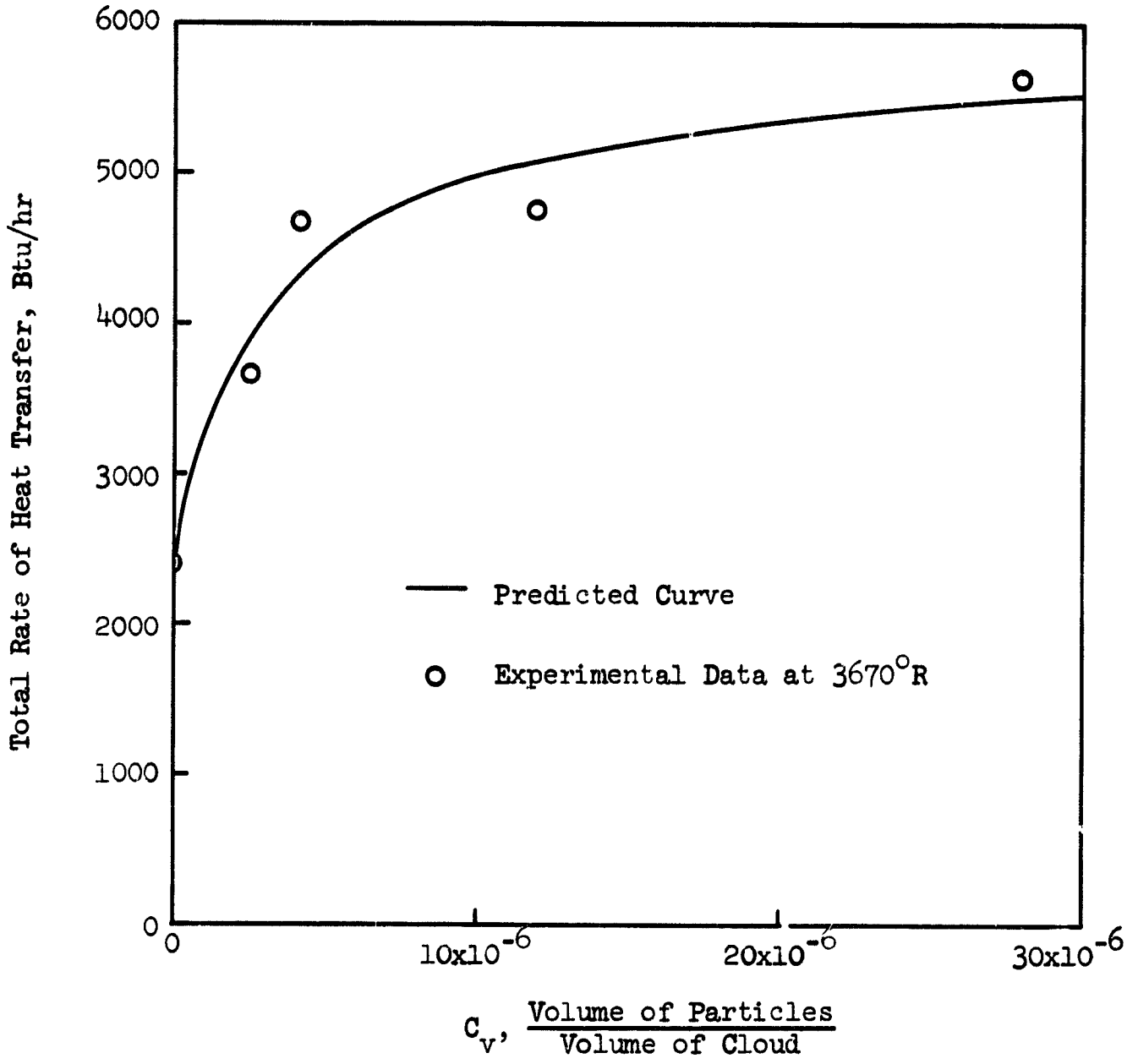

Figure 36. Total Rate of Heat Transfer to Carbon Black Particle Clouds as a Function of Particle Volumetric Concentration.

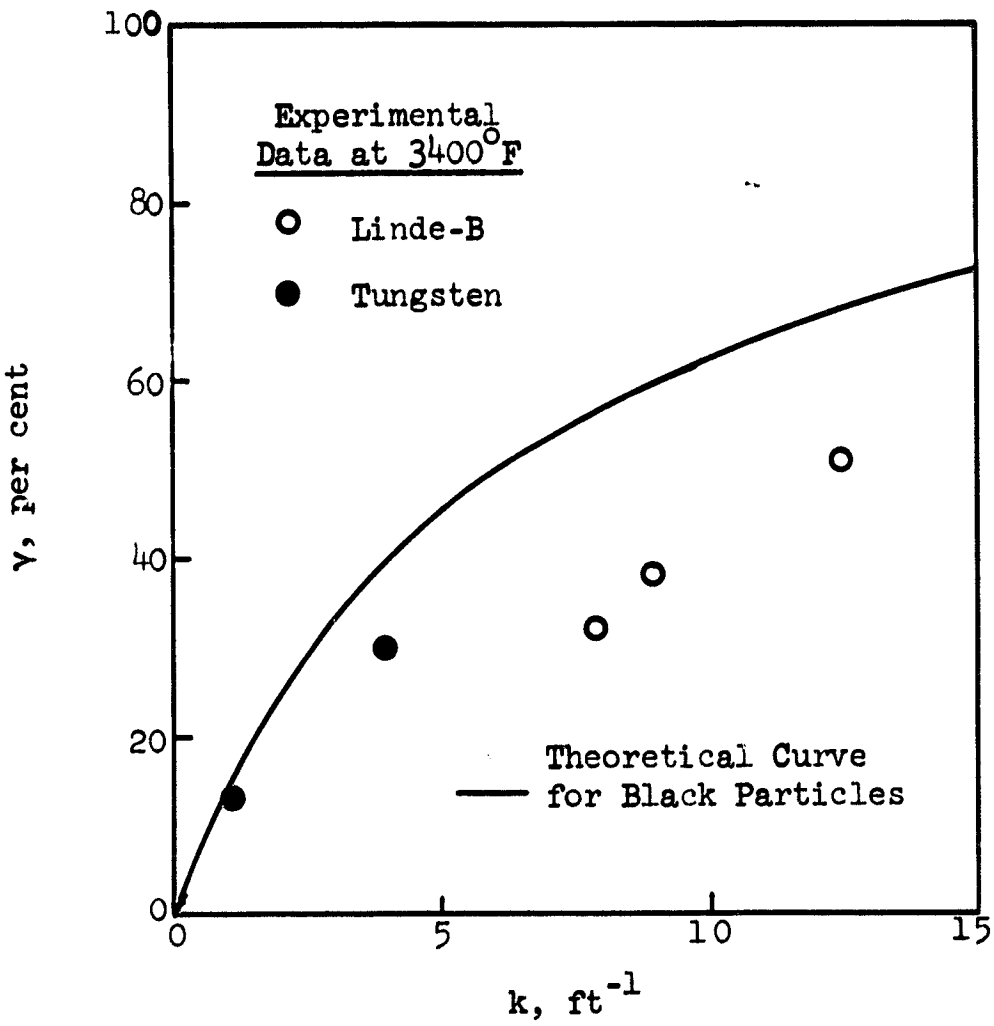

Figure 37. Absorption Efficiency of Linde-B and Tungsten Particle Clouds in a Cylindrical Tungsten Furnace.

0.65. This value was somewhat higher than the value for a flat surface because the agglomerated particles absorbed the reflected radiation from themselves. The net radiant energy absorbed by an agglomerated particle or a particle with rough surface is always higher than a smooth solid sphere of equivalent diameter except for black particles.

Irregularities were observed when tungsten particles were employed. The reliability of the data was thus questionable. The surface of the heating element was usually clean after a test with carbon black clouds, but a relatively heavy deposit of tungsten particles was found after each test with a tungsten cloud. As Figure 38(a) shows, the deposit formed only on the heating element and not on the extensions which were made of the same material, viz., tungsten. Electric power, which was fed only to the heating element, apparently created an electric field and caused the deposition. Figure 38(b) shows three heating elements. The one on the left is new. The one in the middle was used in tests with carbon black clouds. It was broken during disassembly of the furnace, but its surface was clean. The one at the right represents a typical heating element after a test with tungsten. The deposit could be scraped off easily and no fusion between the particles and the surface of the element was evident. The deposit altered the resistance of the heating element and its temperature, however. The emissive property of the surface was also changed. Only the initial temperatures of a test were employed to calculate the data presented in Figure 37. It is questionable if equilibrium and steady state were achieved, however.

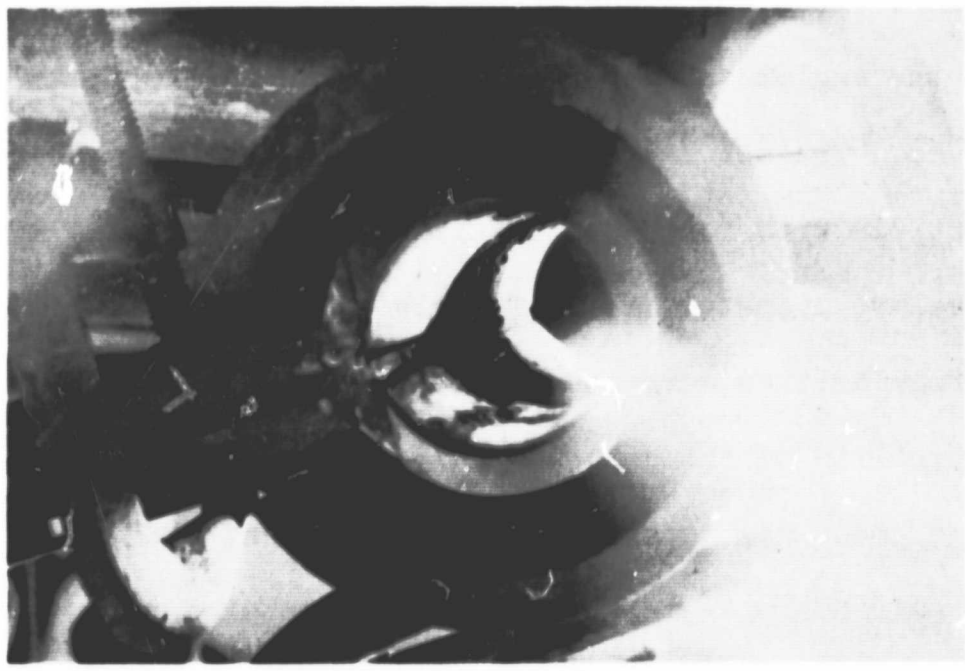

(a) HEATING ELEMENT IN FURNACE

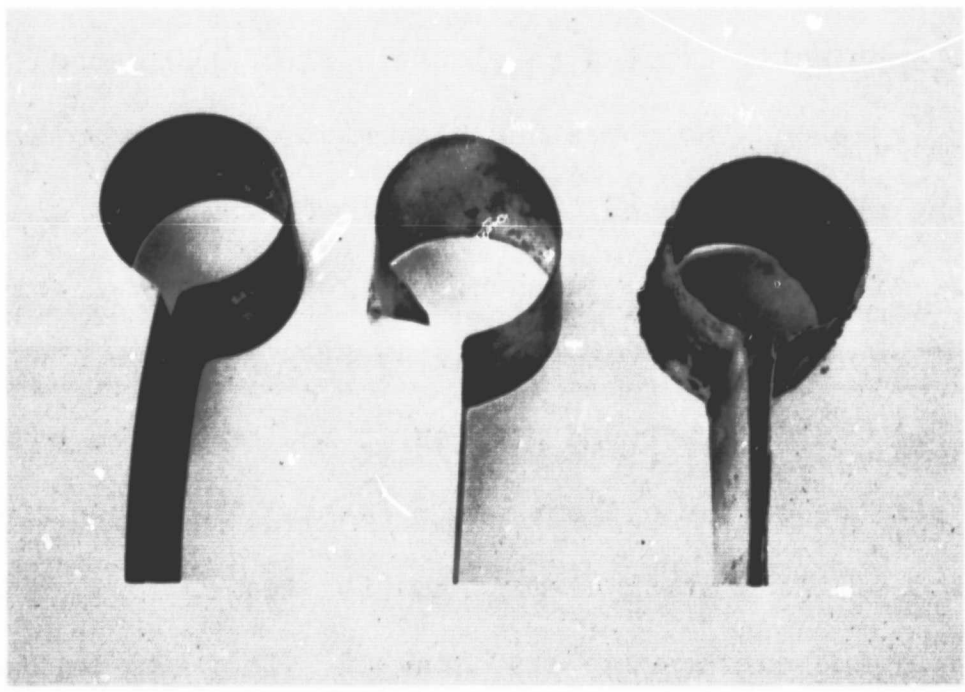

(b) COMPARISON OF THREE HEATING ELEMENTS

Figure 38. Deposition of Tungsten Particles on the Tungsten Heating Element.

IX. STUDY OF PARTICLE DISAPPEARANCE IN RADIANT FIELDS

A. Background of the study

If particles are used to seed the propellant in some future gaseous-core, nuclear rocket, the lifetime and vaporization or sublimation rates of the particles must be well understood. The particles must not lose their absorption function before the propellant gas itself reaches a sufficiently high temperature to become absorbant. If a so-called "window" exists in the propellant system the vessel wall may be damaged.

Theoretically, this rate of disappearance is a very complex problem involving simultaneously momentum, heat, and mass transfer. The heat transfer rate is the most important and it involves conduction, convection, and radiation, the latter being of major concern. The properties of the aerosol mainly involve the concentration and size distribution of the particles; these factors will vary both radially and longitudinally in a cylindrical system if the particles are vaporizing or sublimating. It is expected that a boundary will be formed within the aerosol on one side of which there will be no particles.

Williams[41] studied the vaporization of mist by radiation by assuming uniform radiant energy flux, steady state, and the particles to be nearly transparent spheres. This analysis provides a good starting place for this study. Other sources[42,43] utilizing much simplified conditions are available. No information concerning vaporization and sublimation occuring in a flowing aerosol has been found in the literature.

B. Experimental studies and discussion

The purpose of the experimental work was to find out whether or not the phenomenon of particle disappearance could be investigated in a radiant field generated by an electrically heated furnace. In order to reduce the effects by the heat transferred by convection and conduction, the experimental apparatus was built to avoid direct contact of the aerosol and the hot surface of the heating element.

The radiant heater, which is shown in Figures 39 and 40 consisted of a tungsten heating element, an enclosure, a square glass window, and a cooling system for the enclosure and the window. The heating element was made of a 0.005 inch thick sheet. The element was 3 inches wide by 11 inches long. It was cut into five strips in such a way that each was connected to others at only one end. The resistance crossing the heating element thus was relatively high and the controlling reactor would not be overloaded even at the maximum power the heating element could withstand. The effective heating area was 3 inches by 9 inches as shown in Figure 41. The enclosure was made of brass and the inside was partially gold plated to reduce the absorption of radiation. It was water-cooled, and rubber O-rings were used to seal the top and the window. Several window plates were used; they were 1/8-inch thick pyrex glass and 1/4-inch pyrex and quartz plates. The size of the window was 4 inches by 10 inches. An air cooling system was built outside the window to cool both the window as well as the near side of the rectangular conduit.

The aerosol conduit was made of pyrex glass with a cross-section of 3 inches by 5 inches. The conduit was 2 feet long with aluminum extensions

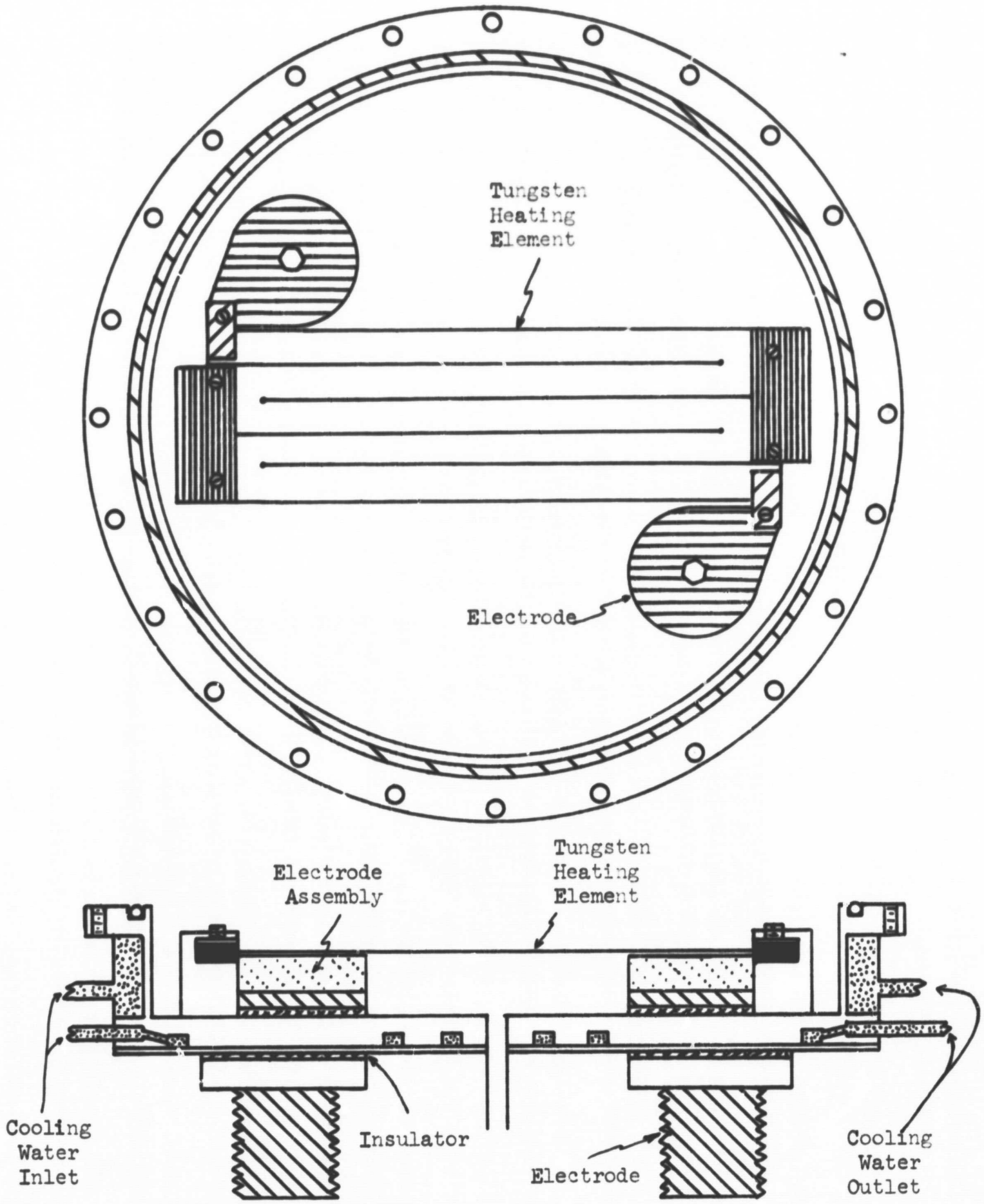

Figure 39. Front and Side Views of the Radiant Heater with Top Removed.

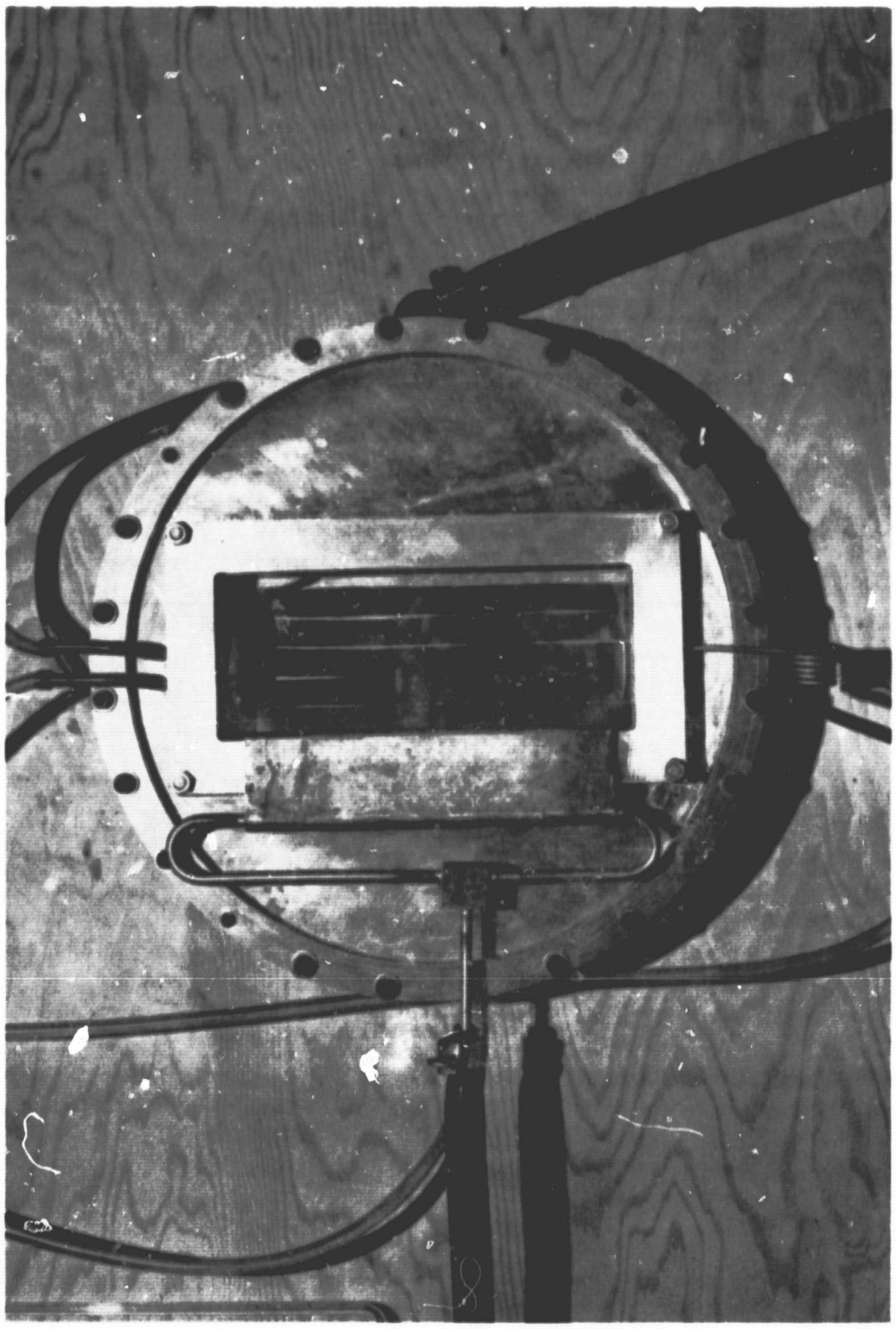

Figure 40. Radiant Heater for Particle Disappearance Studies.

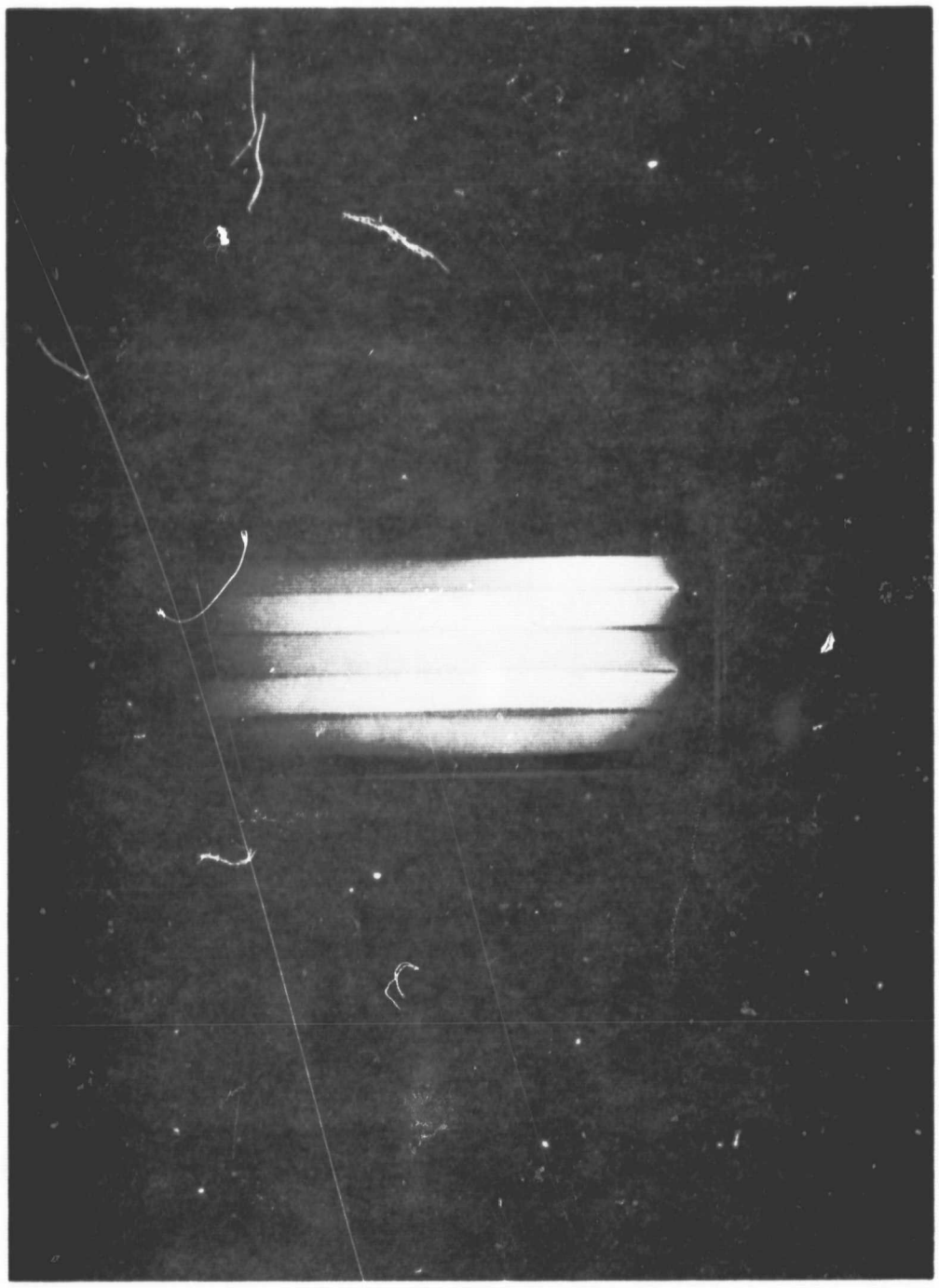

Figure 41. Heating Element of the Radiant Heater with Power On.

on both ends. The inlet section was 3 feet long and the outlet section 1 foot. The arrangement of the conduit is shown in Figure 42.

A water aerosol was generated by an ultrasonic nebulizer (DeVilbiss Model 880). An outside air supply was used so that the concentration and flow rate of the aerosol could be controlled.

To make a test, the aerosol was introduced into the conduit first. A few minutes were usually required to reach a steady flow. Then the cooling air and water were turned on. The power supply was next turned on with a shorting bar placed between the two electrodes as insurance against an initial voltage surge that could damage the heating element. Then the shorting bar was removed. The power controller, finally, was activated until the desired temperature was achieved.

Many tests were made but no significant aerosol disappearance was detected. The water droplets could be seen to evaporate gradually as they passed the radiant field but no clear boundary was observed. The temperature was increased until either the heating element burned out or the window cracked. The enclosure was operated either under vacuum conditions or with helium gas at atmospheric pressure. It was found that a window of 1/8-inch pyrex glass performed when the enclosure was filled with helium gas just as satisfactorily as either the 1/4-inch quartz or pyrex glass either under vacuum or filled with helium. A clean "particulate-free" zone never occurred.

The failure of this experiment is mainly attributed to the lack of a sufficiently intense radiant field and the weak absorption of the fine water mist. A more intense radiant heater than could be obtained was

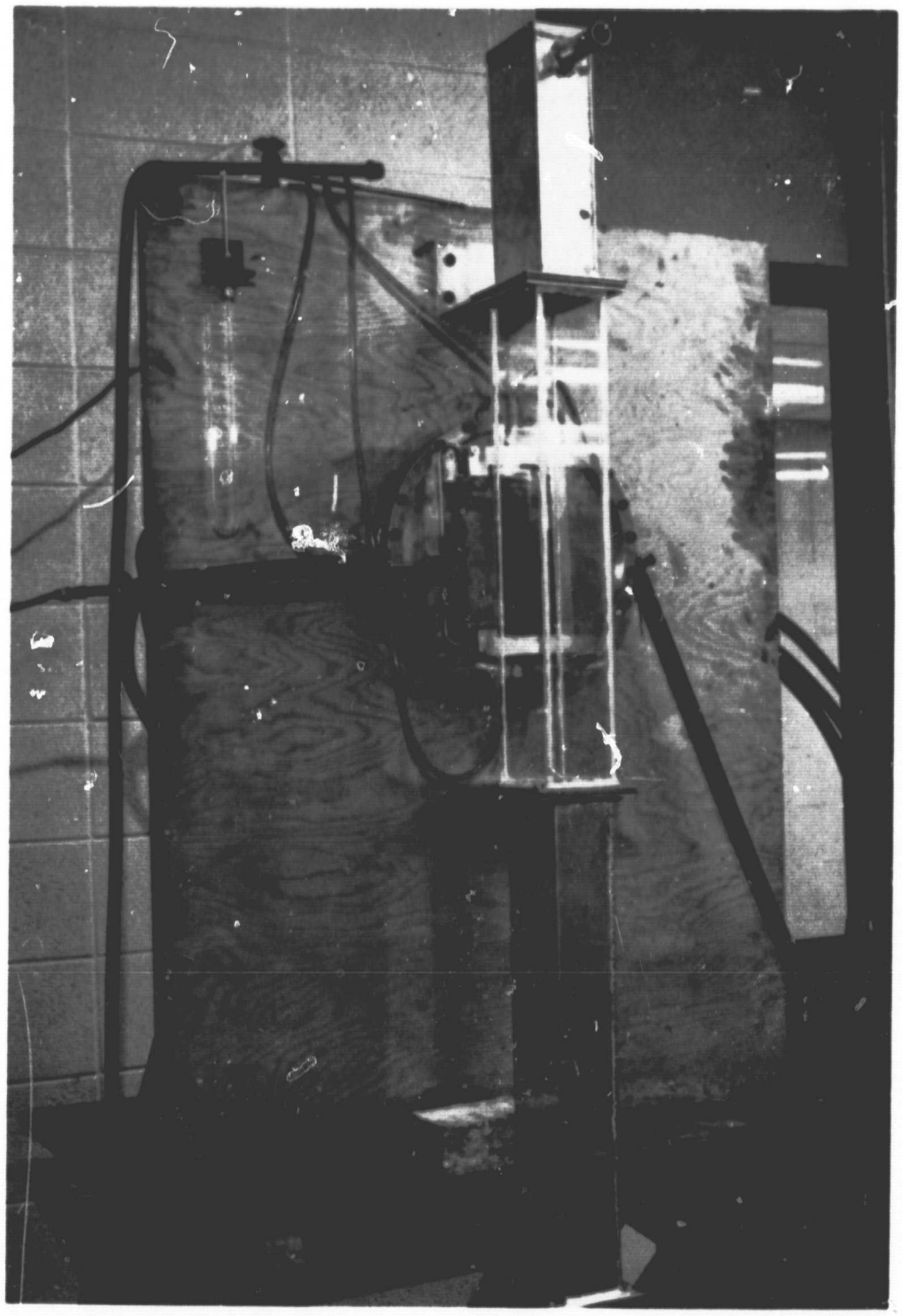

Figure 42. Aerosol Conduit and Radiant Heater.

needed to vaporize such particulates and also more absorbing particulates could have been used. Black ink, for example, added to the water would increase the absorption to some degree.

X. CONCLUDING REMARKS AND RECOMMENDATIONS

The primary purpose of this study was to investigate radiant heat transfer to particle clouds. Many aspects of the problem, both directly and indirectly involved, were studied. Concluding remarks on each of these studies are as follows:

1. Particle clouds having uniform density and a specific concentration are difficult to generate especially when the particle diameter is below one micron. Four types of cloud generators were designed, constructed, modified, and tested. Main factors to be considered in choosing a cloud generator are particle size, density, and surface condition; electrostatic charge generation; desired cloud properties such as optical density, particle concentration, and dispersion condition; quantity of cloud generated per unit time; and the time for generation of the cloud without a stop for refilling. High pressure is required for good dispersion. However, the effectiveness of increasing pressure is gradually diminished as the pressure rises. Complete dispersion of fine particles such as carbon black has not been accomplished with existing techniques.

2. Carbon black clouds yield the highest extinction coefficient among all the materials tested at the same volumetric concentration. The transmissivity of carbon black clouds is essentially independent of the wavelength of the radiation in the range from 0.4 to 0.65 micron.

3. Equations were derived for the rate of radiant heat transfer to black-particle clouds in terms of the mean beam length, particle concentration, particle density, and particle size. Experimental results are in good

agreement with the theoretical predictions. Systems of reflective particles require consideration of the absorption of reflected radiation. A rigorous analysis was not made.

4. View factors were evaluated for black, cylindrical systems by a combination of analytical and numerical methods. These results are presented by figures. Equations were derived for evaluating view factors for non-black body systems from view factor values of black systems.

5. Equations for view factors among zones of any size were also derived. Methods were presented for attacking problems of non-isothermal emission and variable absorption conditions by employing the basic equations for view factors among zones. The rate of radiant absorption of any zone in a conduit thus can be calculated. If the convective heat transfer coefficient is known, the total heat transfer at any local section of any size can be predicted.

6. A cylindrical tungsten furnace (L = D = 1.5 in.) was constructed and tested. The maximum temperature achieved was $4900^{\circ}R$. Radiant heat transfer measurements to carbon black clouds made with it yielded results in good agreement with theoretical calculations that assumed the tungsten surface gray. Irregularity was observed when tungsten particles were used.

7. Particle disappearance in radiant fields was investigated, but satisfactory results were not obtained. The tungsten heating element as employed was not able to generate enough radiant energy to permit obtaining meaningful results. Either a more intense source of radiation must be formed or the clouds must pass directly over the source to give additional heat from the convective process.

Recommendations for future studies are as follows:

1. View factors should be determined for systems having essentially the geometry of conceptual nuclear rocket engines by a combination of analytical and numerical approaches.

2. Back radiation from the aerosol to the surrounding surfaces should be investigated with respect to the particle properties and the system geometry.

3. Theoretical solutions should be further checked by experimental evaluation with emphasis placed on systems of non-uniform emitting surfaces and absorbing media. The equations for radiant heat transfer among zones also need to be confirmed experimentally.

4. Absorption properties of clouds consisting of reflective particles and translucent droplets should be obtained in case non-black particles are selected as the seed material and the particles may melt to droplets before gasification occurs.

5. Further theoretical and experimental investigations should be undertaken into the generation of well-dispersed particle clouds.

6. A high intensity radiation source is needed for particle gasification studies. Theoretical analysis of the gasification of particles in radiant fields and the effects of gasification on the absorption characteristics of the seeded gas are also needed.

Respectfully submitted:

Clyde Orr, Jr.

Clyde Orr, Jr.
Project Director

Approved:

Frederick Bellinger

Frederick Bellinger, Chief
Chem. Sci. and Materials Division

REFERENCES

1. Howell, J. R. and M. K. Strite, Analysis of Heat Transfer Effects in Rocket Nozzles Operating with Very High-Temperature Hydrogen, NASA TR R-220, National Aeronautics and Space Administration, Lewis Research Center, Cleveland, Ohio, 1965.

2. Krascella, N. L., Tables of the Composition, Opacity, and Thermodynamic Properties of Hydrogen at High Temperatures, NASA SP-3005, Washington, D. C., 1963.

3. Burkig, V. C., Thermal Absorption in Seeded Gases, Douglas Report DAC-59985, Douglas Aircraft Company, Inc., Missile and Space Systems Division, Santa Monica, California, 1967.

4. Krascella, N. L., Theoretical Investigation of the Absorption and Scattering Characteristics of Small Particles, United Aircraft Corporation Research Laboratories Report C-910092-1, 1964.

5. Marteney, P. J., Experimental Investigation of the Opacity of Small Particles, United Aircraft Corporation Research Laboratories Report C-910092-2, 1964.

6. Hottel, H. C. and E. S. Cohen, "Radiant Heat Exchange in a Gas-filled Enclosure: Allowance for Non-uniformity of Gas Temperature," American Institute of Chemical Engineers Journal 4, 3-14 (1958).

7. Erkku, H., Radiant Heat Exchange in Gas-filled Slabs and Cylinders, Ph.D. Thesis, Massachusetts Institute of Technology, 1959.

8. Hoffman, T. W. and W. H. Gauvin, "An Analysis of Spray Evaporation in a High Temperature Environment, I. Radiant Heat Transfer to Clouds of Droplets and Particles," Canadian Journal of Chemical Engineering 39, 179-88 (1961).

9. Hoffman, T. W., Theoretical and Experimental Investigation of the Evaporation of Stationary Droplets and Sprays in High Temperature Surroundings, Ph.D. Thesis, McGill University, Canada, 1959.

10. Einstein, T. H., Radiant Heat Transfer to Absorbing Gases Enclosed in a Circular Pipe with Conduction, Gas Flow and Internal Heat Generation, NASA TR R-156, National Aeronautics and Space Administration, Washington, D. C., 1963.

11. Edwards, D. K. and K. E. Nelson, "Rapid Calculation of Radiant Energy Transfer Between Nongray Walls and Isothermal H_2O or CO_2 Gas," Journal of Heat Transfer, Transactions of the American Society of Mechanical Engineers 84, 273-8 (1962).

12. Heaslet, Max and R. F. Warming, "Radiative Transport and Wall Temperature Slip in an Absorption Planar Medium," International Journal of Heat and Mass Transfer 8, 979-994 (1965).

13. Love. T. J. and R. J. Grosh, "Radiative Heat Transfer in Absorption, Emitting, and Scattering Media," Journal of Heat Transfer, Transactions of the American Society of Mechanical Engineers 87, 161-6 (1965).

14. Viskanta, R. and R. J. Grosh, "Heat Transfer in a Thermal Radiation Absorbing and Scattering Medium," International Developments in Heat Transfer, Part IV, ASME, 820-8 (1961).

15. McAlister, J. A., E. Y.H. Keng, and C. Orr, Jr., Heat Transfer to a Gas Containing a Cloud of Particles, NASA CR-325, National Aeronautics and Space Administration, Washington, D. C., 1965.

16. Hamaker, H. C., "The London-van der Waals Attraction Between Spherical Particles," Physica 4, 1058-72 (1937).

17. Haerns, Manfred, "Effect of Interparticle Adhesive Forces on Fluidization of Fine Particles," Industrial and Engineering Chemistry Fundamentals 5, No. 4, 508-16 (1966).

18. Krupp, H. and G. Sperling, "Theory of Adhesion of Small Particles," Journal of Applied Physics 37, No. 11, 4176-80 (1966).

19. Kordecki, M. C. and C. Orr, Jr., "Adhesion of Solid Particles to Solid Surfaces," Archives of Environmental Health 1, 1-9 (1960).

20. McFarlane, J. S. and D. Tabor, "Adhesion of Solids and the Effect of Surface Films," Proceedings of the Royal Society A 202, 224-43 (1950).

21. Morgan, B. B., "The Adhesion and Cohesion of Fine Particles," British Coal Utilization Research Association 25, 125-37 (1961).

22. Keng, E. Y.H. and C. Orr, Jr., "Particle Size and the Rate of Radiant Heat Transfer to Gas-Suspended Particles," Powder Technology 1, 323-7 (1968).

23. Burson, J. H., III, E. Y.H. Keng, and C. Orr, Jr., The Influence of Electrostatic Effects on the Dispersion of Organic Powders, Final Report under Contract No. DA18-035-AMC-1058(A), Georgia Institute of Technology, Atlanta (1968).

24. Williams, J. R., A. S. Shensy, and J. D. Clement, "Radiant Propellant Heating in the Gaseous Core Nuclear Rocket," AIAA 4th Propulsion Joint Specialist Conference, Cleveland, Ohio (1968).

25. Cadle, R. D., Particle Size, Reinhold Publishing Corporation, New York, 1965.

26. Sinclair, D., "Optical Properties of Aerosols," Handbook of Aerosols, Atomic Energy Commission, Washington, D. C. (1950).

27. Hottel, H. C. and A. F. Sarofim, Radiative Transfer, McGraw-Hill Book Company, New York, 1967.

28. McAlister, J. A., E. Y.H. Keng, and C. Orr, Jr., Heat Transfer to a Gas Containing a Cloud of Particles, NASA CR-54441, National Aeronautics and Space Administration, Washington, D. C., 1965.

29. DallaValle, J. M., Micromeritics, Second Edition, Pitman Publishing Corporation, New York, Chapter 3, 1948.

30. McAdams, W. H., Heat Transmission, Third Edition, McGraw-Hill Book Company, Inc., New York, Chapter 4, 1954.

31. Wiebelt, J. A., Engineering Radiation Heat Transfer, Holt, Rinehart, and Winston, Inc., New York, Chapter 7, 1966.

32. Tien, C. L., "Heat Transfer by a Turbulently Flowing Fluid-Solids Mixture in a Pipe," Journal of Heat Transfer, Transactions of the American Society of Mechanical Engineers 83, 183-8 (1961).

33. Farber, L. and M. J. Morley, "Heat Transfer to Flowing Gas-Solids Mixtures in a Circular Tube," Industrial and Engineering Chemistry 49, 1143-50 (1957).

34. Keng, E. Y.H. and C. Orr, Jr., Investigation of Radiant Heat Transfer to Particle-Seeded Gases for Application to Nuclear Rocket Engine Design, NASA CR-953, National Aeronautics and Space Administration, Washington, D. C., 1967.

35. Eckert, E. R. G. and R. M. Drake, Heat and Mass Transfer, McGraw-Hill Book Company, Inc., New York, 1959.

36. Wiebelt, J. A., Engineering Radiation Heat Transfer, Holt, Rinehart, and Winston, Inc., New York, 1966.

37. Fishenden, M. and O. A. Saunders, "The Errors in Gas Temperature Measurements and their Calculation," Journal of The Institute of Fuel 12, No. 64, S5-S14 (March, 1939).

38. Bosanquet, C. H., "The Wall Effect in Gas Temperature Measurement," Journal of The Institute of Fuel 12, No. 64, S14-S17 (March, 1939).

39. Holl, H. B., The Reflection of Electromagnetic Radiation, Redstone Arsenal Report RF-TR-63-4, U.S. Army Missile Command, Huntsville, Ala.

40. Allen, R. D., L. F. Glassier and P. L. Jordan, "Spectral Emissivity, Total Emissivity, and Thermal Conductivity of Molybdenum, Tantanum, and Tungsten Above 2300°K," Journal of Applied Physics 31, 1382-7 (1960).

41. Williams, F. A., "On the Vaporization of Mist by Radiation," International Journal of Heat and Mass Transfer 8, 575-87 (1965).

42. Friedman, M. H. and S. W. Churchill, "The Adsorption of Thermal Radiation by Fuel Droplets," Chemical Engineering Progress Symposium Series 61, No. 57, 1-4 (1965).

43. Downing, C. G., "The Evaporation of Drops of Pure Liquids at Elevated Temperatures: Rates of Evaporation and Wet-Bulb Temperatures," American Institute of Chemical Engineers Journal 12, No. 4, 760-6 (1966).